



Università degli Studi di Cagliari

DOTTORATO DI RICERCA

Biologia e Biochimica dell'Uomo e dell'Ambiente

Ciclo XXVI

TITOLO TESI

Characterization of the mechanism of action of new HIV-1 reverse transcriptase-associated ribonuclease H inhibitors

Settore scientifico disciplinare di afferenza

Microbiologia BIO/19

Presentata da: Angela Corona

Coordinatore Dottorato Prof. Emanuele Sanna

Tutor/Relatore Prof. Enzo Tramontano

Esame finale anno accademico 2012 – 2013

Summary

Abstract.....	6
Chapter 1	
Introduction	8
1.1 The Human Immunodeficiency Virus 1	9
1.1.1 Genome Organization.....	9
1.1.2 Structure	11
1.1.3 Viral replication cycle.....	11
1.2 Approved HIV-1 inhibitors	13
1.3 Retrotranscription process	14
1.4. RT structure and functions	17
1.4.1 RNA- and DNA-dependent DNA synthesis.....	19
1.4.2 RNase H: DNA-directed RNA cleavage.....	20
1.4.3 Strand-transfer.....	21
1.4.4 Pyrophosphorolysis.....	22
1.5 RTIs: structure, mode of action and resistance	22
1.5.1 Nucleoside and Nucleotide RT inhibitors (NRTIs and NtRTIs)	22
1.5.2 Non-Nucleoside RT Inhibitors (NNRTIs).....	23
1.6. RNase H function as a drug target	25
1.6.1 Metal chelating active site inhibitors.	26
1.7.2 Allosteric inhibitors.....	27
1.7 Objectives	29
Chapter 2.	
Material and Methods	31
2.1 Prototype Foamy Virus Reverse Transcriptase	31
2.1.1 Protein purification.....	31
2.1.2 PFV RT DNA polymerase-independent RNase H activity determination.	31
2.1.3 PFV RNA dependent DNA polymerase activity determination.	31
2.1.4 NMR analyses.....	31
2.2 HIV-1 Reverse Transcriptase	32
2.2.1 Site-directed Mutagenesis.....	32
2.2.2 Protein expression and purification	33
2.2.4 HIV-1 DNA polymerase-independent RNase H activity determination.	34
2.2.5 HIV-1 RNA-dependent DNA polymerase activity determination.	34
2.2.6 Evaluation of DNA polymerase-independent RNase H and RDDP kinetic efficiencies.....	35
2.2.7 Yonetani-Theorell	35

2.2.9 Detection of protein inhibitor interactions by Differential Scanning Fluorimetry (ThermoFluor).	35
2.3 HIV-1 Integrase	36
2.3.1 Protein expression and purification	36
2.3.2 HIV-1 integrase activity.....	36
2.3 Cells and viruses.	37
2.3.1 Viral replication titration	37
2.3.2. MTT cytotoxicity assay.....	37
2.3.3 Quantification of viral DNA genomes.	37
2.4 Molecular Modeling	38
2.4.1 Molecular modeling on FVRT.....	38
2.4.2 Molecular Modeling on HIV-1 RT for DKAs binding study	38
2.4.2 Molecular Modeling on HIV-1 RT for RMNC6 binding study.....	40
 Chapter 3.	
Foamy virus reverse transcriptase as a tool to characterize human immunodeficiency virus type 1 ribonuclease H inhibitors	42
3.1 Introduction	42
3.2 Inhibition of PFV PR-RT enzyme activities by RHIs	43
3.3 Effect of the NNRTI EFV on the PFV PR-RT enzyme activities	46
3.4 NMR titration experiments with PFV RNase H.	46
3.5 Molecular modeling of RDS1643 on the PFV RNase H domain.	50
3.6 Structure comparison between the HIV-1 and PFV RNase H domains.	50
3.7 Discussion	52
 Chapter 4.	
A combined cell-based and site-directed mutagenesis approach defines highly conserved residues involved in the selective inhibition of the HIV-1 RNase H function by DKA derivatives	55
4.1 Introduction	55
4.2 Inhibition of HIV-1 RT-associated DNA polymerase-independent RNase H activity by DKAs.	56
4.3 Molecular docking	57
4.4 Catalytic efficiency of mutant HIV-1 RTs	62
4.5 Evaluation of the effects of DKA derivatives on mutant RTs	63
4.6 Characterization of the mechanism of DKA inhibition in cell-based assays	65
4.7 Discussion	70
 Chapter 5	
Site directed mutagenesis studies on HIV-1 RT shed light on the mechanism of action of a new RT-associated RNase H and RDDP dual inhibitor	72
5.1 Introduction	72
5.2 Comparison with known RNase H inhibitors.	74
5.3 Comparison with EFV: Yonetani-Theorell analysis and NNRTI resistant mutants.	75
5.4 Blind docking analysis.	76

5.5 Influence of the amino acid residues in pocket 1 on HIV-1 RT inhibition by RMNC6.	80
5.6 Influence of the amino acid residues in pocket 2 on HIV-1 RT inhibition by RMNC6	81
5.7 Kinetic studies on mutants	82
5.8 Discussion	83
Chapter 6.	
Conclusions	87
Acknowledgements.....	90
References.....	92

Abstract

HIV-1 the Reverse Transcriptase (RT), the most renowned retroviral specific enzyme, was the first anti-HIV target to be exploited, as. HIV-1 RT combines two functions essential for viral replication: DNA polymerase, synthesis DNA either in a RNA dependent (RDDP) or DNA dependent (DDDP) manner, and Ribonuclease H (RNase H). The RNase H activity catalyzes highly specific hydrolytic events on the RNA strand of the RNA/DNA replication intermediate, critical to the synthesis of integration-competent double-stranded proviral DNA. Because of its essential role, RNase H is a promising target for drug development. However, despite years of efforts, no RNase H inhibitor (RHI) has yet reached clinical approval.

In this work we pursued the identification and characterization of new promising RHIs targeting either the RNase H active site itself (RNase H active site chelating agents) or both RNase H and RDDP activities (allosteric dual inhibitors).

The first approach faced the challenging nature of the RNase H active site region, the morphology of which is, more open than that of the relatively similar, HIV-1 integrase (IN). This hampers the identification of a druggable pocket. We initially used Foamy Virus RT as a tool, to perform NMR and docking analyses on the interaction between FV RT RNase H domain and a previously identified diketo acid (DKA) derivative, inhibitor RDS1643. The amino acid residues of the FV RNase H active site region (T641, I647, Y672 and W703) were established to be important for the interaction with the inhibitor and analogous residues were successfully identified in the HIV-1 RNase H domain using structural overlays. Further docking and site directed mutagenesis studies were performed using six couples of ester/acid DKA, derived from RDS1643, showing for the first time, a broad interaction between RHIs and conserved residues in the HIV-1 RNase H active site region (R448, N474, Q475, Y501 and R557). Moreover, ester and acid derivatives exhibited a different binding orientation, that reflected a different specificity for RNase H versus IN. Among the synthesised derivatives one, RDS1759, showed to be an RNase H selective active site inhibitor characterized also, for the first time, in cell-based assays.

The second approach focused on the determination of the mechanism of action of a new isatine-derived RNase H/RDDP dual inhibitor, RMNC6. Docking analysis and site directed mutagenesis

results supported the hypothesis of a two-sites mode of action, with an independent role for two pockets, to be further characterized for a rational optimization of the scaffold.

Chapter 1.

Introduction

Acquired immunodeficiency syndrome (AIDS) has been the object of intensive research since mid-1981 when it was first described by the Center for Disease Control (CDC) (Anon 1981) and the scientific community deployed all resources to halt the lethal progression of the disease. A new retrovirus, first categorized as a T-lymphotropic virus, HTLV-III, was reported to have been found in tissues from AIDS patients in 1983 (Barré-Sinoussi et al. 1983). The causative relationship between AIDS and this virus, later named Human Immunodeficiency Virus (HIV) (Coffin et al. 1986), was established in 1984 (Broder & Gallo 1984). HIV-1 causes slow unremitting disease, targeting various lineages of CD4⁺ hematopoietic cells, particularly T-helper lymphocytes, differentiated macrophages, and some populations of dendritic cells. In particular, three different phases of infection have been characterized. The first, an “Acute retroviral syndrome” (ARS), occurs within 2-4 weeks after HIV infection in which the virus uses CD4⁺ cells to replicate massively, seeding and integrating its genome in various organs, particularly lymphoid organs such as the thymus, spleen, and lymph nodes. Plasma level of CD4⁺ cells drops down dramatically and a high number of HIV copies spread throughout the body. The immune system fights back with killer T cells (CD8⁺ T cells) and B-cell-produced antibodies. At this point, HIV levels in the blood are dramatically reduced. At the same time, CD4⁺ T cell counts rebound, and for some people the cell number rises to its original level. Shielded from the immune system, the virus lies dormant for an extended period of time, staying at a constant level called viral set point. During this second phase, called “Clinical latency stage”, the HIV virus continues to reproduce at very low plasma levels. For untreated people the clinical latency stage lasts an average of 10 years. During this time viral load will slowly begin to rise and CD4⁺ count to decline. The third phase, named as “full-blown AIDS”, starts when the number of CD4 cells falls below 200 cells/mm³; the human organism becomes vulnerable to opportunistic infections. Without treatment, people who progress to AIDS typically survive about 3 years, but the occurrence of dangerous opportunistic illnesses decreases the life-expectancy without treatment to about 1 year. The Joint United Nations Programme on

HIV/AIDS (UNAIDS) and World Health Organization (WHO) now estimates that the mean time from infection with HIV to AIDS and death, without treatment, is approximately 11 years. In 1986 a related, but immunologically distinct human retrovirus, now called HIV-2, was identified in Africa (Clavel et al. 1986). Compared to HIV-1, HIV-2 causes a slower decline in CD4+ levels, a longer clinical latency and a lower mortality rate (Gottlieb et al. 2002).

Nowadays, over 30 years of intensive research on HIV-1 have transformed this highly lethal infection into a chronic disease (Tsibris & Hirsch 2010) that can currently be treated with 25 drugs in different therapeutic combination regimens. However, despite these efforts, AIDS is still the first health emergency in the world. The last UNAIDS global report estimated 35.3 (32.2–38.8) million HIV-1 infected people and 2.3 (1.9–2.7) millions global new HIV infections in 2012. It has been estimated that more than 25 million people worldwide have already died of AIDS-related diseases and opportunistic infections, with an estimated 1.6 (1.4–1.9) million AIDS-related deaths in 2012 (Feinstein & Dimomfu 2013). Therefore the scientific community is still focusing on finding new targets and drugs to combat this threat.

1.1 The Human Immunodeficiency Virus 1

1.1.1 Genome Organization

HIV-1 belongs to the family of *Retroviridae*, lentivirus genus. Like all prototypic lentiviruses, HIV-1 has a (+) strand RNA genome that contains three major genes, *gag*, *pol*, *env*, encoding the major structural proteins as well as essential enzymes (Freed 2001). The HIV genome has several overlapping open reading frames and employs a sophisticated system of differential RNA splicing to obtain nine different gene products encoding 15 different proteins from its 9.2 kb genome. The three primary HIV-1 translation products are initially synthesized as polyprotein precursors, which are subsequently processed by viral or cellular proteases into mature proteins (Fig. 1). The *gag* gene encodes the proteins for the infrastructure of the internal part of the virus: the *gag* encoded p55^{gag} protein is cutted during the virion maturation to obtain the structural proteins MA, CA, NC and p6 (Briggs et al. 2004). The *pol* reading frame codes for the polyproteins Pr160, subsequently cutted to originate the enzymes that are essential for viral replication: the integrase (IN), protease, and reverse transcriptase (RT). The *env* gene codes for the two subunits of the surface

glycoprotein complex gp120 and gp41. In addition, like most complex retroviruses, HIV-1 has multiple regulatory elements. The two main regulatory proteins are Tat and Rev, others important accessory proteins are Nef, Vpr, Vif and Vpu, which are not essential for replication in certain tissues. Moreover, several conserved secondary structure elements, also called cis-acting RNA, have been identified within the HIV-1 RNA genome, as series of stem-loop structures connected by small linkers. These include the trans-activation region (TAR) element, the 5'-polyadenylation signal [poly(A)], the Primer binding site (PBS), the dimerization initiation sequence (DIS), the major splice donor (MSD) and the ψ hairpin structure located within the 5' end of the genome and the HIV Rev response element (RRE) within the *env* gene (Damgaard et al. 2004). These elements are reported to mediate elongation of viral RNA transcripts, genomic RNA dimerization, splicing and packaging of full length viral RNA (Freed & Martin 2007).

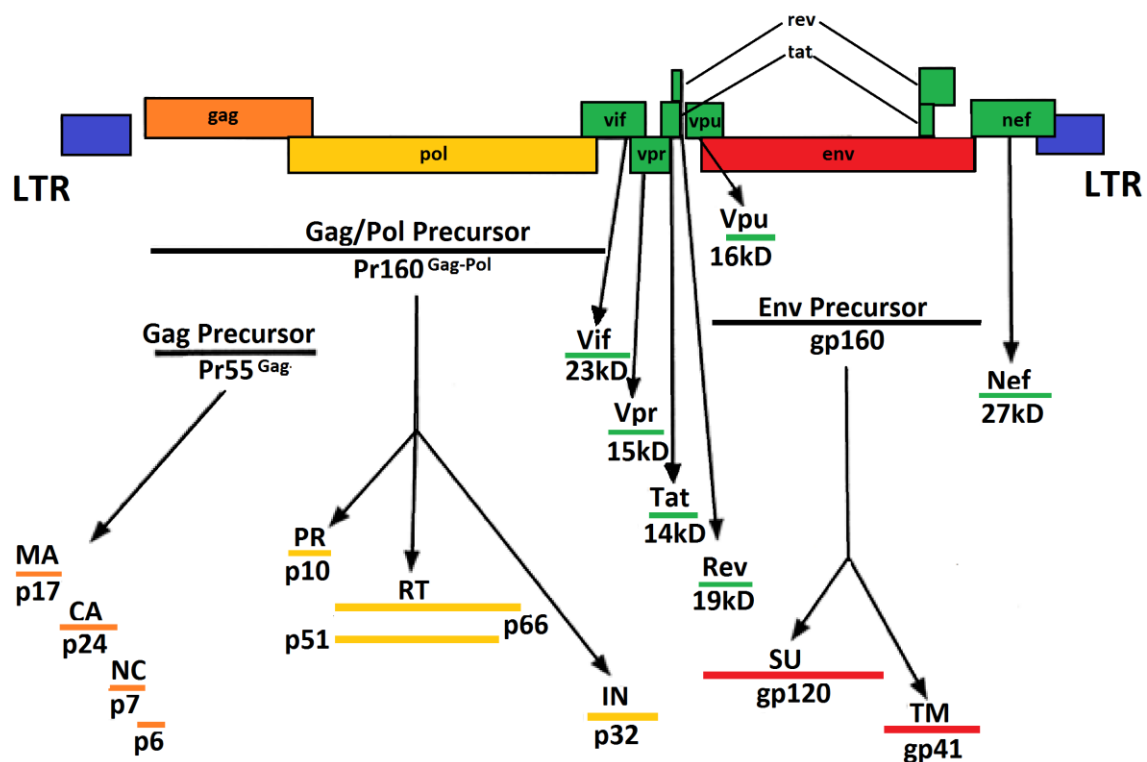


Figure 1. Human Immunodeficiency virus encoded proteins. The location of HIV genes, the sizes of primary translation products and the processed mature viral proteins are indicated. Modified from (Freed & Martin 2007).

1.1.2 Structure

The virion of HIV-1 is a roughly spherical particle with a diameter between 100 and 180 nm (Ganser-Pornillos et al. 2012). The virion is surrounded by a cell-derived lipid membrane containing surface proteins. Some of these membrane proteins are products of the viral genome (surface glycoprotein gp120/gp41), while others are captured from the host cell during viral budding and can perform supporting functions. Directly below the viral lipid membrane is a matrix layer composed of trimers of matrix protein (p17). Inside the HIV particle is a cone-shaped structure, named capsid, composed of approximately 250 hexamers and 12 pentamers of capsid protein (p24). The capsid contains two copies of positive single-stranded viral RNA bound by the NC (p7) protein and the enzymes (RT and IN) necessary for replication of the virus (Fig. 2).

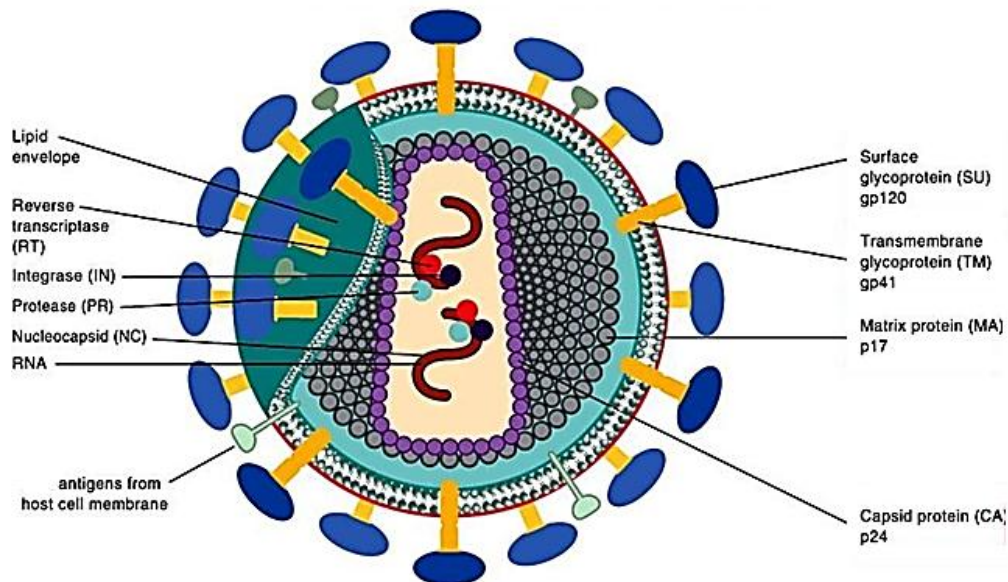


Figure 2. Schematic representation of the mature HIV-1 virion structure.

1.1.3 Viral replication cycle

Once in the host organism, HIV-1 uses the gp120/gp41 glycoprotein to target the CD4 receptor located on the surface of susceptible cells. A subsequent conformational switch allows the interaction with chemokine co-receptors CXCR4 and CCR5 on the cell surface, promoting the fusion of viral and cell membranes (Doms 2000). During entry, the disaggregation of the matrix shell permits the release of the core in the host cytoplasm. Here subviral particles are partially

uncoated maintaining protection of the viral RNA genome while permitting access to the deoxyribonucleoside triphosphates (dNTPs) necessary for proviral DNA synthesis. The genomic RNA is reverse transcribed into a linear integration competent double-stranded DNA molecule, which, associated with IN and viral cofactors in the “preintegration complex”, is imported into the

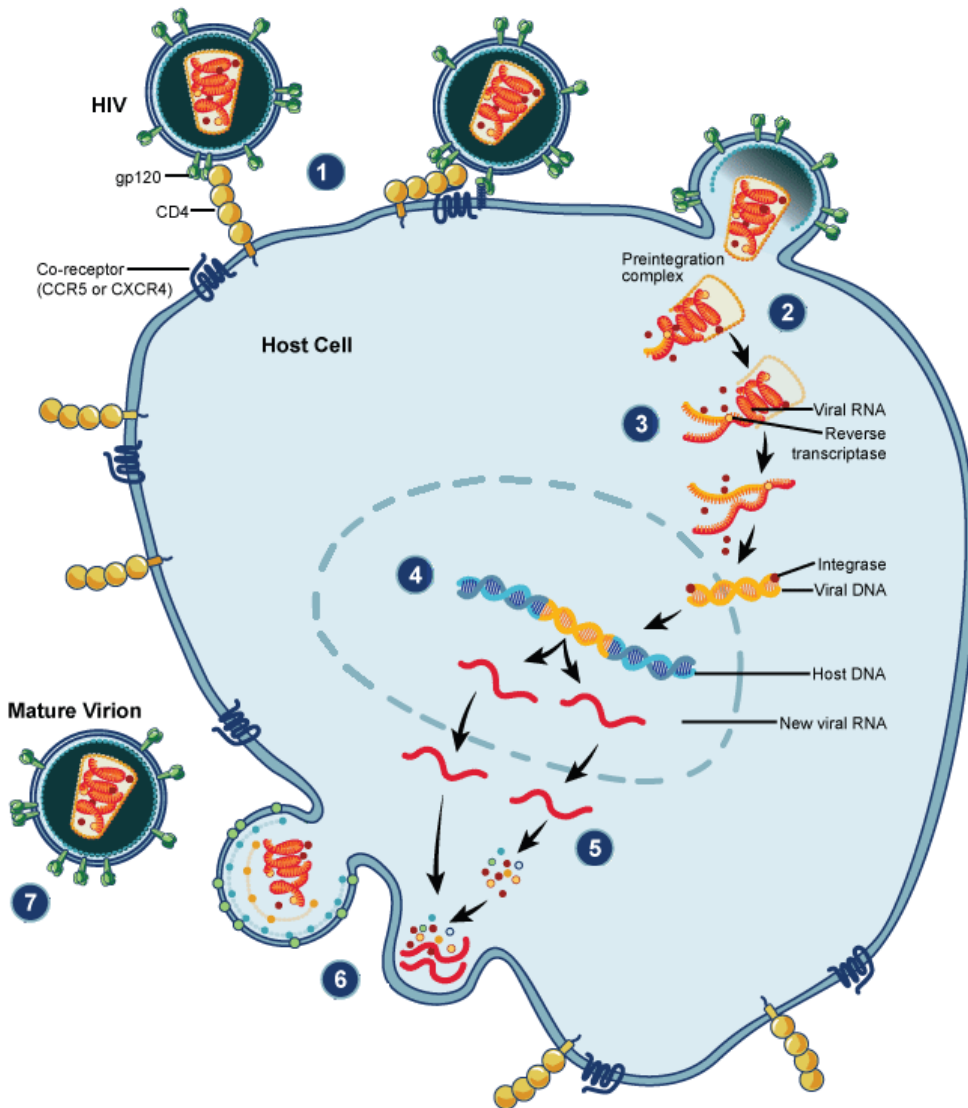


Figure 3. HIV-1 replication cycle. 1. Fusion of the HIV cell to the host cell surface. 2. HIV RNA, reverse transcriptase, integrase, and other viral proteins enter the host cell. 3. Viral DNA is formed by reverse transcription. 4. Viral DNA is transported across the nucleus and integrates into the host DNA. 5. New viral RNA is used as genomic RNA and to make viral proteins. 6. New viral RNA and proteins move to cell surface and a new, immature, HIV virus forms. 7. The virus matures by protease releasing individual HIV proteins. Source modified from : National Institute of Allergies and Infectious Diseases, Biology of HIV.

nucleus and integrated into the host genome (Fig.3). The integration of viral DNA is catalyzed by the viral coded enzyme IN and enhanced by the viral nucleic acid chaperone protein NC, which also protects viral DNA from degradation. HIV-1 preferentially integrates in active transcriptional units in human cells. The stably integrated HIV-1 provirus serves as a template for the transcription of viral messengers and genomic RNA by the cellular RNA polymerase II. The viral promoter, situated in the U3 part of the 5'-LTR (Fig.5), requires activation by cellular transcription factors, together with the binding of the viral transactivator protein Tat to the stem-loop trans-acting response element (TAR) present in 5'-LTR region. The synthesized full length HIV-1 transcripts are transported to the cytoplasm either unspliced (genomic RNA, which also serves as the Gag and Gag-Pol mRNA), partially spliced (encoding Vif, Vpr, Vpu and Env) or fully spliced (encoding Tat, Rev and Nef). The viral Rev protein links the incompletely spliced and unspliced viral RNAs to the export machinery, allowing unspliced RNA to exit from the nucleus. In the cytoplasm, mRNAs are translated into viral proteins and the enzymatic polyproteins precursors Gag and Gag-Pol. These are transported via different pathways to the plasma membrane, where they concentrate in lipid rafts that putatively serve as assembly platforms, while other components accumulate close by. When the number of densely packed viral polyproteins beneath the plasma membrane reach 1500 to 2000 units, it induces membrane curvature and then the subsequent formation of a membrane-coated spherical particle. The HIV-1 p6 part of Gag mediates the final viral release. The newly released particles have an immature morphology, without a condensed core. Shortly after the budding is finished, the viral protease is auto-activated and cleaves both Gag and Gag-Pol precursors into their sub-components which then reorganize into the characteristic conical inner core.

1.2 Approved HIV-1 inhibitors

The HIV-1 life cycle, with its many steps and virus-regulated or catalyzed events, presents many potential opportunities for therapeutic intervention (Fig. 4). During the entry, Gp41 and the coreceptor CCR5 are the targets for two approved entry agents: the peptide-based fusion inhibitor, enfuvirtide, and the small-molecule CCR5 chemokine receptor antagonist, maraviroc. The second critical step of the replication cycle is the reverse transcription of (+) ssRNA genome,

wich lasts the first 10 hours of infection and is the target for two distinct classes of RT inhibitors (RTI): the nucleoside RTIs (NRTIs) zidovudine, didanosine, zalcitabine, stavudine, lamivudine, abacavir, emtricitabine and tenofovir, all of which are analogs of native nucleoside substrates, and the non-nucleoside RTIa (NNRTIs) delavirdine, efavirenz, etravirine, nevirapine and rilpivirine, all of which bind to a non-catalytic RT allosteric pocket. Both RTI classes affect the RT DNA polymerization activity and block the generation of full-length viral DNA. A third step targeted by approved drugs is the proviral DNA integration. Two IN inhibitors (INIs) are currently available: Raltegravir and the recently licensed Dolutegravir. Both of them specifically inhibit IN strand-transfer activity and block the integration of the HIV-1 DNA into the cellular DNA. A fourth process blocked by HIV-1 approved inhibitors is the processing of viral polyproteins by the viral encoded Protease that is the target of eight approved drugs: atazanavir, fosamprenavir, daruavir, ritonavir, nelfinavir, squinavir, tipranavir, indinavir.

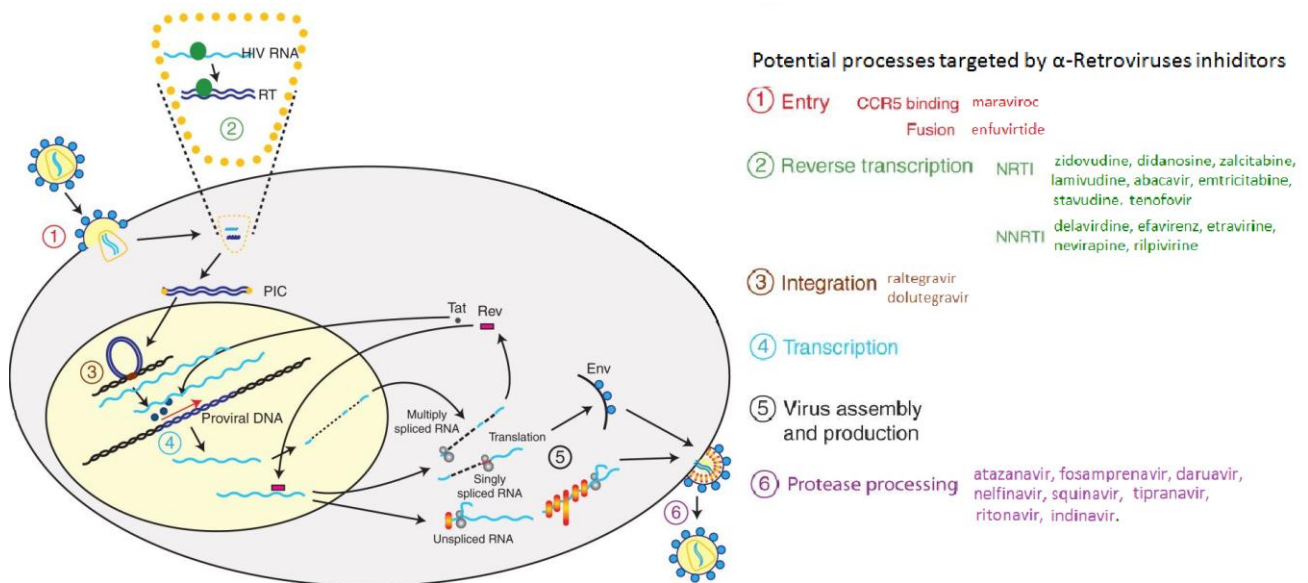


Figure 4. Schematic of the HIV-1 life cycle in a susceptible CD4⁺ cell. Potential or current antiretroviral drug target are highlighted . FDA-approved inhibitors are listed in relation to specificity of action and drug target (Modified from Arts et al. 2012).

1.3 Retrotranscription process

Among the 25 HIV-1 inhibitors, the 12 drugs that target the reverse transcription account for nearly half of all approved antiretroviral drugs. The retrotranscription process (Fig. 5) is characteristic of all retroviruses and requires viral as well as cellular elements among which the

most important is the virus-encoded RT protein, a multifunctional enzyme that performs the viral genome replication using two associated enzyme functions: DNA polymerase and ribonuclease H (RNase H).

As briefly introduced before, each HIV particle contains two copies of (+) ssRNA genome sequence 9,2 kb long (Ratner et al. 1985), which codes for structural and non-structural proteins and has two identical sequences at its the 5'- and 3'-ends,. Near the 5'-end of the viral genome there is a 18 nucleotides long segment, termed primer binding site (PBS), that is complementary to the 3' 18 nucleotides of the human tRNA^{Lys3}. When the cellular tRNA is hybridized to the PBS, it serves as a DNA primer and the RT-associated DNA polymerase function can initiate the first (-) strand ssDNA synthesis using the viral RNA genome as a template. The (-) strand ssDNA synthesis generates an RNA:DNA hybrid that is a substrate for the RT-associated RNase H function which selectively degrades the RNA strand of the RNA:DNA hybrid. During (-) ssDNA synthesis, RT pauses at the TAR hairpin, realizing the first (-) strand strong-stop DNA and promoting RNA cleavage approximately 14-20 nucleotides downstream from the pause site within the polyA hairpin in the copied template. This cleavage exposes the (-) ssDNA to an interaction with the polyA hairpin present in the R sequence of the 3' end genome. Therefore, a (-) strand-transfer occurs from the R region at the 5'-end of the genome to the equivalent R region at the 3'-end. The presence of two RNA genome molecules in a single virion particle allows (-) strand strand-transfer to occur either intra- or inter-molecularly (Chen et al. 2003). After this step, (-) strand synthesis can continue along the viral RNA starting from its 3'-end. Whilst DNA synthesis proceeds, the RNase H function cleaves the RNA strand of the RNA:DNA at numerous points. Although most of the RNase H cleavages do not appear to be sequence specific, there are two conserved purine-rich sequences, known as the polypurine tracts (PPTs), that are resistant to RNase H cleavage and remain annealed to the nascent (-) strand DNA. These two well-defined sites are located in the central part of the HIV-1 genome. In particular, the 3'-end PPT defines the 5'-end of the viral coding (+) strand DNA synthesis since this PPT serves as DNA primer (Huber & Richardson 1990; Rausch & Le Grice 2004). The (+) strand DNA synthesis continues until the 5'-end of the (-) strand DNA and also uses the 18 nucleotide PBS sequence of the tRNA as a template. Importantly, the 19th base from the 3'-end of tRNA^{Lys3} is a methylated Alanine, and the presence of this modified base blocks the RT,

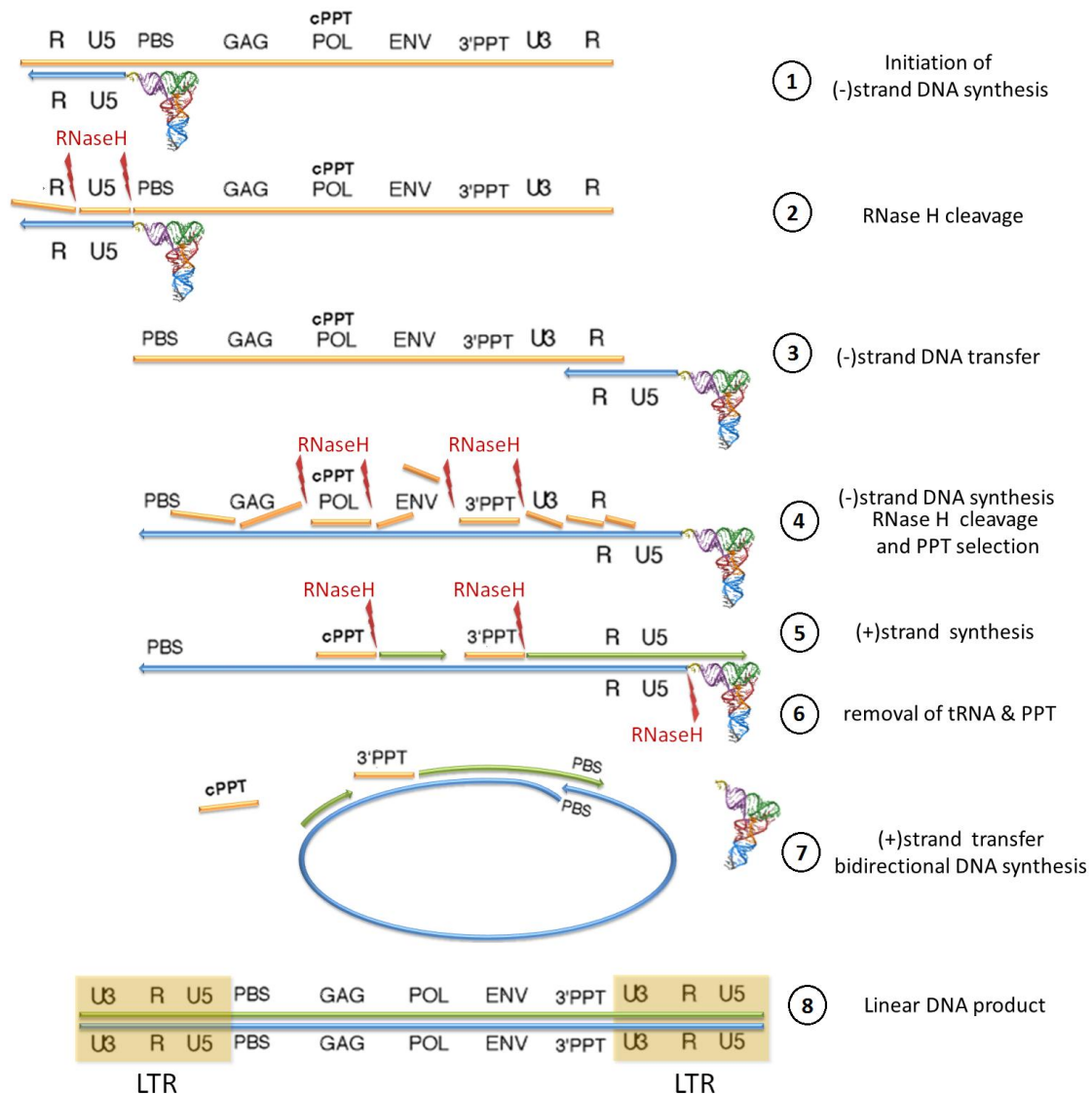


Figure 5. HIV-1 reverse transcription process. Step 1: host cell tRNA^{Lys3} hybridizes to the PBS near the 5'-end of the (+) strand RNA genome (orange). (-) strand DNA (blue) synthesis starts using host tRNA^{Lys3} as a primer. DNA synthesis proceeds up to the 5'-end of the RNA genome. Step 2: RNase H hydrolysis of the RNA portion of the RNA:DNA hybrid product exposes the ssDNA product determining the (-) strand strong stop DNA. Step 3: strand transfer of the (-) strand DNA through its hybridization with the R region at the 3'-end of the ssRNA genome and further elongation of the (-) strand DNA. Step 4: DNA synthesis proceeds and the RNase H function cleaves the RNA strand of the RNA:DNA at numerous points leaving intact two specific sequences (cPPT, 3'PPT) resistant to the RNase H cleavage. Step 5: (-) strand DNA synthesis (green) initiation using PPTs as primers. Step 6: RNase H hydrolysis of the PPT segments and the junction of the tRNA:DNA hybrid, freeing the PBS sequence of the (+) strand DNA. Step 7: strand transfer of the PBS sequence of the (+) strand DNA that anneals to the PBS on the (-) strand DNA. DNA synthesis then continues with strand displacement synthesis. Step 8: the product is a linear dsDNA with long terminal repeats (LTRs) at both ends. From (Esposito et al. 2012).

generating a (+) strand strong-stop DNA. Subsequently, the RNase H function precisely cleaves the RNA segment of the tRNA:DNA hybrid, freeing the PBS sequence of the (+) strand DNA and allowing it to anneal to the complementary site near the 3'-end of the extended (-) strand DNA (Basu et al. 2008). Then, a bidirectional synthesis occurs to complete a viral dsDNA that has a 90 nucleotides single-stranded flap at the center. This unusual situation is thought to be solved by host mechanisms and one candidate for flap removal is the flap endonuclease-1 (FEN-1) (Rausch & Le Grice 2004). Finally, a specific RNase H cut removes the PPT primers and exposes the integration sequence to facilitate the insertion of the viral dsDNA into the host chromosome.

1.4. RT structure and functions

As a major target for anti-HIV therapy, RT has been the subject of extensive research through crystal structure determinations, biochemical assays and single-molecule analyses. RT derives from a Gag-Pol polyprotein that is processed by the viral-encoded protease to give rise to two related subunits of different length, p66 and p51, that share a common amino terminus and combine in a stable asymmetric heterodimer (Divita et al. 1995). Analysis of the crystal structure of RT (Fig. 6) reveals that p66 is composed of two spatially distinct domains: the polymerase domain and the RNase H domain. The polymerase domain shows a characteristic highly conserved right hand-like structure, consisting of the fingers domain (residues 1-85 and 118-155), the palm domain (residues 86-117 and 156-237) and the thumb domain (residues 238-318). The p66 subunit also comprise the connection domain (residues 319-426) and RNase H domain (residues 427-560) (Kohlstaedt et al. 1992; Jacobo-Molina et al. 1993). The p51 subunit lacks the RNase H domain and has the same four subdomains of the p66 polymerase domain. The relative subdomain positions, however, are different from p66. Because of its different folding, p51 does not have enzymatic activities but serves to stabilize the proper folding of the p66 subunit which performs all the catalytic functions (Esposito et al. 2012).

RT is primarily responsible for several distinct activities that are all indispensable for the retrotranscription process: RNA- and DNA-dependent DNA synthesis, RNase H activity, strand-transfer, and strand displacement synthesis (Liu et al. 2008). The presence of all these functions in a single protein together with its highly dynamic RT nature which allows it to spontaneously slide

over long distances of RNA:DNA and DNA:DNA duplexes, to target the primer terminus for DNA polymerization, to rapidly access multiple sites and, hence, to make up for its low processivity. RT sliding does not require energy from nucleotide hydrolysis, and it is thought to be a thermally driven diffusion process (Liu et al. 2008).

It has recently been shown that RT can bind to the nucleic acid substrates in two different orientations, termed “RNase H cleavage competent orientation” and “polymerase competent orientation”, each of which allows one of the two enzymatic activities (Abbondanzieri et al. 2008). These two binding modes are in a dynamic equilibrium and it has been demonstrated that RT can

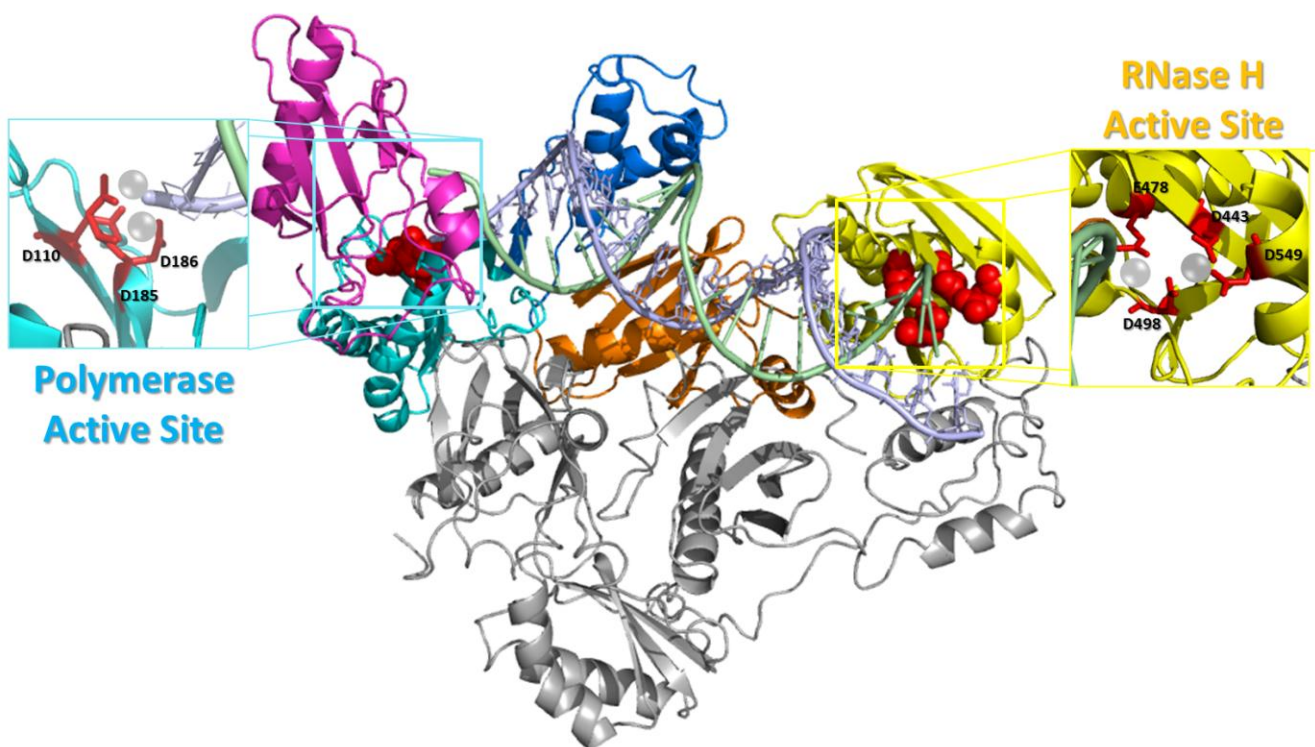


Figure 6. Structure of HIV-1 RT. The enzyme has two domains: the p66 (colored) and the p51 (gray). The polymerase domain shows a characteristic highly conserved structure that resembles a right hand, consisting of the fingers domain (magenta), the palm domain (cyan), and the thumb domain (blue). The p66 subunit also comprises the connection domain (orange) and RNase H domain (yellow). The polymerase active site is located in the middle of the palm, fingers and thumb subdomains. The three catalytic aspartic acid residues (D110, D185 and D186) located in the palm subdomain of p66 that bind the cofactor divalent ions (Mg^{2+}) are shown (red). The RNase H domain is located at C-terminus of the p66 subunit, 60 Å from the polymerase active site. The RNase H active site contains a DDE motif comprising the carboxylates residues D443, E478, D498 and D549 (shown in red) that can coordinate two divalent Mg^{2+} (shown as a cream spheres).

spontaneously and rapidly switch between these orientations without dissociating from the substrate. This flipping can be influenced by the presence of small molecules such as nucleotides, that stabilize the polymerase competent orientation, or NNRTI inhibitors that, conversely, destabilize it (Abbondanzieri et al. 2008). Together, shuttling and switching, give rise to a very complex series of conformational changes that increase the replication efficiency.

1.4.1 RNA- and DNA-dependent DNA synthesis

The DNA synthesis, catalyzed by both RT-associated RNA- and DNA-dependent DNA polymerase activities (RDDP and DDDP, respectively), occurs with a mechanism that is similar to the one of all others DNA polymerases (Steitz 1999) The polymerase active site is located in the middle of the palm, fingers and thumb subdomains. In particular, the thumb subdomain is very important for a correct substrate binding since its $\beta 12$ – $\beta 13$ sheets, termed the “primer grip”, extensively interact with the phosphate backbone (Dash et al. 2008). Three aspartic acid residues (D110, D185 and D186) located in the palm subdomain of p66 bind the divalent ion cofactor (Mg^{2+}) through their catalytic carboxylate groups and are essential for catalysis (Fig. 6) (Sarafianos et al. 2009). The DNA synthesis requires that RT binds to the template primer on the priming binding site, and this interaction is stabilized by a change of the conformation of the thumb (from close to open). Then, an incoming dNTP is admitted on the nucleotide binding site to form a ternary complex. Then, a conformational change of the fingers traps the dNTP, precisely aligning the α -phosphate of the dNTP and the 3'-OH of the primer inside the polymerase active site (this is the rate limiting step). Now, the enzyme catalyzes the formation of a phosphodiester bond between the primer 3'-OH and the dNMP, while releasing a pyrophosphate. The fingers weaken the grip around the substrate and allow the pyrophosphate free to leave the catalytic site. Finally, a translocation of the elongated DNA primer frees the nucleotide-binding site for the next incoming dNTP. Alternatively RT can dissociate from the complex. Compared to cellular DNA polymerases, RT exhibits a very low processivity, typically dissociating from the substrate after synthesizing only a few hundred nucleotides. This fact decreases the RT fidelity and results in the accumulation of mutations during reverse transcription. Error rates have been reported to fluctuate between 5.8×10^{-5} and 1.2×10^{-5} per nucleotide per replication cycle. Precise rate differ between different HIV-1

genetic subtypes and significantly increase at temperatures above 37°C (Menéndez-Arias 2008; Álvarez & Menéndez-Arias 2014).

Importantly, during its DNA polymerase activity RT can run up against several template secondary structures, particularly in case of the RNA template that can form stable RNA:RNA interactions, which can occlude the polymerization site and/or displace the primer terminus. In this case, RT has been shown to realize a strand displacement synthesis, in which the sliding movement can contribute to the re-annealing of the primer, displacing the RNA (Sarafianos et al. 2009).

1.4.2 RNase H: DNA-directed RNA cleavage

RT is able to nonspecifically hydrolyze the RNA strand of the RNA:DNA replication intermediate, as well as to catalyze highly specific hydrolytic events. Prominent among these is precise removal of the RNA primers that initiate (-) and (+) strand DNA synthesis (a host-coded tRNA and the poly-purine tract, respectively). These events ultimately define 5'- and 3'-LTRs, sequences that are essential for efficient integration of viral DNA. This RNase H function is essential for virus replication as RNase H-deficient viruses are non-infectious (Schatz et al. 1990).

The RNase H domain is located at the C-terminal end of the p66 subunit, 60 Å far from the polymerase active site (Fig. 6). This distance is equivalent to the length of 17 nucleotides of a DNA:DNA duplex or 18 nucleotides of a RNA:DNA hybrid (Nowotny et al. 2005). The RNase H active site contains a highly conserved, essential DDE motif, which includes the carboxylate residues D443, E478, D498 and D549. These coordinate two divalent Mg^{2+} cations, consistent with the proposed phosphoryl transfer geometry (Rosta et al. 2011). Mutations in any of the D443, D498 and E478 residues abolish enzyme activity (Schatz et al. 1989; Mizrahi et al. 1990; Mizrahi et al. 1994). The RNase H domain can catalyze a phosphoryl transfer through nucleophilic substitution reactions on phosphodiester bonds. This action occurs through the deprotonation of a water molecule, producing a nucleophilic hydroxide group that attacks the scissile phosphate group of RNA previously activated by coordination with the Mg^{2+} cofactor (Beilhartz & Götte 2010). RNase H cleavage specificity for the RNA portion of RNA:DNA hybrid mainly relies on the particular minor groove width of such hybrids and its interaction with the “primer grip”. The latter refers to an extensive network of contacts between the hybrid phosphate backbone and several

residues ~ 4 -9 bp far from the RNase H active site (Dash et al. 2008). The RNA:DNA helical structure has a minor groove width of ~ 9 -10 Å, which is intermediate between the A- and B-form of the others double-stranded nucleic acids (dsNA). The HIV-1 RNase H hydrolyzes hybrids with lower minor groove widths much less efficiently, such as the PPT containing hybrids which show widths of only 7 Å probably due to the presence of polyA-tracts. (Sarafianos et al. 2001; Sarafianos et al. 2009) This fact allows recognition of PPT sequences as RNA primers for DNA synthesis by RT, and may also represent a further specific target for development of antiviral drugs.

The RNase H catalysis can occur “polymerase-dependently” or “polymerase independently”, and it is possible to distinguish three different cleavage types “(Menéndez-Arias et al. 2008; Champoux & Schultz 2009). “DNA 3'-end-directed cleavage” acts during (-) strand DNA synthesis, when the RNase H active site cleaves the RNA in a position based on the binding of the polymerase active site to the 3'-end of the new (-) DNA (Furine & Reardon 1991). “RNA 5'-end-directed cleavage” acts when RT binds to a recessed RNA 5'-end annealed to a longer DNA strand, and RNase H function cleaves the RNA strand 13-19 nucleotides away from its 5'-end. The “internal cleavage” cleavage occurs because the RNA cleavage is slower than DNA synthesis and, given that, a viral particle contains 50-100 RT molecules and only two copies of (+) RNA, all non-polymerizing RTs can bind to the hybrid and degrade the RNA segment by a polymerase-independent mode (Dash et al. 2008)

1.4.3 Strand-transfer

The strand-transfer is a critical step during the reverse transcription process in which two complementary ssNAs have to anneal to allow the completion of DNA synthesis. In both the (-) and (+) strand transfer the ssNA develops secondary structures: the 97 nt R element folds into two conserved stem loop structures: the trans activation response element (TAR) and a poly(A) hairpin (Goff 2007; Damgaard et al. 2004). The PBS sequence at the 3'-end of the (-) strand DNA can also form a stable hairpin structure. Strand transfer by RT is promoted by the presence of viral-encoded nucleocapsid (NC) protein (Ji et al. 1996). The strand transfer process, together with the RT fidelity and the presence of other host factors such as APOBEC (Aguiar & Peterlin 2008)

underlie the high rates of mutagenesis and recombination, events that allow HIV to rapidly evolve and develop resistance against drugs.

1.4.4 Pyrophosphorolysis

Like most DNA polymerases, RT can catalyze the reversal of the dNTP incorporation, which is termed pyrophosphorolysis. RT uses a pyrophosphate (ppi) molecule or an NTP, such as ATP, as acceptor substrate (Arion et al. 1998). The reaction produces a dinucleotide tetraphosphate (formed by the excised dNMP and the acceptor ATP substrate), leaving free the 3'-OH DNA end. This RT function is particularly important in some drug resistant mechanisms. This will be discussed more in detail later on.

1.5 RTIs: structure, mode of action and resistance

The approved combination treatments used for HIV-1 include two classes of RTIs that target the viral enzyme with two different mechanisms of action. The first class comprises compounds known as NRTIs while the second class comprises compounds known as NNRTIs.

1.5.1 Nucleoside and Nucleotide RT inhibitors (NRTIs and NtRTIs)

There are currently eight NRTIs clinically available, structurally resembling both pyrimidine and purine analogues (Mehellou & De Clercq 2010; Arts & Hazuda 2012; Esposito et al. 2012) (Fig. 7). Pyrimidine nucleoside analogues include thymidine analogues zidovudine (AZT), stavudine (d4T) and cytosine analogues such as lamivudine (3TC), zalcitabine, (ddC), emtricitabine (FTC). Purine nucleoside analogues include abacavir (ABC) and didanosine (ddI), guanosine and adenine analogues, respectively. In order to inhibit reverse transcription, these agents have to be phosphorylated by cellular kinases to their triphosphate derivatives. All NRTIs follow the same mechanism of RT inhibition: once activated to their triphosphate form, they enter the DNA polymerase active site (Fig. 5) and are incorporated by RT into the growing DNA competing with the natural dNTPs and terminating the elongation of the growing dsDNA due to their lack of a 3'-hydroxyl group (Fig. 7). Therefore, once incorporated into dsDNA they prevent the further incorporation of incoming nucleotides. Importantly, while the HIV-1 RT uses these NRTIs as

substrates, the cellular DNA polymerases do not recognize them with the same affinity. The “second-generation” nucleoside analogues (Mehellou & De Clercq 2010) are also equipped with a phosphonate group which cannot be cleaved by hydrolysis (by esterases), making them more resistant to cleavage once incorporated compared to their regular dNTP counterparts. The only approved member of this class is tenofovir (PMPA).

Under selective drug pressure, viral mutants resist to NRTIs by two general mechanisms: NRTI discrimination, which reduces the NRTI incorporation rate usually by steric hindrance (Schinazi 1993, Schuurman 1995), and NRTI excision, which eliminates NRTI after incorporation. The M41L, D67N, D70R, L210W, T215F/Y and K219Q mutations, located around the dNTP binding pocket and also termed thymidine analogs mutations (TAMs), increase NRTI excision (Fig. 8) (Arion et al. 1998; Dharmasena et al. 2007; Yahi et al. 2005; Meyer et al. 1999). Recently, mutations in the connection and RNase H domains have also been shown to confer NRTI resistance (Nikolenko et al. 2007; Yap et al. 2007; Delviks-Frankenberry et al. 2008; Brehm et al. 2007; Hachiya et al. 2008) by reducing RNase H activity. This RNase H-dependent mechanism of NRTI resistance has been proposed to be due to an increase in NRTI excision determined by a reduction of RNase H activity, because the time available for nucleotide excision is limited by the degradation of the template by RNase H. Therefore, when mutations in the RNase H domain decrease its activity and consequently the HIV-1 RT template-switching, the excision rate is augmented, but only during RNA-dependent DNA synthesis and not during DNA-dependent DNA synthesis (Roquebert & Marcelin 2008)

1.5.2 Non-Nucleoside RT Inhibitors (NNRTIs)

NNRTIs are a structurally and chemically diverse group of compounds that inhibit RT by binding to the enzyme in a hydrophobic pocket (NNIBP) located in the palm domain of the p66 subunit of the heterodimeric RT, approximately 10 Å from the catalytic site of the enzyme. This class counts five approved drugs with remarkably heterogeneous scaffolds: nevirapine, efavirenz, delavirdine, etravirine and rilpivirine (Fig. 8).

The NNRTI binding pocket contains the side chains of aromatic and hydrophobic amino acid residues Y181, Y188, F227, W229, Y318, P95, L100, V106, V108, V179, L234 and P236 from the p66

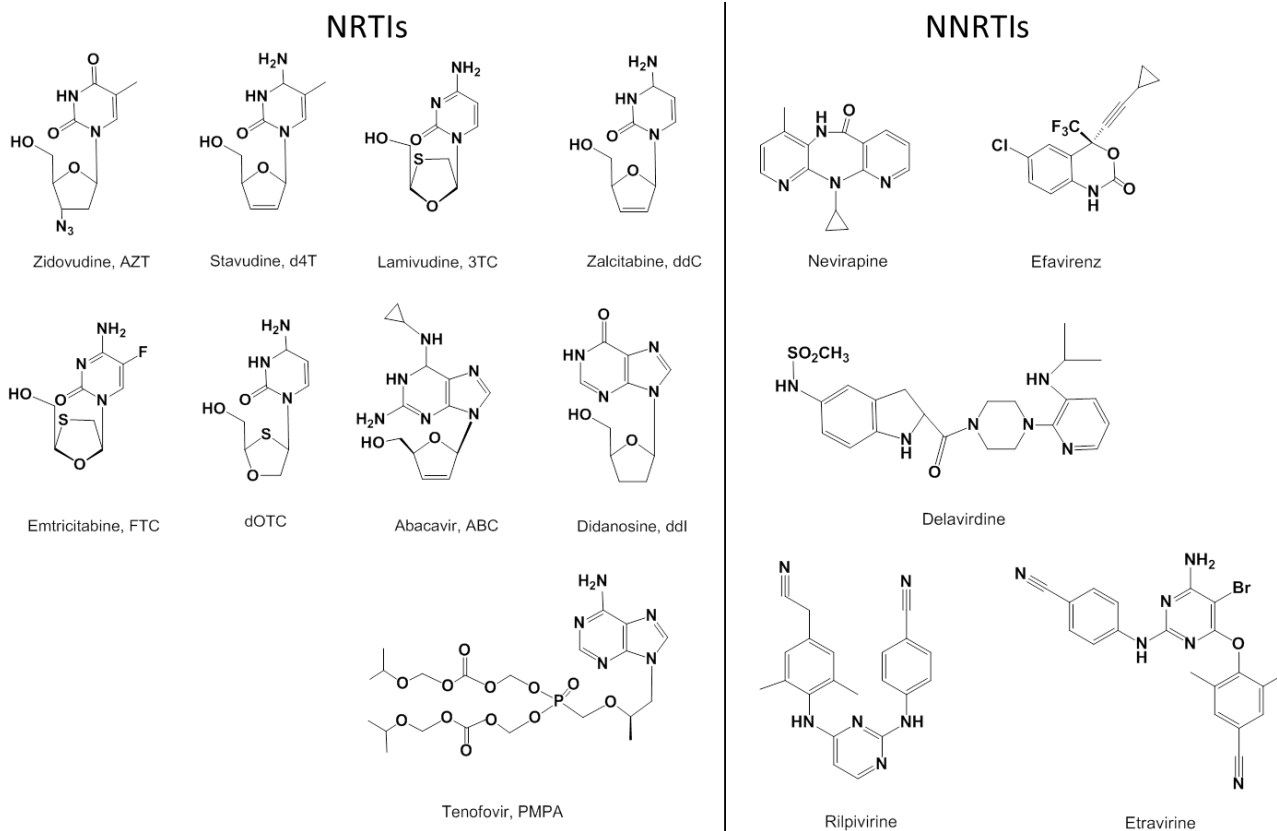


Figure 7. Chemical structures of approved NRTIs and NNRTIs.

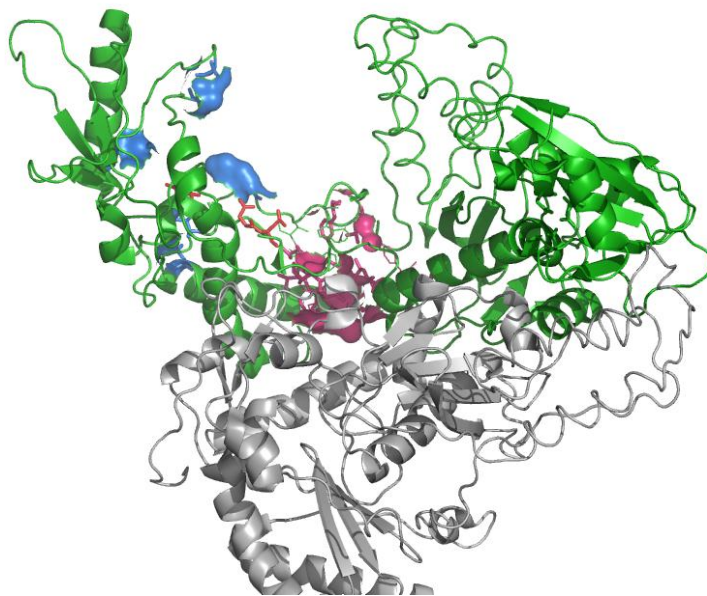


Figure 8. Pockets involved in RDDP inhibitor binding to HIV-1 RT. The two HIV-1 RT subunits are in green (p66) and in gray (p51). The catalytic residues of the RDDP active site are shown in red. NRTIs interact with residues close to the polymerase active site, some of which are mutated in TAM resistant viruses (blue). NNRTIs bind in a hydrophobic pocket next to the polymerase active site (dark pink).

subunit (Distinto et al. 2013) (Fig. 8). The NNIBP is flexible and its conformation depends on the size, shape, and binding mode of the different NNRTI. It can accommodate a space of about 620-720 Å, which is approximately more than twice the volume occupied by most of the present NNRTIs. This explains the large variety of chemical scaffolds of this class of inhibitors (Mehellou & De Clercq 2010) whose shapes inspired authors to create imaginative names to describe them, e. g. “butter-fly” (Ding et al. 1995), “horseshoe” (Das et al. 2005) and “dragon” (Das et al. 2011). The binding of NNRTI causes the dislocation of the β 12- β 13- β 14 sheets that results in a movement of the primer grip away from the polymerization site sheet (Das et al. 1996). Importantly, unlike NRTIs, NNRTIs do not require intracellular metabolic processing to exert their activity. The stabilization of the NNRTI binding in the allosteric site is accomplished through i) stacking interactions between the NNRTI aromatic rings and the side chains of Y181, Y188, W229 and Y318 residues in the lipophilic pocket of the RT; ii) electrostatic forces (particularly significant for K101, K103 and E138 residues); iii) van der Waals interactions with L100, V106, V179, Y181, G190, W229, L234 and Y318 residues; iv) hydrogen bonds between NNRTI and the main chain (carbonyl/amino) peptide bonds of the RT (Mui et al. 1992; Schäfer et al. 1993; Balzarini 2004). First-generation NNRTIs, such as nevirapine and delavirdine, easily become ineffective through selection of resistant RTs that contain single aminoacid mutations. Such commonly observed resistance mutations in NNRTI-treated patients include L100I, K103N, V106A, Y181C, Y188L, and G190A (Ren & Stammers 2008). These mutations occur alone or in combination and cause clinically relevant drug resistance, directly, by altering the size, shape, and polarity of different parts of the NNIBP or, indirectly, by affecting access to the pocket.

1.6. RNase H function as a drug target

Because of its peculiar role, RNase H function has been the object of intensive efforts to identify RNase H inhibitors (RHIs), and, through the past decade, a number of classes of molecules able to inhibit RNase H function have been identified (Tramontano 2006; Tramontano & Di Santo 2010; Corona et al. 2013). RNase H inhibitors can be categorized in two classes based on their binding site and mode of action: metal-chelating active site inhibitors (Fig.9) and allosteric inhibitors (Fig.10).

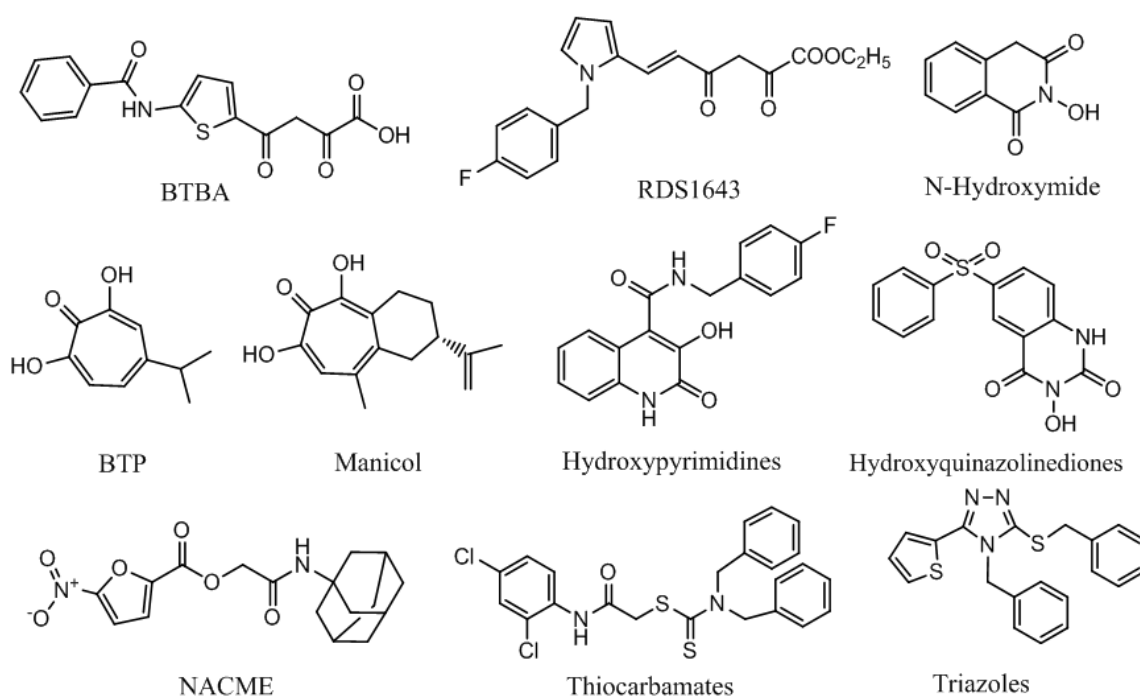


Figure 9. Chemical structure of RNase H active site inhibitors.

1.6.1 Metal chelating active site inhibitors.

Metal chelating active site inhibitors binds into the RNase H active site coordinating the two Mg^{2+} ion cofactors. The first reports of a compound inhibiting RNase H function was a diketoacid (DKA) derivative ,BTBA, which was first developed against HIV-1 IN (Shaw-Reid et al. 2003), and N-Hydroxyimides (Klumpp 2003). The first proof of RHI DKA RDS1643 inhibits viral replication (Tramontano et al. 2005) encouraged the development of different classes of Mg^{2+} chelating agents: hydroxilated tropolones betathujaplicinol (BTP) and manicol, (Budihias et al. 2005; Chung et al. 2011), hydroxypyrimidines (Kirschberg et al. 2009) and hydroxyquinazolinones (Lansdon et al. 2011), naphthyridinones (Su et al. 2010), Nitrofuran-2-carboxylic Acid Carbamoylmethyl Esters (NACME) (Fuji et al. 2009), thiocarbamates and triazoles (Di Grandi et al. 2010) (Fig. 9). Unfortunately, in all co-crystallized structures of RT/RNase H prototypes with RNase H inhibitors coordinating the cofactors into the active site (Chung et al. 2011; Su et al. 2010; Klumpp & Mirzadegan 2006; Lansdon et al. 2011) the compounds exhibited an orientation of binding that did not allow extended secondary interactions between enzyme and inhibitor, with the exception

of residue H539 (Lansdon et al. 2011), not allowing further insights for improve binding affinity and inhibitor specificity.

1.7.2 Allosteric inhibitors.

A number of structurally different compounds have been reported to inhibit HIV-1 RNase H activity without chelation (Corona et al. 2013). Among them are Vinylogous Ureas (Chung et al. 2010) (Chung et al. 2012), Thienopyrimidinones (Masaoka et al. 2013), Anthraquinones (Esposito et al. 2011), Hydrazones (Himmel 2006), and isatine derivatives (Distinto et al. 2013) (Fig. 10). These classes of compounds exhibited different binding in three different allosteric pockets.

In particular, vinylogous urea and thienopyrimidinone derivatives have been proposed to occupy a site at the interface of the two RT subunits that comprises p51 subunit residues C280-T290 and p66 subunit P537-E546 (Chung et al. 2012) (Fig. 11). Since x-ray crystal data suggests that the RNA/DNA hybrid binding is accompanied by movement of the p51 thumb and p66 RNase H domain as a single unit, it has been proposed that these compounds inhibit the subdomain/subunit flexibility that is an integral component of catalysis. In perspective, given the requirement for RT flexibility in accommodating and processing the RNA/DNA replication intermediate, the subunit interface may indeed offer a druggable pocket for compounds that can alter the RT subdomain and subunit motion.

Other compounds such as Hydrazones (Himmel et al. 2006), anthraquinones (Esposito et al. 2011) and isatine derivatives (Distinto et al. 2012) have been reported to have an interesting dual inhibition profile, since they inhibit both RT-associated RNase H and RDDP functions. They have been proposed to bind either to i) an allosteric site located between the polymerase catalytic region and the pocket where most of known polymerase inhibitors bind (50 Å from the catalytic site) including amino acid residues V108, D186, L187, Y188, L223, P227, L228 and W229 (Himmel et al. 2006); ii) a site located between the RNase H active site and the substrate-handle region including amino acid residues W401, T403, E404, K431, E430, Q507, and W535 on p66 and K331, L422 and L425 on p51. (Felts et al. 2011); iii) both sites at the same time (Distinto et al. 2013) (Fig. 11).

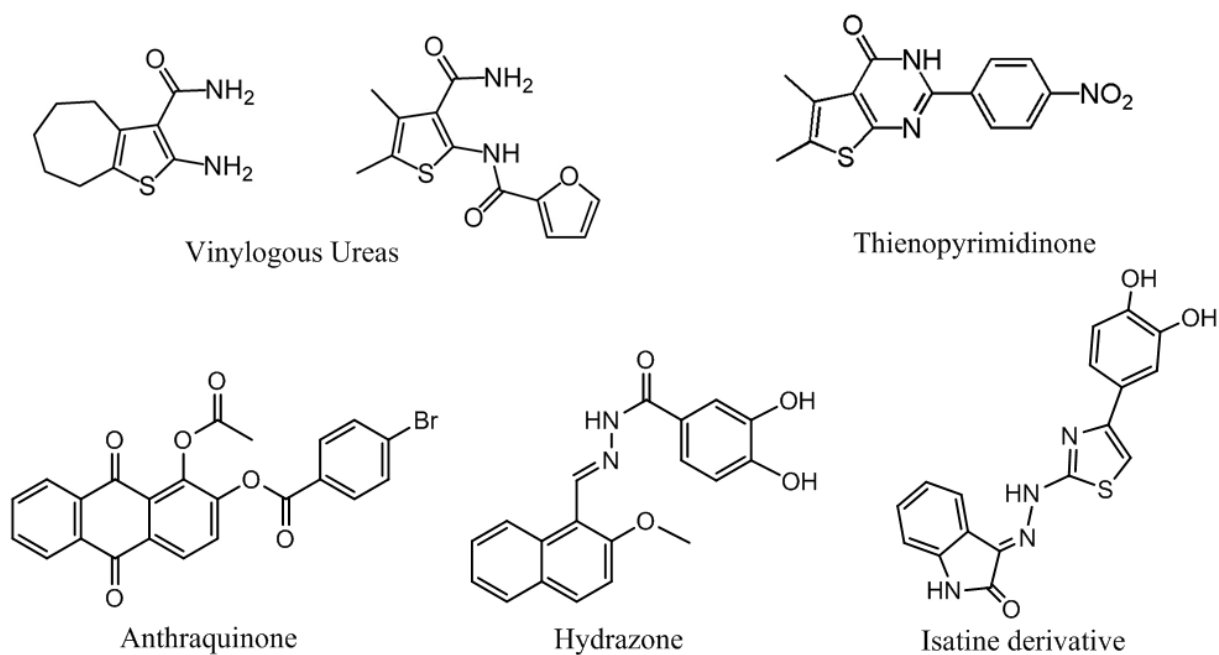


Figure 10. Chemical structure of allosteric RNase H inhibitors

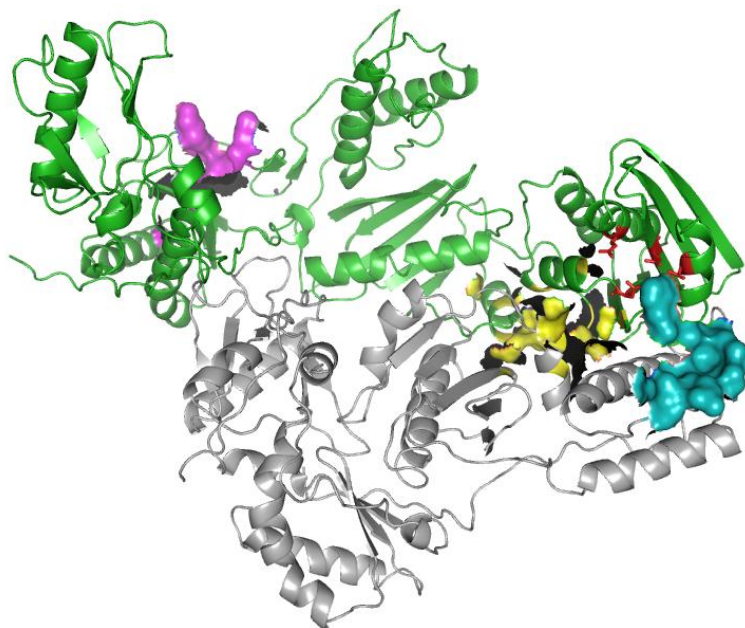


Figure 11. Pockets involved in RHI binding to HIV-1 RT. The two HIV-1 RT subunits are shown in green (p66) and in gray (p51). The catalytic residues of the RNase H active site are enlightened in red. The Hydrazone binding site, described by Himmel et al (Himmel et al. 2006), is located between the polymerase active site and the NNRTI binding pocket (sharing a few residues with it) (purple). A second Hydrazone binding site proposed by Felts et al (Felts et al. 2011), is located between the RNase H and the connection domain (yellow). The putative binding site for Vinylogous ureas is a hydrophobic pocket at the interface between the RNase H domain and the p51 subunit (cyan).

The high RT plasticity, together with the notion that NNRTIs such as nevirapine and efavirenz show long-range effects (increased RNase H catalytic activity) have led to the proposal of combined of short-range and long-range effects for the inhibition of RDDP and RNase H functions (Distinto 2013). However, the real mechanism of action is not determined yet and the role played by the two binding sites is controversial.

1.7 Objectives

The HIV-1 RT-associated RNase H function is essential for retroviral replication and is an attractive drug target given that no RNase H inhibitor has been approved yet. The purpose of this thesis work has been to identify and characterize new selective and potent RNase H inhibitors to be further developed into drug candidates.

Given the available informations produced in the field of RNase H inhibition until 2011 by my research group at the University of Cagliari, I pursued this goal focusing both on characterization of RNase H active site chelating agents and on determination of the mechanism of action of RNase H and RDDP dual inhibitors, starting either from already identified RNase H inhibitors or new promising scaffolds, identified in our laboratory by virtual and *in vitro* screening.

In both cases I carried out a combination of *in vitro* and *in silico* analysis to understand the chemical determinants involved in the binding of the inhibitor to the targeted protein. I explored the putative binding sites, dissecting the pocket/s by site-directed mutagenesis of residues hypothesized to be critical for binding. Finally, when possible, I validated the target in cell-based assays.

RNase H active site chelating agents have been reported since 2005 as promising RNase H inhibitors (Tramontano et al. 2005). However, the lack of improvements in potency of inhibition, together with information coming from crystal structures of RNase H domain interacting with active site inhibitors bound in an orientation unfavorable for ligand optimization, dejected pharmaceutical companies and academia from further research in that direction. In the absence of crystal structure information of HIV-1 RNase H domain with our DKA inhibitors, we considered the high similarity between HIV-1 and Foamy virus prototype (FV) RTs. Given the recent resolution via

NMR of the FV RT we decided to use it as a tool to explore the mechanism of action of known RNase H inhibitors. We characterized the mode of binding of inhibitors active against FV RT by NMR analysis to acquire information about their binding sites. With opportune comparative structural analysis this information was then translated to the HIV-1 RNase H domain, and confirmed by docking on HIV-1 RT and site directed mutagenesis to identify and characterize residues involved in binding. The DKA selectivity for the target has been evaluated both in biochemical assays and in cell culture assays.

Dual allosteric inhibitors of both RNase H and RDDP are a fascinating possibility to overcome the rapid selection of viral strains resistant to the currently approved single target drugs. Until now, none of the approved antiviral drugs is active on both functions, although a number of compounds have been reported to inhibit both RT functions *in vitro* (Distinto et al. 2013), and two binding sites located in different areas of the enzyme have been reported and hypothesized: the first one near the polymerase active site, the second one close to the RNase H active site. A recent virtual screening campaign conducted by our group has identified a promising isatine-derived scaffold active on both functions in the low micromolar range (Distinto et al. 2012). In this thesis I have explored the possibilities of binding of a newly synthesized isatine-derivative into the whole HIV-1 RT using a blind docking experiment and site directed mutagenesis that confirmed and characterized the *in silico* outcomes. I identified two independent binding pockets and I looked for an exhaustive explanation of this singular mechanism of inhibition, in the attempt to discriminate between the respective role of the two pockets involved.

Chapter 2.

Material and Methods

2.1 Prototype Foamy Virus Reverse Transcriptase

2.1.1 Protein purification.

Purification of PFV PR-RT and ¹⁵N labelled PFV RNase H was performed as described previously (Hartl et al. 2010; Leo, Schweimer, et al. 2012).

2.1.2 PFV RT DNA polymerase-independent RNase H activity determination.

The PFV RT-associated RNase H activity was measured in 100 µL reaction volume containing 50 mM Tris HCl pH 8.1, 6 mM MgCl₂, 1 mM dithiothreitol (DTT), 80 mM KCl, hybrid RNA/DNA (5'-GTTTTCTTTTCCCCCTGAC-3'-Fluorescein, 5'-CAAAAGAAAAGGGGGGACUG-3'-DabcyI) and 2 nM PFV RT. The reaction mixture was incubated for 1 hour at 37°C, the reaction was stopped by addition of EDTA and products were measured with a Victor 3 (Perkin) at 490/528 nm.

2.1.3 PFV RNA dependent DNA polymerase activity determination.

The PFV RT-associated RNA-Dependent DNA Polymerase (RDDP) activity was measured in 50 µL volume containing 60 mM Tris-HCl pH 8.1, 8 mM MgCl₂, 60 mM KCl, 13 mM DTT, 100 µM dTTP, 5 nM PFV RT and poly(A)-oligo(dT) (EnzCheck kit Invitrogen). The reaction mixture was incubated for 30 min at 37°C. The enzymatic reaction was stopped by addition of 50µl of 0.5M EDTA pH 8.0. Reaction products were detected by picogreen addition and measured with a Victor 3 (Perkin) at 502/523 nm (excitation/emission wavelength).

2.1.4 NMR analyses.

Standard NMR HSQC experiments were recorded using 50 - 80 µM ¹⁵N PFV labelled RNase H in 5mM Na-phosphate pH 7.0, 100 mM NaCl, 6 mM MgCl₂, 0.5 mM DTT, 10% D₂O (v/v), 6 % deuterated DMSO at 25°C on Bruker Avance 700 and 800 MHz spectrometers partially equipped with a cryogenically cooled probe. In-house protocols were used to process the NMR data and the program NMRView was utilized for analysis (B.A. Johnson, Merck, Whitehouse Station, NJ, USA).

Inhibitors were dissolved in 100% deuterated DMSO to a final concentration of 100 mM and added at the concentrations indicated in the Results section. Control HSQC spectra of PFV RNase H at various concentrations of deuterated DMSO were recorded for each titration step. Final DMSO concentrations for RDS1643 did not exceed 11%.

Changes in the chemical shifts were expressed by calculating the weighted geometric average (equation 1, $c_{15N} = 0.1$) of chemical shifts of ^1H and ^{15}N spins. A chemical shift change with a weighted geometric average of greater or equal 0.02 ppm was considered as significant.

$$\text{equation 1: } \Delta_{\text{norm}} = \sqrt{\Delta\delta_{1\text{H}}^2 + (c_{15\text{N}} \cdot \Delta\delta_{15\text{N}})^2}$$

2.2 HIV-1 Reverse Transcriptase

2.2.1 Site-directed Mutagenesis.

RTs strains naturally resistant to NNRTIs (K103N, Y181C, Y188L) have missense mutations on both p66 and p51 enzymatic subunits. Amino acid substitutions were introduced in both p51 and p66 subunits by mutating the RT wt gene coded together with the protease gene in a *p(His)6-tagged p66/p51 HIV-1HXB2 RT-prot*. Mutagenesis was realized using the QuikChange protocol (Agilent Technologies Inc., Santa Clara, CA). The plasmids were kindly provided by Stuart Le Grice Laboratory (NCI Frederick).

In the mutants RTs realized for binding characterization purposes the mutations were selectively introduced in the p66 subunit only.

Amino acid substitutions in the RT p66 RNase H domain (R448A, N474A, Q754A, Y501A, A502F, A508V, R557A) were selectively introduced mutating the RT wt gene coded together with the protease gene in the p6HRT-prot plasmid. Since all mutated residues are located in the RNase H domain, and because of proteolytic events occurring after expression delete the RNase H domain from the resulting p51, this leads to mutated p66/ wt p51 RT heterodimers.

Amino acid substitution in the RT p66 polymerase domain (V106A, V108A, Y188A, E224A, P225A, P226A, F227A, L228A, W229A, M230A, G231A). Amino acid substitutions were introduced selectively into the only p66 subunit of HIV-1 RT coded in a p66RT plasmid (not His-tagged). RTs

with mutated p66/ wt p51 were obtained co-purifying mutated p66 together with His-tagged wt p51 after separate expression.

2.2.2 Protein expression and purification .

Heterodimeric wt RT, NNRTI resistant RTs and mutant RTs containing amino acid substitutions in the RNase H domain only were expressed essentially as described (Le Grice et al., 1995). Monomeric subunits of recombinant RTs containing mutation in the p66 polymerase domain only were expressed separately (p66 and p6H51) using the same protocol.

Briefly, *E. coli* strain M15 containing the pRT-prot or vector, wt or mutated, were grown up to an OD600 of 0.7 and induced with 1.7 mM isopropyl β -D-1-thiogalactopyranoside (IPTG) for 4 h. SDS-PAGE followed by Coomassie staining was used to verify the final product of expression.

Lysis protocol: cell pellets were resuspended in Lysis buffer (50 mM Sodium Phosphate pH 7.8, 0.5 mg/mL lysozyme), incubated on ice for 20 min, added 0.3 M final NaCl, sonicated and centrifuged at 30,000 \times g for 1 h. The supernatant was recovered for protein purification. In the case of p66 polymerase domain mutants the pellet containing p66RT expression was combined in an equal ratio with pellet of expression of p6H51 (his-tagged wt subunit) before the lysis and the supernatant was gently stirred overnight at 4°C to allow heterodimer reconstitution.

Protein purification was carried out with an BioLogic LP (Biorad) with a combination of Immobilized Metal Ion Affinity Chromatography and Ion Exchange chromatography. The supernatant was loaded onto a Ni²⁺-sepharose column pre-equilibrated with Loading Buffer (50 mM Sodium Phosphate pH 7.8, 0.3M NaCl, 10% glycerol, 10 mM imidazole) and washed thoroughly with Wash Buffer (50 mM Sodium Phosphate pH 6.0, 0.3 M NaCl, 10% glycerol, 80 mM imidazole). RT was gradient-eluted with Elute Buffer (Wash buffer with 0.5 M imidazole). Fractions were collected, protein purity was checked by SDS-PAGE and found to be higher than 90%. Enzyme-containing fractions were pooled and diluted 1:1 with Dilute Buffer (50 mM Sodium Phosphate pH 7.0, 10% glycerol) then loaded onto a Hi-trap Heparine HP GE (Healthcare lifescience) pre-equilibrated with 10 column volumes of Loading Buffer 2 (50 mM Sodium Phosphate pH 7.0, 10% glycerol, 150 mM NaCl). The column was then washed with Loading Buffer2 and RT was gradient eluted with Elute Buffer 2 (50 mM Sodium Phosphate pH 7.0, 10%

glycerol, 150 mM NaCl). The fractions were collected, the protein was dialyzed and stored in Buffer containing 50 mM Tris HCl pH 7.0, 25 mM NaCl, 1mM EDTA, 50% glycerol. Protein concentration was determined by BSA Standard curve. Enzyme-containing fractions were pooled and aliquots were stored at -80°C .

2.2.4 HIV-1 DNA polymerase-independent RNase H activity determination.

The wt and mutant HIV RT-associated RNase H activity was measured in 100 μL reaction volume containing 50 mM Tris HCl pH 7.8, 6 mM MgCl_2 , 1 mM dithiothreitol (DTT), 80 mM KCl, hybrid RNA/DNA (5'-GTTTTCTTTTCCCCCTGAC-3'-Fluorescein, 5'-CAAAGAAAAGGGGGGACUG-3'-Dabcyl). Enzyme catalytic activities were determined via dose-response curve, in presence of increasing amount of enzyme: 0.9ng, 1.87 ng, 3.75 ng, 7.5ng, 15ng, 30 ng, 60 ng, 120ng,240ng, 480 ng, 1 μg , 2 μg . Different amount of enzymes according to a linear range of dose-response curve were used for experiments of RNase H function inhibition: 20 ng of wt RT; 60 ng K103N; 37.5 ng V106A; 75 ng V108A; 5 ng Y181C; 50 ng Y188A; 30 ng Y188L; 100ng E224A; 37.5 ng P225A; 20 ng P226A; 18 ng F227A; 30ng L228A; 30 ng W229A; 10 ng M230A; 30 ngG231A; 37.5 ng R448A; 62.5 ng N474A; 300 ng Q475A; 1 μg Y501A; 100ng A502F; 37.5 ng A508V; 75 ng R557A. The reaction mixture was incubated for 1 h at 37°C , the reaction was stopped by addition of 0.5M EDTA pH 8.0 and products were measured with a Victor 3 (Perkin) at 490/528 nm (excitaion/emission wavelength).

2.2.5 HIV-1 RNA-dependent DNA polymerase activity determination.

The HIV-1 RT-associated RNA-Dependent DNA Polymerase (RDDP) activity was measured in 25 μL volume containing 60 mM Tris-HCl pH 8.1, 8 mM MgCl_2 , 60 mM KCl, 13 mM DTT, poly(A)-oligo(dT), 100 μM dTTP. Enzyme catalytic activities were determined via dose-response curve, in presence of increasing amount of enzyme: 0.9ng, 1.87 ng, 3.75 ng, 7.5ng, 15ng, 30 ng, 60 ng, 120ng,240ng, 480 ng, 1 μg , 2 μg . Different amount of enzymes according to a linear range of dose-response curve were used for experiments of RDDP function inhibition: 6 ng wt RT; 30 ng K103N RT; 12 ng V106A RT; 19 ng V108A RT; 1,5 ng Y181C RT; 45 ng Y188A RT; 15 ng Y188L RT; 30 ng E224A RT; 15 ng P225A RT; 18 ng P226A RT; 23 ng F227A RT; 15 ng L228A RT; 30 ng W229A RT; 30 ng M230A RT;

15 ng G231A RT; 30 ng R448A, 30 ng N474A, 100 ng Q475A, 30 ng Y501A, 15 ng A502F RT; 19 ng A508V RT; 30 ng R557A RTs. After enzyme addition the reaction mixture was incubated for 30 min at 37 °C and enzymatic reaction was stopped by addition of 2 µl of 0.2 M EDTA pH 8.0. Reaction products were detected by picogreen addition and measured with a Victor 3 (Perkin) at 502/523 nm (excitation/emission wavelength).

2.2.6 Evaluation of DNA polymerase-independent RNase H and RDDP kinetic efficiencies.

Kinetic analyses of the DNA-polymerase independent RNase H and RDDP activities were performed according to Lineaweaver–Burke plots using the Sigmaplot11.0 software. Velocity (v) was expressed as fmoles/min.

2.2.7 Yonetani-Theorell

Yonetani-Theorell analysis was carried out according to Yonetani (Yonetani 1982). Briefly RDDP reaction velocity was measured following the RDDP function inhibition experimental protocol at several fixed concentrations of the inhibitor I_1 RMNC6 (1.25 µM; 2.5 µM; 5 µM) while titrating the second inhibitor I_2 EFV (4 nM; 8 nM; 16 nM). Reaction products were measured with a Victor 3 (Perkin) at 502/523 nm (excitation/emission wavelength). The reciprocal of velocity ($1/v$) was plotted as a function of concentration for RMNC6. The interaction constant α was calculated according to the Yonetani Theorell equation (Yonetani 1982).

2.2.9 Detection of protein inhibitor interactions by Differential Scanning Fluorimetry (ThermoFluor).

Thermal stability assays were performed according to Nettleship et al. 2008 (Nettleship et al. 2008). To a LightCycler 480 96-well plate (Roche) 1 µL of 500 µM inhibitor in DMSO was added, followed by 49 µL of 300 nM HIV-1 RT in reaction buffer containing 20 mM HEPES, pH 7.5, 10 mM MgCl₂, 100 mM NaCl, and a 1:1000 dilution of Sypro Orange dye (Invitrogen). The mixture was heated from 30 to 90°C in increments of 0.2°C every 5 seconds. Fluorescence intensity was measured using excitation and emission wavelengths of 483 and 568 nm, respectively. Changes in protein thermal stability (ΔT_m) upon inhibitor binding were analyzed by using LightCycler 480 software. All assays were performed in triplicate.

2.3 HIV-1 Integrase

2.3.1 Protein expression and purification

HIV-1 IN was expressed essentially as reported in (Zamborlini et al. 2011). Briefly, His-tagged IN was produced in *E. coli* BL21-CodonPlus (DE3)-RIPL (Agilent, Santa Clara, USA) and purified under non-denaturing conditions. Protein production was induced at an OD₆₀₀ of 0.6 to 0.8, by adding IPTG to a concentration of 0.5 mM. Cultures were incubated for 3 h at 37°C and then centrifuged 20 min at 1100 g, 4°C. Cells were resuspended in buffer A (50 mM Tris-HCl (pH 8), 1 M NaCl, 4 mM β-mercaptoethanol) and lysed by passage through a French press. The lysate was centrifuged (30 min at 12,000xg at 4 °C), and the supernatant was filtered (pore size 0.45 μM) and incubated with nickel-nitrilotriacetic acid agarose beads (Qiagen, Venlo, The Netherlands) for at least 2 hours at 4 °C. The beads were washed with buffer A and then with buffer A supplemented with 80 mM imidazole. His-tagged proteins were then eluted from the beads in buffer A supplemented with 1 M imidazole and 50 μM zinc sulfate. They were then dialyzed overnight against 20 mM Tris-HCl (pH 8), 1 M NaCl, 4 mM β-mercaptoethanol and 10% glycerol. Aliquots of the purification products were rapidly frozen and stored at -80°C.

2.3.2 HIV-1 integrase activity.

Strand transfer reaction was performed as described previously (Delelis et al. 2007). Oligonucleotides (ODN) HIV-1B (5'-TGTGGAAAATCTCTAGCA-3') and HIV-1A (5'-ACTGCTAGAGATTTTCCACA-3') were used for the strand transfer-reaction. ODNs were purchased from Eurogentec (Liege, Belgium) and further purified by electrophoresis in a denaturing 18% acrylamide/urea gel. HIV-1B was radiolabelled with T4 polynucleotide kinase (Biolabs) and γ[32-P]ATP (3000 Ci/mmol) (Amersham), and purified on a Sephadex G-10 column (GE Healthcare). Double-stranded ODNs were obtained by mixing equimolar amounts of complementary strands (HIV-1A) in the presence of 100 mM NaCl. Strand-transfer reactions were carried out at 37°C, in a buffer containing 10 mM HEPES (pH 7.2), 1 mM DTT, 7.5 mM MgCl₂ or MnCl₂ in the presence of 12.5 nM DNA substrate. Products were separated by electrophoresis in denaturing 18% acrylamide/urea gels. Gels were analysed with a Molecular Dynamics STORM phosphoimager and quantified with Image Quant™ 4.1 software.

2.3 Cells and viruses.

2.3.1 Viral replication titration

MT4 and 293T cells were cultured in RPMI1640 and DMEM medium, respectively. Both mediums were supplemented with 10% fetal calf serum. HIV-1 stocks were prepared by transfecting 293 T with the HIV-1 molecular clone derived from pNL4-3 (Δ env viruses)(Gelderblom et al. 2008) Δ env viruses NLENG1-ES-IRES WT encode the WT integrase. Pseudotyping of Δ env viruses was performed by co-transfection of 293 T cells with a VSV-G plasmid using the calcium phosphate method. Viral supernatants were filtered (0.45 μ m) after 30 min of centrifugation at 4500 g and frozen at -80°C . HIV-1 p24gag antigen content in viral supernatants was determined by enzyme-linked immunosorbent assay (Perkin-Elmer Life Sciences). For infection were used 120 ng of p24gag antigen per 10^6 cells, corresponding to a multiplicity of infection (m.o.i.) of 0.3. When required, cells were treated in the presence of integrase inhibitor RAL (100 nM) or efavirenz (100 nM). Flow cytometry analysis was performed on a FACSCalibur flow cytometer (BD Bioscience) to measure cell viability and percentage of infected cells. Results were analysed using the ImageQuant software.

2.3.2. MTT cytotoxicity assay.

MT4 cell proliferation was measured by seeding 1×10^4 cells/well in 96-well plates in 100 μ L of RPMI/FBS (10%), penicillin (100 U/mL), streptomycin (200 μ g/mL). Cells were treated with increasing concentration of different inhibitors and subjected to MTT assay after 48 hours of growth. Briefly, after discarding the supernatant, 100 μ L of MTT dilution (5 mg/mL in DMEM 10% FBS) were added and cells were incubated for 2 hours at 37°C 5% CO_2 . Then, after addition of 100 μ L of Lysis Solution (20 mM HCl, 0.1% SDS), cells were incubated for 2 hours. 100 μ L of final solution of each sample was then transferred to a new 96-well plate for quantification on a plate-reader Spectramax at 570 nM.

2.3.3 Quantification of viral DNA genomes.

Quantitative PCR (qPCR) was performed as described previously (Munir et al. 2013). Briefly, MT4 cells were infected and treated with inhibitors at time zero and 10 hours post infection. RDS1759

and RDS1760 inhibitors were used at concentration of 10 μ M, and known inhibitors Raltegravir and Efavirenz were used as a control at a concentration of 200 nM and 100 nM, respectively. Two to five millions cells were collected at each time point. Cells were washed in PBS, and dry cell pellets were frozen at -80°C until use. DNA from infected cells was purified using a QIAamp DNA Blood mini kit (Qiagen) according to the manufacturer's instructions. Quantifications of total viral DNAs, 2-LTRc and integrated DNAs were performed on a Light cycler instrument (Roche Diagnostics) using the second-derivative-maximum method provided by the Light Cycler quantification software, version 3.5 (Roche Diagnostics). Amplification of the β -globin gene (two copies per diploid cell) was performed to normalize the results using commercially available materials (Control kit DNA; Roche Diagnostics). The quantification results for two-LTR circle, total HIV-1 DNA, and integrated HIV-1 DNA were expressed as copy numbers per μ g DNA.

2.4 Molecular Modeling

2.4.1 Molecular modeling on FVRT.

Docking experiments were performed using the program AutoDock Vina (Trott & Olson 2010). Non-polar hydrogen atoms were removed from both protein and ligand and saved in a pdbqt format. A grid box was set. with 20*36*28 points in x, y, z directions and -8.5, -18, 7 as the grid center for PFV RNase H (PDB ID: 2LSN). The grid box included the active site residues and the adjacent residues exhibiting significant chemical shift changes. These parameters were saved in a configuration text file (config.txt) followed by autodocking. The results generated were visualized in PyMOL. Among the inhibitor binding orientations obtained the orientation fitting best to the NMR data was chosen.

2.4.2 Molecular Modeling on HIV-1 RT for DKAs binding study

Ligands preparation: the DKAs three dimensional structures were generated with the Maestro Build Panel (Anon n.d.) and were then submitted to Polak-Ribiere conjugate gradient minimization (0.0005 kJ/(Å mol) convergence using MacroModel (version 9.9) (Anon n.d.). Ligands were modeled in their enolate form, since such compounds mainly exist in their enolic form in solution (Maurin et al. 2004) and also given the influence of the two metal cations in the binding site.

Protein preparation: for docking we selected the crystal structure of the full-length HIV-1 RT in complex with a naphthyridinone inhibitor bound to the RNase H active site (PDB ID: 3LP1). The missing residue R557, which is part of the RNase H active site, was modeled using the coordinates of the PDB ID: 3K2P crystal structure (structure of HIV-1 RT with the inhibitor beta-thujaplicinol bound at the RNase H active site). The receptor was prepared using the “Protein Preparation Wizard” panel of Schrödinger 2012 molecular modeling package (Anon n.d.). The bond orders and disulfide bonds were assigned, all hydrogen atoms were added, and all water molecules deleted. An optimization of the hydrogen-bonding network was performed using the “H-bond assignment” tool. Finally, using the “improp utility”, the positions of the hydrogen atoms were optimized by keeping all the heavy atoms in place.

Docking calculations: docking studies were carried out with Glide v. 5.8 (Schrödinger)(Anon n.d.). Glide is a grid-based ligand docking program with energetics approach and searches for favorable interactions between ligands and receptors. The shape and properties of the receptor are represented on a grid by different sets of fields that provide progressively more accurate scoring of the ligand position. These fields are generated as preprocessing steps in the calculation and hence need to be computed only once. For the grid generation, a box centered on the active site Mg^{2+} ions was created. This box gives a more precise measure of the effective size of the search space. However, ligands can move outside this box during grid minimization. The Cartesian coordinates of the outer box, X, Y, and Z lengths were each set to 20 Å. The conformational space of the ligand is defined by Glide by several lowest-energy poses that are subjected to a Monte Carlo procedure that examines nearby torsional minima. This procedure is needed in some cases to properly orient peripheral groups and occasionally alters internal torsion angles. The default value (1.00) for the van der Waals radii scaling factor was chosen, which means no scaling for the nonpolar atoms was performed. In the present study, the standard precision (SP) mode of GlideScore function was used to score the obtained binding poses. The force field used for the docking was the OPLS-2005 (Jorgensen et al. 1996). All of the pictures were rendered with pymol (www.pymol.org).

2.4.2 Molecular Modeling on HIV-1 RT for RMNC6 binding study

Ligand preparation: a theoretical 3D model of RMNC6 was built using Maestro. (Schrödinger LLC., Maestro GUI, New York, NY, USA, 2012.) The inhibitor structure was optimized by means of an energy minimization carried out using the MMFFs force field (T. Halgren, J. Comput. Chem. 1996, 17(5-6), 520-552), the GB/SA (Hasel et al. 1988) water implicit solvation model and the Polak-Ribier Conjugate Gradient (PRCG) method, converging on a gradient with a threshold of $0.05 \text{ kJ}(\text{mol} \cdot \text{Å})^{-1}$.

Protein preparation: the coordinates for reverse transcriptase enzymes were taken from the RCSB Protein Data Bank (Berman et al. 2000) (PDB codes 1vrt (Ren et al. 1995), 2zd1 (Das et al. 2008), 1ep4 (Ren 2000), 3qo9 (Das et al. 2011), 1rti (Ren et al. 1995) 1tv6 (Pata et al. 2004) , 3lp2 (Himmel et al. 2009). The proteins were prepared using the Maestro Protein Preparation Wizard. Original water molecules were removed and termini were capped. The bond orders and formal charges were added for hetero groups, and all the hydrogen atoms were added in the structure. Missing hydrogens atoms were included. After preparation, the structures were refined in order to optimize the hydrogen bond network using OPLS_2005 (Kaminski et al. 2001) force field. The minimization was terminated when the energy converged or the RMSD reached a maximum cut-off of 0.30 Å .

Docking protocol: molecular docking studies were performed using the QMPL workflow protocol. (Schrödinger LLC., QMPolarized protocol, in Schrodinger Suite, New York, NY, USA). Grids were defined around the refined structure by centering on the residue W229 (located in the NNRTI binding pocket) and Q500 (located in the RNase H domain) and fixing the box volume at $97,336 \text{ Å}^3$, covering the whole p66 and most of p51 subunit. The extra precision (XP) docking algorithm was applied for scoring theoretical poses. The other settings were left as default. The same protocol was applied to all simulations.

Post docking protocol: 10,000 steps of the Polak-Ribier conjugate gradient (PRCG) minimization method were conducted on the top ranked theoretical complexes using OPLS_2005 force field. The optimization process was performed up to the derivative convergence criterion equal to $0.01 \text{ kJ}/(\text{mol} \cdot \text{Å})^{-1}$. The binding free energies ($\Delta G(\text{Bind})$) were computed applying molecular mechanics

and continuum solvation models with the molecular mechanics generalized Born/surface area (MM-GBSA) method (Kollman et al. 2000).

Chapter 3.

Foamy virus reverse transcriptase as a tool to characterize human immunodeficiency virus type 1 ribonuclease H inhibitors

3.1 Introduction

The *retroviridae* family is divided into two major subfamilies: the *orthoretrovirinae*, including α to ϵ and lentiviruses, and the *spumaretrovirinae*, and one more that include the only genus of FVs (Linial 2007). FVs differ from *orthoretrovirinae* in many aspects of the retroviral replication cycle, e.g. reverse transcription takes place before the virus buds from the host cell, so that DNA is found in extracellular FV particles, similar to hepadnaviruses (Yu et al. 1996). Moreover, in FVs only the IN is cleaved off from the Pol precursor, leading to a mature, multifunctional protease-RT (PR-RT) enzyme in the virus particle. In contrast, all other retroviruses – including HIV-1 – cleave off the PR domain from Pol (Pfrepper et al. 1998; Roy & Linial 2007).

Therefore, in FVs, the mature PR-RT carries out the functions of the PR and the RT, including the RT-associated RDDP and RNase H activities (Rinke et al. 2002; Boyer et al. 2007; Hartl et al. 2010). A few studies have characterized the enzymatic properties of prototype FV (PFV) PR-RT, particularly in comparison with the HIV-1 RT, showing that PFV PR-RT-associated RDDP activity is more processive than HIV-1 RT (Hartl et al. 2011); it has the same fidelity as HIV-1 RT (Boyer et al. 2007), while its K_M values for dNTPs are 5-30 fold lower than the one of HIV-1 RT (Boyer et al. 2004). Overall, these differences in the polymerization properties appear to reflect the ability of FVs to replicate only in dividing cells (with high dNTPs concentrations). PFV PR-RT has been shown to be monomeric and able to catalyze all RT related functions (Boyer et al. 2004), while PR activation requires dimer formation of the PR domain via binding of PR-RT to a specific element on the viral RNA, called PARM (protease activating RNA motif) (Hartl et al. 2010). Hence, for the retrotranscription functions PFV PR-RT differs from alpharetroviral and lentiviral RTs (including HIV-1 RT) that are dimeric, and is similar to the gammaretroviral RTs that are monomeric

(Herschhorn & Hizi 2010). In addition, the PFV RNase H domain possesses a basic protrusion, including a basic loop and the so-called C-helix, which has been proposed to be important for activity and substrate binding and is absent from the HIV-1 RNase H domain (Leo, Hartl, et al. 2012; Leo, Schweimer, et al. 2012; Esposito et al. 2012).

However, despite this, comparison of the structural features of the PFV RNase H domain with the HIV-1 RNase H domain, showed that they are highly similar (Leo, Schweimer, et al. 2012). In fact, superimposition of the two RNase H domains showed a good structural alignment, in particular in the domain portion that makes contacts with the hybrid substrate (Fig. 12). Therefore, we asked whether the PFV RNase H domain could be used as tool to investigate the interactions between RHIs and the RNase H domain.

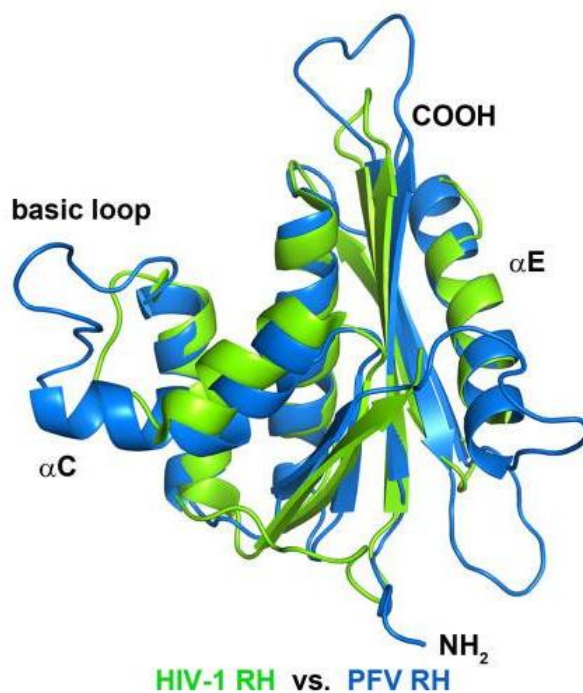


Figure 12 Superposition of PFV- RT and HIV-1 RT RNase H domains.PFV (blue) (PDB ID: 2LSN) and HIV-1 (green) (PDB ID: 1HYS) (Leo, Schweimer, et al. 2012)

3.2 Inhibition of PFV PR-RT enzyme activities by RHIs

To verify this hypothesis, we first tested the effect of known HIV-1 RT RHIs on both the PFV RT and HIV-1 RT RNase H and RDDP activities. In particular, we chose to test the DKA derivative RDS1643 (Tramontano et al. 2005), the 3-hydroxy-4-propionyl-3,4-dihydroquinolin-2(1H)-one (DHQ)

(Suchaud et al. 2012), the natural product β -Thujaplicinol (BTP) (Chung et al. 2011), all of which are chelating agents. Among the allosteric RHIs we chosen the VU urea derivative 2-amino-4,5,6,7-tetrahydrobenzo[b]thiophene-3-carboxamide (VU6) (Chung et al. 2010), and the hydrazonoindolin-2-one derivative (Z)-3-(2-(4-(3,4-dihydroxyphenyl)thiazol-2-yl)hydrazono)indolin-2-one (NSC657589) that was shown to inhibit both, HIV-1 RT-associated RDDP and RNase H activities, possibly by binding to a site located in a region between the polymerase catalytic aspartate triad (Asp110, Asp185, Asp186) and the NNRTI pocket, hence contiguous to the NNRTI pocket but different from it (Distinto et al. 2012)(fig. 13).

When these HIV-1 RHIs were tested on PFV PR-RT in biochemical assays using the methods previously described for HIV-1 RT-associated RNase H and polymerase functions (Distinto et al. 2012) and the reaction conditions previously optimized for PFV PR-RT (Hartl et al. 2010), we observed that all selected RHIs inhibited the PFV PR-RT (Fig. 13). In particular, the metal chelating catalytic site binder RHIs, RDS1643, DHQ and BTP inhibited the PFV PR-RT RNase H activity with IC_{50} values comparable to the ones obtained for HIV-1 RT, with the exception of DHQ, which was 2.5-fold less potent on PFV PR-RT than on HIV-1 RT. Unexpectedly, while RDS1643 and DHQ have both been reported to be selective for the HIV-1 RNase H function (Table 1), they also inhibited the PFV PR-RT associated RDDP activity with the same potency shown for the RNase H function (Figure 2). In contrast, BTP did not inhibit the RDDP activity of either enzyme (Table 1, Figure 13).

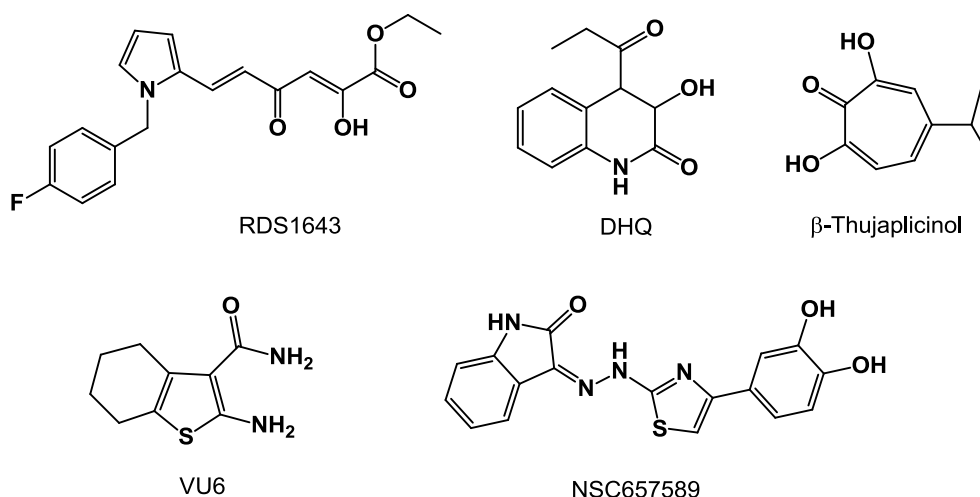


Figure 13. Chemical structures of HIV-1 RHIs.

Table 1. PFV PR-RT inhibition by HIV-1 RT RHIs

Compound	PFV PR-RT		HIV-1 RT	
	^a RNase H IC ₅₀ (μM)	^b RDDP IC ₅₀ (μM)	^a RNase H IC ₅₀ (μM)	^b RDDP IC ₅₀ (μM)
RDS1643	7.6 ± 2.0	5.2 ± 0.5	8.0 ± 1.5	> 100
DHQ	41 ± 8	41 ± 12	16 ± 4.0	> 100
BTP	0.3 ± 0.1	> 100	0.22 ± 0.03	> 100
VU6	6.5 ± 0.4	15.2 ± 1.8	18.7 ± 4.8	> 100
NSC657589	1.7 ± 0.3	2.0 ± 0.5	4.4 ± 1.3	7.4 ± 1.7
Efavirenz	> 20	> 20	> 20	0.015 ± 0.005

^aCompound concentration required to inhibit RT-associated RNase H activity by 50%.

^bCompound concentration required to reduce RT-associated RDDP activity by 50%.

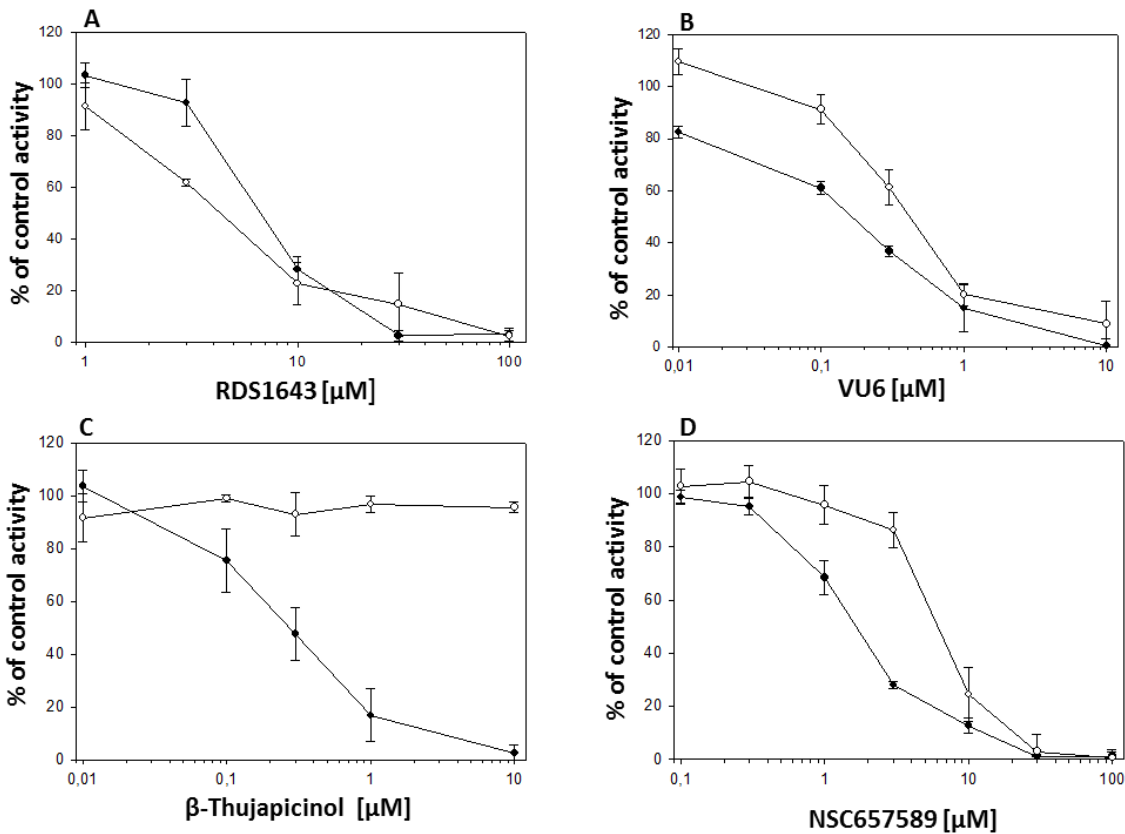


Figure 14. Dose dependent PFV PR-RT inhibition by HIV-1 RHIs. PFV PR-RT associated RNase H (●) and RDDP (○) activities were assayed at 37 °C as described for 1 hour (RNase H) and 30 minutes (RDDP) in the absence and in the presence of different concentration of RDS1643 (Panel A); β-Thujaplicinol (Panel B); VU6 (Panel C); NSC657589 (Panel D). Results represent averages and standard deviations of three independent experiments.

Next we assayed the VU derivative VU6, showing that it inhibited the PFV PR-RT associated RNase H function 2.9-fold more potently than the HIV-1 RT. Interestingly, VU6 was also able to inhibit the PFV PR-RT associated RDDP activity, while it was inactive on the HIV-1 RT RDDP (Table 1). Subsequently, we tested the hydrazonoindolin-2-one derivative NSC657589 that has been reported previously to inhibit both HIV-1 RT associated functions (Distinto et al. 2012). Our data reveal that this compound also inhibited both PFV PR-RT RNase H and RDDP functions. However, the IC₅₀ values observed for PFV PR-RT inhibition by NSC657589 were 2 to 3-fold lower than the ones observed for HIV-1 RT inhibition.

3.3 Effect of the NNRTI EFV on the PFV PR-RT enzyme activities

Given the ability to inhibit the PFV RT-associated RDDP activity shown by the tested RHIs, we asked whether the NNRTI EFV was also able to inhibit the PFV PR-RT functions. It is worth to note that it is known that the NNRTI binding pocket is present only in HIV-1 RT but not in the highly homologous HIV-2 RT (30) and that the HIV-1 RT tyrosines, Y181 and Y188, close to the active site motif Y¹⁸³MDD (...VIY¹⁸¹QYMDDLY¹⁸⁸V...) as well as the mutation K103N are involved in EFV resistance (30). Sequence comparisons show that in PFV RT only the tyrosine corresponding to Y188 is present (...NVQVYVDDIY³¹⁷L...), however, due to the low sequence identity (ca. 26 %) it is difficult to judge whether the lysine corresponding to K103 is present in PFV RT. Results showed that EFV was not able to inhibit either PFV PR-RT functions (Table 1) confirming that the NNRTI binding pocket is not present in PFV PR-RT and suggest that the hydrazonoindolin-2-one derivative NSC657589 binds to a site which is different from the NNRTI binding pocket.

3.4 NMR titration experiments with PFV RNase H.

To learn more about RNase H inhibitor binding, the binding of several of the inhibitors, namely RDS1643, NSC657589 and VU6, to the free PFV RNase H domain was tested in NMR titration experiments. An NMR spectrum correlating the resonance frequencies of chemical shifts of amide protons directly bonded to ¹⁵N labeled nitrogen atoms (2D [¹H-¹⁵N] HSQC, heteronuclear single quantum correlation) allows the individual detection of peptide backbone signals. Each signal in the spectrum represents a single amino acid of the peptide chain and can be assigned to an

individual residue. Changes in the chemical environment of a magnetically active atom, e.g. binding of an inhibitor or ligand, lead to changes of chemical shifts of the signal. Thus, HSQC spectra can be used to investigate inhibitor binding.

The structure of the PFV RNase H has previously been solved by NMR spectroscopy (PDB ID: 2LSN) (Leo, Schweimer, et al. 2012). Thus, NMR assignment and structural information can be used for inhibitor titration experiments. However, measurements using the RNase H inhibitors and PFV RNase H were partially hampered by the low solubility of the inhibitors in aqueous solutions and the high inhibitor concentrations needed in NMR spectroscopy since concentrations of ^{15}N labeled enzyme of around 50 – 100 μM are necessary to obtain analyzable signals. In fact, addition of NSC657589 and VU6 to ^{15}N labeled PFV RNase H resulted in partial precipitation of the inhibitors. Final concentrations of about 2 mM NSC657589 (ca. 32-fold excess) or 12 mM VU6 (ca. 194-fold excess) were added to ^{15}N labeled PFV RNase H. However, due to partial precipitation of inhibitors and possibly enzyme even at lower inhibitor concentrations during the measurements, the spectra could not be evaluated (data not shown). In contrast, addition of the inhibitor RDS1643 (49-fold excess) gave rise to relevant chemical shift changes of certain residues in the HSQC spectrum (Fig. 15, 16). A chemical shift change of 0.02 ppm or greater was considered meaningful (Fig. 15, Fig16A).

Significant chemical shift changes upon inhibitor addition could be observed with residues T598, A614, G617, T641, I647, A648, T668, Y672, A674, W703, K722, H732 and T733. The overlays of the HSQC spectra of residues T641 and W703 recorded at various inhibitor concentrations are illustrated in Figure 15B. The data confirm that RDS1643 binds to the RNase H domain and suggest that effects on polymerization are indirect. However, we cannot exclude a second binding site in the polymerase domain.

In Figure 17A the residues exhibiting significant chemical shift changes upon inhibitor addition are highlighted in the three-dimensional structure of PFV RNase H. The ribbon diagram and the surface representation in Figure 17B show that amongst the residues with significant chemical shift changes, T598, A614, G617, A648, T668 and A674 are not surface exposed, while residues, T641, I647, Y672 and W703 are spatially close together and oriented towards the protein surface.

Residues T598, I647, A648 and T668 are adjacent to the active site residues D599, E646, and D669 respectively. W703 is in the alpha helix D, which follows the basic loop that has been shown to be involved in nucleic acid substrate binding (Leo, Schweimer, et al. 2012). T641 is located at the beginning of alpha helix A, which also harbors the active site residue E646.

These data indicate that the inhibitor binding pocket is located next to the active site and could be formed by the surface exposed residues T641, I647, Y672 and W703. Residues K722, H732 and T733 located at the beginning of alpha helix E and the adjacent N-terminal loop are also surface exposed. However, they exhibited only small chemical shift changes (< 0.03 ppm), which could be due to minor direct or indirect conformational changes induced by the binding of the inhibitor.

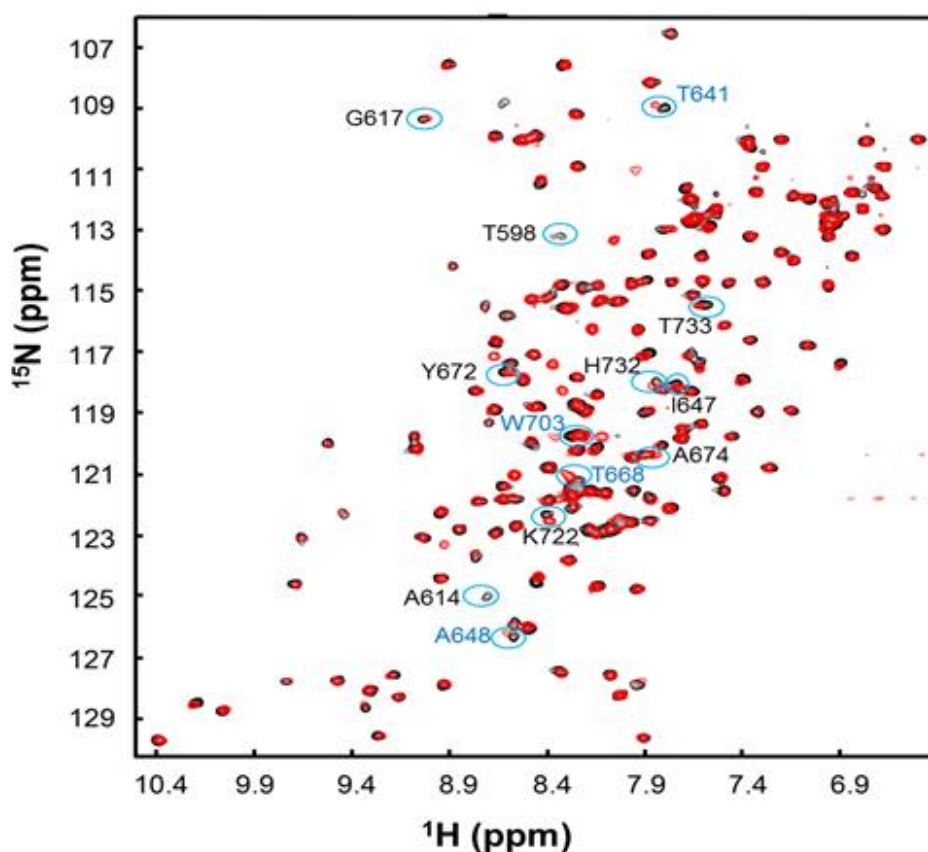


Figure 15: Interaction of PFV RNase H with inhibitor RDS1643. Overlay of [$^1\text{H}^{15}\text{N}$] HSQC spectra of 80 μM ^{15}N labeled PFV RNase H in the absence (black) and presence of 3.9 mM RDS1643 (red). Resonances with significant changes of chemical shifts are labeled.

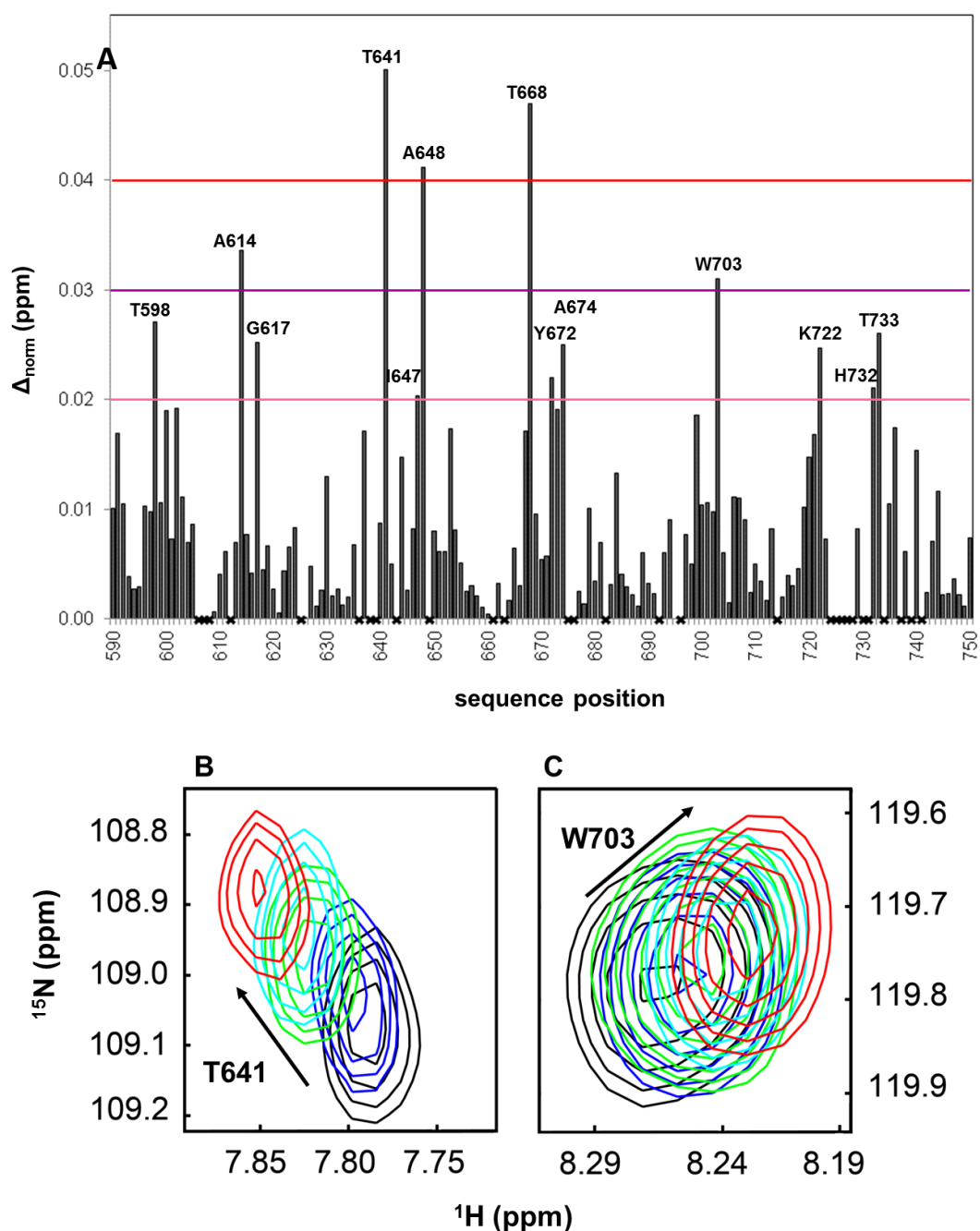


Figure 16. Backbone chemical-shift changes upon inhibitor binding. (A) Changes of chemical shifts of PFV RNase H after addition of 3.9 mM RDS1643 as a function of the primary sequence. Chemical-shift changes larger than 0.02 ppm, indicated by a horizontal red line, were considered significant. Residues that were not assigned are marked by an x on the X. axis (B). [^1H ^{15}N] HSQC overlays of the T641 (left panel) and W703 (right panel) amide cross peaks at each inhibitor titration step shown in different colors (black: 0 mM; blue: 1.0 mM; green: 2.0 mM; cyan: 3.0 mM; red: 3.9 mM;RDS1643)

Most of the other residues shown in Figure 16A are located in the interior of the protein (Figure 17B) and therefore do not come into consideration for direct inhibitor contact. Rather, binding of the inhibitor might lead to indirect changes in the local structure of the protein, by changing side chain orientations.

3.5 Molecular modeling of RDS1643 on the PFV RNase H domain.

To show how the nucleic acid substrate is bound in relation to the putative inhibitor binding pocket, we modeled the RNA/DNA substrate of the human RNase H/RNA/DNA complex (PDB ID: 2QK9) onto the PFV RNase H (Leo, Schweimer, et al. 2012). For clarity, only the nucleic acid without human RNase H is presented. It has been shown previously by UV/Vis spectroscopy and isothermal titration calorimetry that RDS1643 and other DKAs chelate Mg^{2+} or Mn^{2+} (Tramontano et al. 2005; Shaw-Reid et al. 2005) and thus may interact with the metal ions in the active site of RNase H. This is consistent with our observation of chemical shift changes in the NMR titration experiment close or next to the active site residues. Overall, these data suggest that RDS1643 can chelate the Mg^{2+} into the RNase H active site and that it can make additional interactions with residues next to it to stabilize its binding. To further verify this mode of interaction we performed docking calculations with RDS1643 and PFV RNase H using the program AutoDock Vina (Trott & Olson 2010). Based on our NMR data we limited the potential binding site to the active site and the area including residues T641, I647, Y672 and W703.

Figure 17D depicts a possible binding mode of the inhibitor that is in good agreement with our results. The keto-groups of RDS1643 reach into the RNase H active site and thus may be able to chelate the metal ions while the hydrophobic part of the molecule is close to Y672 and W703.

3.6 Structure comparison between the HIV-1 and PFV RNase H domains.

To elucidate the binding of RDS1643 to HIV-1 RNase H, a secondary structure alignment of HIV-1 RNase H and PFV RNase H was performed (Figure 18A). In HIV-1 RNase H residues T473, L479, Y501 and V518 correspond to T641, I647, Y672 and W703, in the inhibitor binding pocket of PFV RNase H. The structural overlay of PFV RNase H with HIV-1 RNase H presented in Figure 18B implies that in HIV-1 RNase H binding of the inhibitor could take place in a similar way.

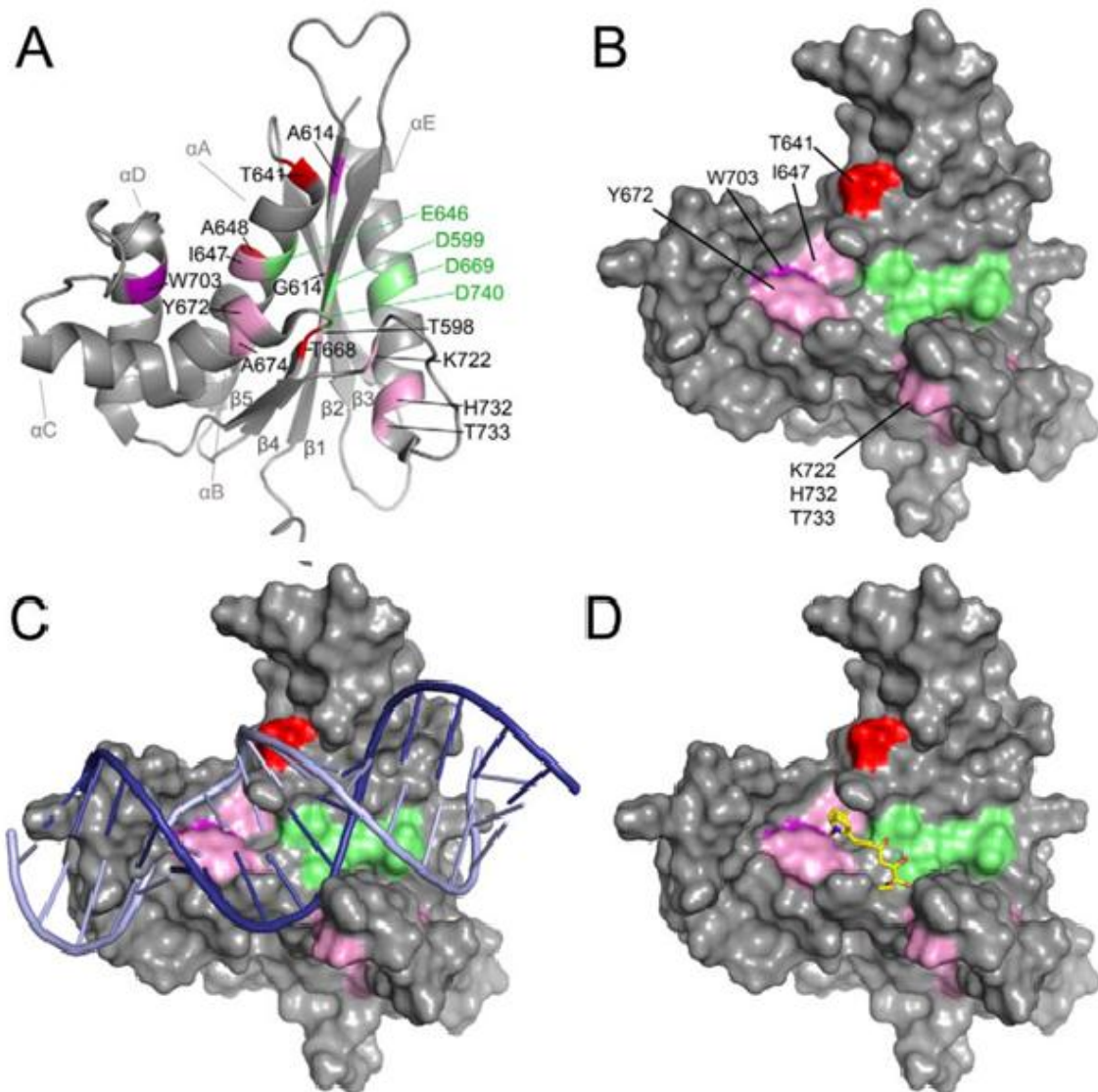


Figure 17. Identification of the putative inhibitor binding site on the structure of PFV RNase H. The normalized chemical shift changes (weighted geometric average of $^1\text{H}^N$ and ^{15}N chemical shift changes) are shown in the PFV RNase H. Amino acids showing significant chemical shift changes at an RDS1643 concentration of 3.9 mM are highlighted. Changes equivalent or larger than 0.02 ppm are illustrated in pink, changes larger than 0.03 ppm in violet and changes larger than 0.04 ppm are shown in red. The active site residues are represented in green. (A) Ribbon presentation of PFV RNase H (PDB: 2LSN). (B) Surface presentation of PFV RNase H highlighting the surface exposed residues with significant chemical shift changes. (C) Surface presentation of PFV RNase H with an RNA/DNA hybrid. Based on the structure of the human RNase H/substrate complex (PDB: 2QK9) a structural alignment of the PFV and human RNase H was performed to model the RNA/DNA substrate of the human RNase H onto PFV RNase H (Rmsd: 2.35 Å) (Leo, Schweimer, et al. 2012). The RNA strand is shown in dark blue, the DNA strand in light blue. (D) Inhibitor modeling. RDS 1643 was modeled onto the structure of the PFV RNase H using the modeling program AutoDock Vina (Trott & Olson 2010).

However, we have also shown that RDS1643 binding to the RNase H has different effects on the RDDP activity of the two enzymes (table 1). This is likely due to additional structural differences, i.e. heterodimer vs. monomer.

3.7 Discussion

To attempt to better understand the mode of action of a series of HIV-1 RT RHIs, we used the PFV RT as a model to gain important insights. This was possible because the structural features of HIV-1 and PFV RNase H domain are in good agreement (Fig.12). We demonstrated that, surprisingly, RDS1643 and DHQ, HIV-1 RNase H active site inhibitors, are active on both PFV PR-RT DNA polymerase and RNase H functions, suggesting on the one hand similarity in the RNase H domains of the two enzymes, on the other hand differences in enzyme flexibility/dynamics. This can be explained by three different hypotheses. Firstly RDS1643 and DHQ may be able to chelate the Mg^{2+} ions in the PFV PR-RT DP site as well as in the RNase H active site, while BTP is not able to act on the DP site. However, in all the retroviral RTs crystallized so far, the geometry of the two sites is quite different and this hypothesis is not very likely. A second possibility is therefore more likely in which binding of RDS1643 and DHQ at the PFV RNase H active site reduces the PFV PR-RT flexibility and, through a long-range effect, it can also affect its RDDP activity. In fact, it has been shown that HIV-1 RT possesses a peculiar ability to flip orientations on the nucleic acid template and that it has high flexibility (Liu et al. 2008) and PFV could show a similar flexibility. It is likely, given the small nature of the the BTP, that the interactions with the amino acid residues in the PFV PR-RT RNase H site do not involve the same residues that instead interact with RDS1643 and DHQ, so that the long-range effect do not take place. The third possibility is that the compounds that inhibit both functions have two different binding sites on the PFV RT.

Therefore, further studies on PFV PR-RT may elucidate whether the inhibition of its DNA polymerase activity by RNase H active site inhibitors is due to long-range effects of compounds binding to the RNase H pocket, which may be stronger in a monomeric protein such as PFV PR-RT, or whether it is due to an intrinsic lower protein flexibility that, therefore, is more easily inhibited by a drug binding anywhere on the enzyme.

Interestingly, the allosteric RHIs NSC657589 and VU6 also inhibited both FV-PR RT functions. NSC657589 has been proposed to inhibit HIV-1 RT by binding a site close to, but distinct from, the

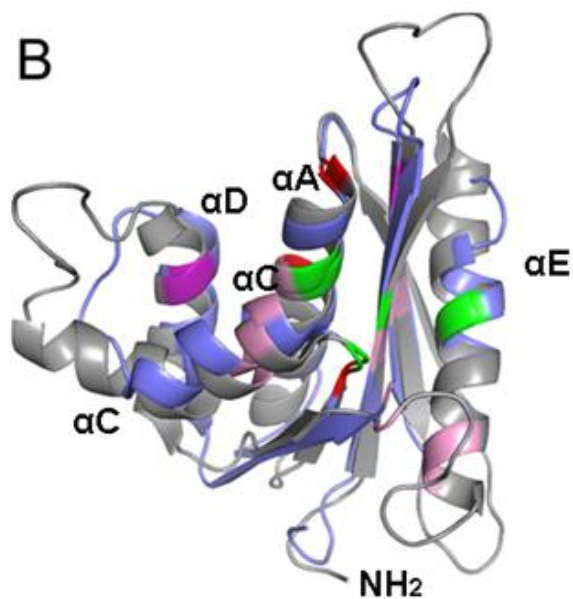
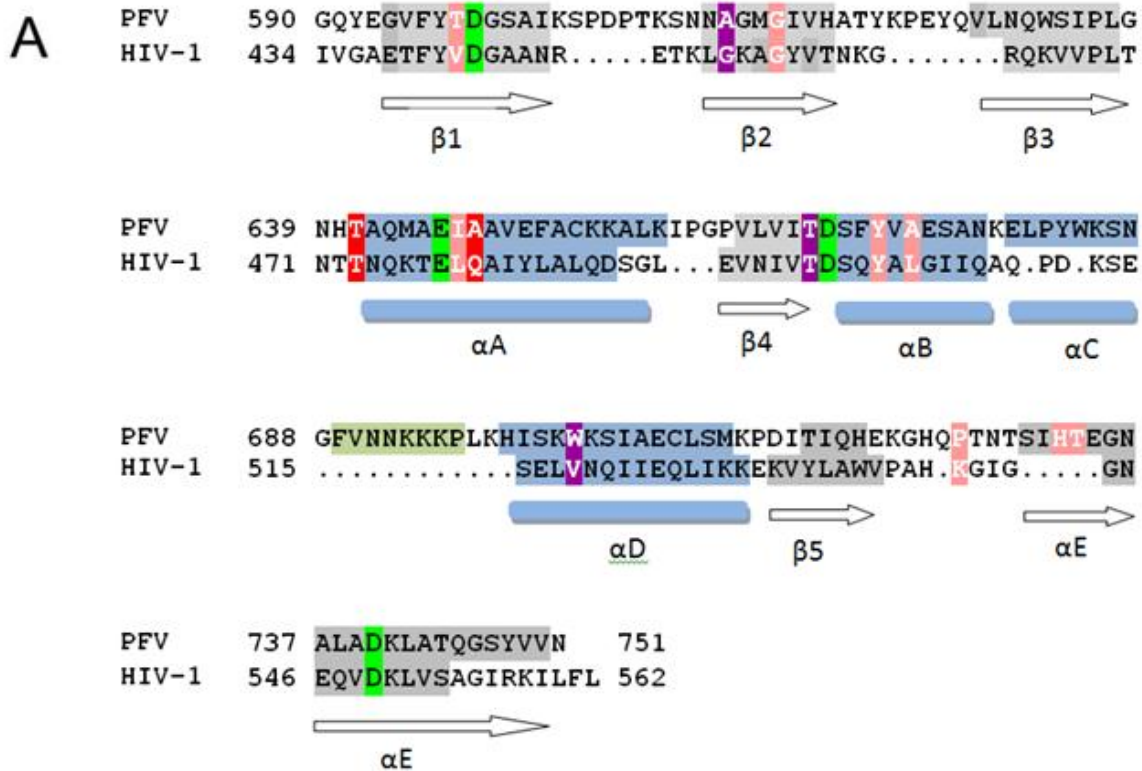


Figure 18. Identification of the putative inhibitor binding pocket in HIV-1 RNase H. (A) Sequence and secondary structure alignment of PFV and HIV-1 RNase to identify the corresponding residues HIV-1 RNase H (PDB ID: 1HRH). The active site residues are highlighted in green. The four residues in HIV-1 RNase H that are equivalent to the ones in PFV RNase H exhibiting chemical shift changes at 3.9 mM RDS1643 are labeled equivalent to the colour coding in Figure 4A. (B) Structural overlay of the RNases H from PFV (PDB ID: 2LSN) (gray) and HIV-1 (PDB ID: 1HRH). (blue). Colour coding of relevant residues as in Figure 17A.

NNRTI binding pocket (Distinto et al. 2012), the reported results may suggest either that this pocket is also present in the PFV PR-RT or that the NSC657589 activity on HIV-1 RT is due to the binding to a different site/s, possibly close to the RNase H binding pocket. This hypothesis is further corroborated by the observation that EFV was not able to inhibit either PFV PR-RT functions, as reported for other retroviruses with monomeric RTs (Figueiredo et al. 2006). This confirms that a pocket equivalent to the one of NNRTIs is not present in PFV PR-RT, and that, therefore, NSC657589 acts on RDDP function with a mechanism different from NNRTIs.

VU6 derivatives also inhibited both PFV PR-RT functions. Vinillogous ureas have been proposed to inhibit HIV-1 RNase H allosterically, by binding a pocket located at the junction between the p51 subunit thumb subdomain and the p66 RNase H domain and, in particular, to interact with an α -helix adjacent to the RNase H domain in the p51 subunit. It is possible that even though HIV-1 RT is a heterodimer and PFV PR-RT is a monomer, this pocket is present in both proteins. Therefore, the VU6 inhibition of both PFV PR-RT RNase H and RDDP functions seems to reinforce the hypothesis that the binding of RHIs to PFV PR-RT may decrease its flexibility leading to a complete loss of its catalytic activities.

NMR titration experiments with FV RNase H and the inhibitor RDS1643 identified the putative binding site in the RNase H, located next to the PFV RNase H active site and could be formed by the surface exposed residues T641, I647, Y672 and W703. Sequence and structure alignments with HIV-1 RNase H were used to reveal the corresponding putative binding site in HIV-1 RNase H, suggesting that in HIV-1 RT the compound may interact with the corresponding residues T473, L479, Y501 and V518, some of which are highly conserved since part of the RNase H primer grip motif (Rausch et al. 2002). This observation makes appealing the further investigation on DKA binding mode into HIV-1 RNase H active site, by docking of RDS1643 in the HIV-1 RT RNase H domain and site directed mutagenesis of the residues identified as critical for the inhibitor binding.

Chapter 4.

A combined cell-based and site-directed mutagenesis approach defines highly conserved residues involved in the selective inhibition of the HIV-1 RNase H function by DKA derivatives

4.1 Introduction

Diketo acid (DKA) derivatives are among the first compounds reported to chelate the Mg^{2+} cofactors in the active site of influenza virus endonuclease (Tomassini et al. 1994), HIV-1 IN (Wai et al. 2000)ⁱ and HIV-1 RNase H (Sluis-Cremer et al. 2004; Hazuda et al. 2004; Enzo Tramontano et al. 2005). In particular, the ester DKA derivative RDS1643 has been shown to inhibit HIV-1 RNase H in biochemical assays and to inhibit viral replication in cell culture (Tramontano et al. 2005). Recently, new DKA derivatives active against both HIV-1 IN and RNase H activities have been reported (Costi et al. 2013).

NMR studies reported in chapter 3 gave important insights into the possible interactions between RDS1643 and HIV-1 RNase H domain. With the aim of clarifying whether the catalytic region of the RNase H can offer additional anchor point that could be targeted by drugs, we explored the DKAs molecular determinants required for the interaction with the HIV-1 RT RNase H domain and that are responsible for the specific RNase H inhibition while not influencing the HIV-1 IN activities. Starting from the DKA prototype RDS1643, we synthesized 6 couples of ester/acid derivatives by introducing different substituents either in the benzyl moiety or in the pyrrole ring. Biochemical assays revealed that such derivatives inhibit both RNase H and IN activities in the low micromolar range. Out of these 12 compounds, 8 also inhibited viral replication in cell culture. Subsequent molecular modeling studies suggested interactions between DKAs and a number of residues lining the enzyme active site. Guided by these studies we therefore mutated these residues into Ala, and biochemical assays on single mutant HIV-1 RTs allowed us to probe their involvement in DKAs binding. Cell based assays were then used to characterize the mechanism of action for a selected couple of ester/acid derivatives confirming the inhibition pattern observed in enzyme assays. In

summary, our data establish a well-defined interaction pattern for DKA derivatives with highly conserved amino acid residues in the RNase H active site. Furthermore we show that derivative RDS1759 effectively inhibits HIV reverse transcription in cells, laying the foundations for further development of RHIs.

4.2 Inhibition of HIV-1 RT-associated DNA polymerase-independent RNase H activity by DKAs.

To investigate the structural features of DKAs required for binding to the RNase H active site, starting from the DKA prototype RDS1643 (Tramontano et al. 2005) a new series of DKAs derivatives were designed and synthesized by introducing different substituents either in the benzyl moiety or in the pyrrole ring (Fig. 19)

These modifications were realized to specifically explore the effects on the RNase H inhibitory activity of i) halogens or alkylic substituents at different positions on the benzyl ring (RDS1643-1644; RDS 1759-1760; RDS1822-1823; RDS2291-2292), ii) the shift of the diketoester chain from position 3 to position 2 on the pyrrole ring (RDS2400-2401; RDS1711-1712), and iii) the insertion of a further phenyl ring in position 4 of the pyrrole ring (RDS1711-1712). In addition, we synthesized each derivative both in their ester and acidic forms to evaluate whether the different nature of the DKA branch could modulate the activity profile of our compounds.

The six ester/acid couples were tested for their ability to inhibit the HIV-1 DNA-polymerase independent RNase H function and the IN activity in biochemical assays and viral replication in cell-based assays (Table 2). All the newly synthesized DKAs inhibited the RNase H activity, with ester derivatives generally being more potent than the acidic counterparts. This effect was more evident for derivatives RDS1759, RDS2291 and RDS2400 that showed IC_{50} values for RNase H activity of 7.3, 8.2 and 11.2 μ M respectively, whilst completely inactive as IN inhibitors. Conversely, in the case of HIV-1 IN, all the acid derivatives were more potent than their ester counterparts, as reported in a previous work (Costi et al. 2013). The different activity profile of ester/acid DKAs on HIV-1 RNase H and IN functions may arise from the different electrostatic properties of the active site of the two enzymes. In particular, in RNase H

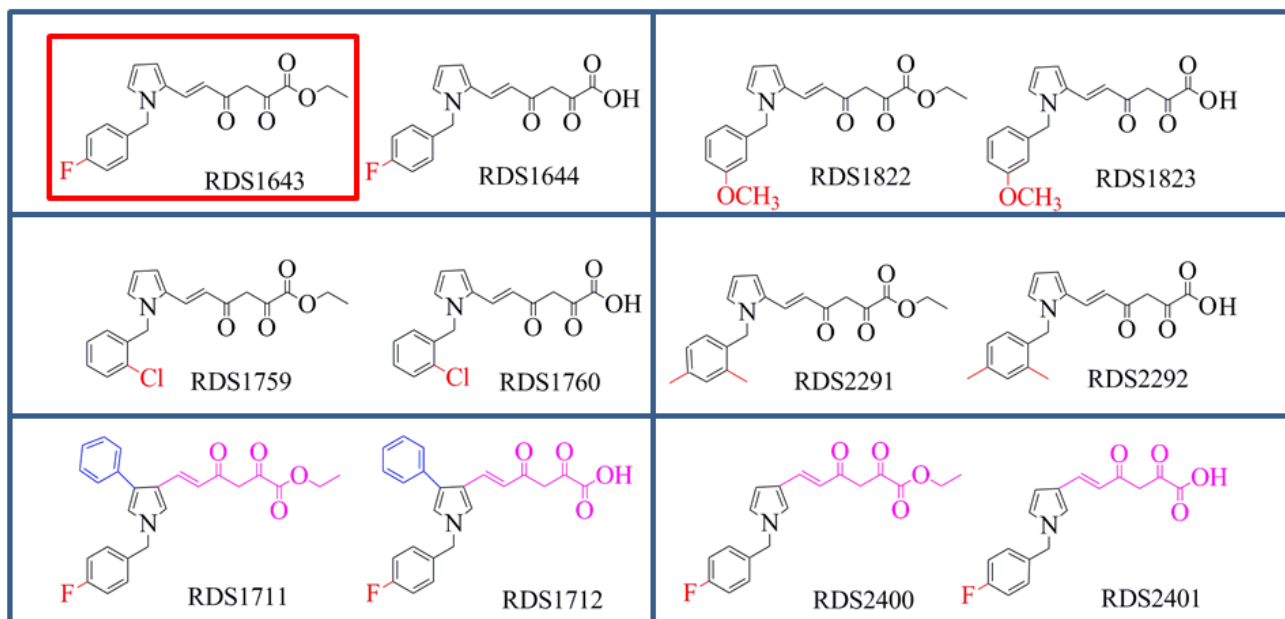


Figure 19. Chemical structures of DKA derivatives

The prototype RDS1643 is depicted in the red square. Substituents in the benzyl moiety are shown in red, additional phenyl ring is shown in blue, displaced diketoester chain is shown in purple.

four catalytic acid residues (D443, E478, D498 and D549) completely neutralize the four positive charges of the two active site Mg^{2+} ions. On the other hand, the IN active site is positively charged since only three acidic residues (D64, D116, D152) counterbalance the four positive charges of the two catalytic Mg^{2+} cations. In this perspective, negatively charged acidic compounds may bind more favorably to HIV-1 IN than to the RNase H active site. To test this hypothesis, it was verified whether both ester and acid DKAs effectively chelate the Mg^{2+} ions in the RNase H active site. To this aim, the DKAs UV spectra were recorded in absence and presence of magnesium ions. The results showed that the maximum absorbance of each compound shifted in the presence of 6 mM $MgCl_2$, confirming that both ester and acid DKAs are able to chelate Mg^{2+} (Fig.20-21). Finally, when tested on HIV-1 replication, four ester/acid couples were able to selectively inhibit viral replication, while couples RDS2400-2401 and RDS2291-2292 were inactive (Table 2).

4.3 Molecular docking

To elucidate the binding mode of our ester/acid DKAs at into the RNase H active site at a molecular level, molecular docking studies were performed. For docking the crystal structure of

the full-length HIV-1 RT in complex with a naphthyridinone inhibitor bound into the RNase H active site (PDB ID:3LP1) was selected. The missing residue R557, which is part of the RNase H active site, was modeled using the coordinates of the PDB ID:3K2P crystal structure of the HIV-1 RT isolated RNase H domain with the inhibitor β -thujaplicinol bound at the active site (see Methods for details). Dockings of RDS1643 and RDS1644 show that both ester and acid DKAs binds at the RNase H active site coordinating the two catalytic Mg^{2+} ions. However, docking predicts that esters and acids should adopt slightly different binding orientation because of the steric hindrance of the ethyl substituent in the ester derivatives (Fig. 22A-22B). Besides the coordination of the metal ions, both RDS1643 and RDS1644 were hypothesized to interact with a number of RNase H active site residues, some of them located in the primer grip region, with important structural and functional roles (Rausch et al. 2002). In particular, the diketo-ester branch of RDS1643 makes H-bonds with the N474 side chain and establishes lipophilic interactions with the A445 and I556 residues through its ethyl substituent (Fig. 22A), while the DKA moiety of RDS1644 forms a salt-bridges with the R557 side chain (Fig. 22B). Additionally, the benzyl ring of both ester and acidic

Table 2. Biological effects of DKA derivatives on the HIV-1 RT-associated RNase H and processing activities and HIV-1 replication

Compound	RNase H ^a IC ₅₀ (μM)	IN ^b IC ₅₀ (μM)	HIV-1 ^c EC ₅₀ (μM)	MT4 ^d CC ₅₀ (μM)	^e SI
RDS1643	8.6 ± 1.3	20.7 ± 3,6	15.5	>50	>3.22
RDS1644	16.1 ± 2.3	0.16 ± 0.025	0.29	>50	>172
RDS1711	8.0 ± 0.2	21.5 ± 12.0	4.3	26.9	6.3
RDS1712	7.7 ± 0.5	1.55 ± 0.15	17.2	>50	>2.9
RDS1759	7.3 ± 0.03	>100	2.10	>50	>23.8
RDS1760	19.4 ± 0.8	0.59 ± 0.77	15.4	>50	>3,2
RDS1822	6.3 ± 1.8	42.7 ± 28	3.4	14.1	4.14
RDS1823	87 ± 5.1	0.59 ± 0.19	3.2	>50	>15.6
RDS2291	8.2 ± 1.2	>100	>15.4	15.4	=
RDS2292	19.3 ± 2.6	26.21	>25.5	25.5	=
RDS2400	11.2 ± 1.1	>100	>50	>50	=
RDS2401	28.4 ± 5.4	27.8	>50	>50	=

^aCompound concentration (± standard deviation) required to inhibit HIV-1 RT-associated RNase H activity by 50%.

^bCompound concentration (± standard deviation) required to inhibit HIV-1 IN activity by 50%.

^cCompound concentration required to decrease viral replication in MT-4 cells by 50%.

^dCompound concentration required to reduce infected MT-4 cells viability by 50%.

^eSelectivity index (CC₅₀/EC₅₀ ratio).

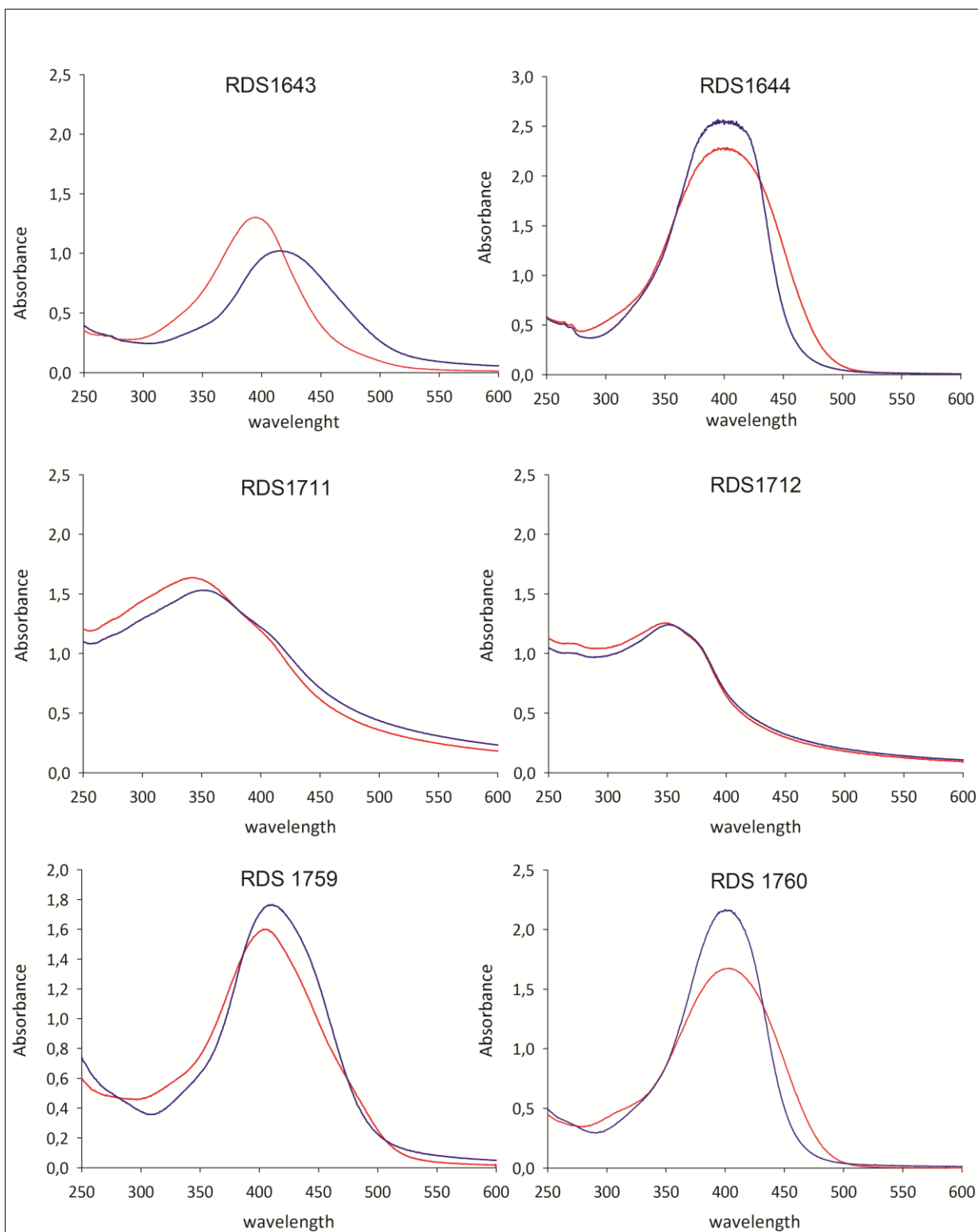


Figure 20. Effect of MgCl₂ on the spectrum of absorbance of dual RTIs.

Chelation of Mg²⁺ by UV-vis spectrum was measured in presence of 100 μM concentration of compound alone (red line) or in the presence of 6mM MgCl₂ (blue line).

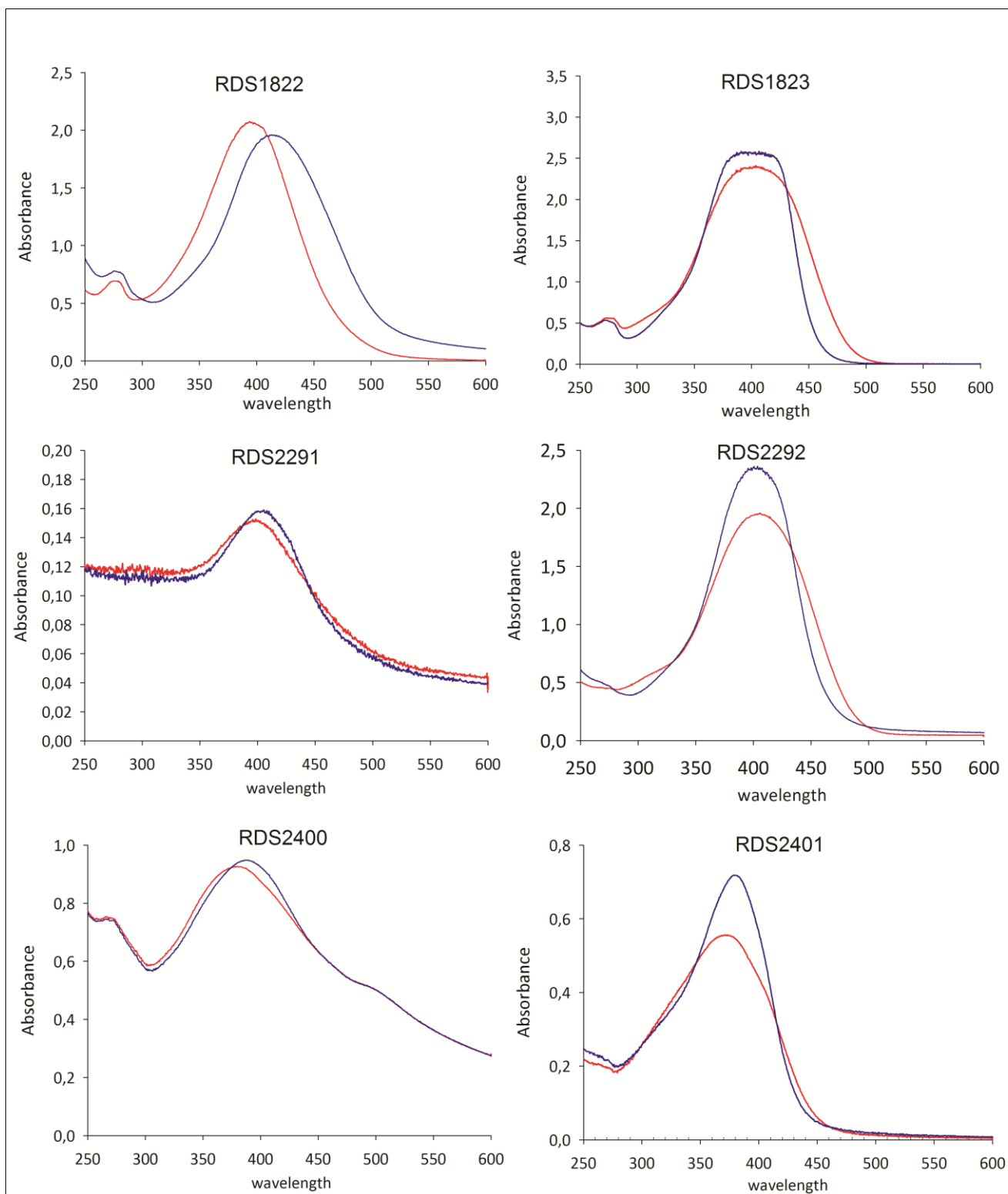


Figure 21. Effect of MgCl₂ on the spectrum of absorbance of dual RTIs.

Chelation of Mg²⁺ by UV-vis spectrum was measured in presence of 100 μM concentration of compound alone (red line) or in the presence of 6mM MgCl₂ (blue line).

derivatives can form parallel-displaced interactions with the Y501 side chain, while the pyrrole ring of RDS1643 can establish further lipophilic interactions with the C α and C β carbons of the Q475 residue. Finally, docking of the ester derivative RDS1711 (Fig. 22C) indicates that this compound is able to form an additional cation- π interaction with the R448 guanidinium group through its benzyl substituent, while the phenyl at position 4 on the pyrrole ring interacts with the Y501 side chain (Fig. 22C). Conversely, the corresponding acid RDS1712 is not predicted to interact with the R448 side chain, whilst its 4-phenyl substituent interacting with the Y501 side chain and its N-benzyl group contacting residue W535 (Fig. 22D).

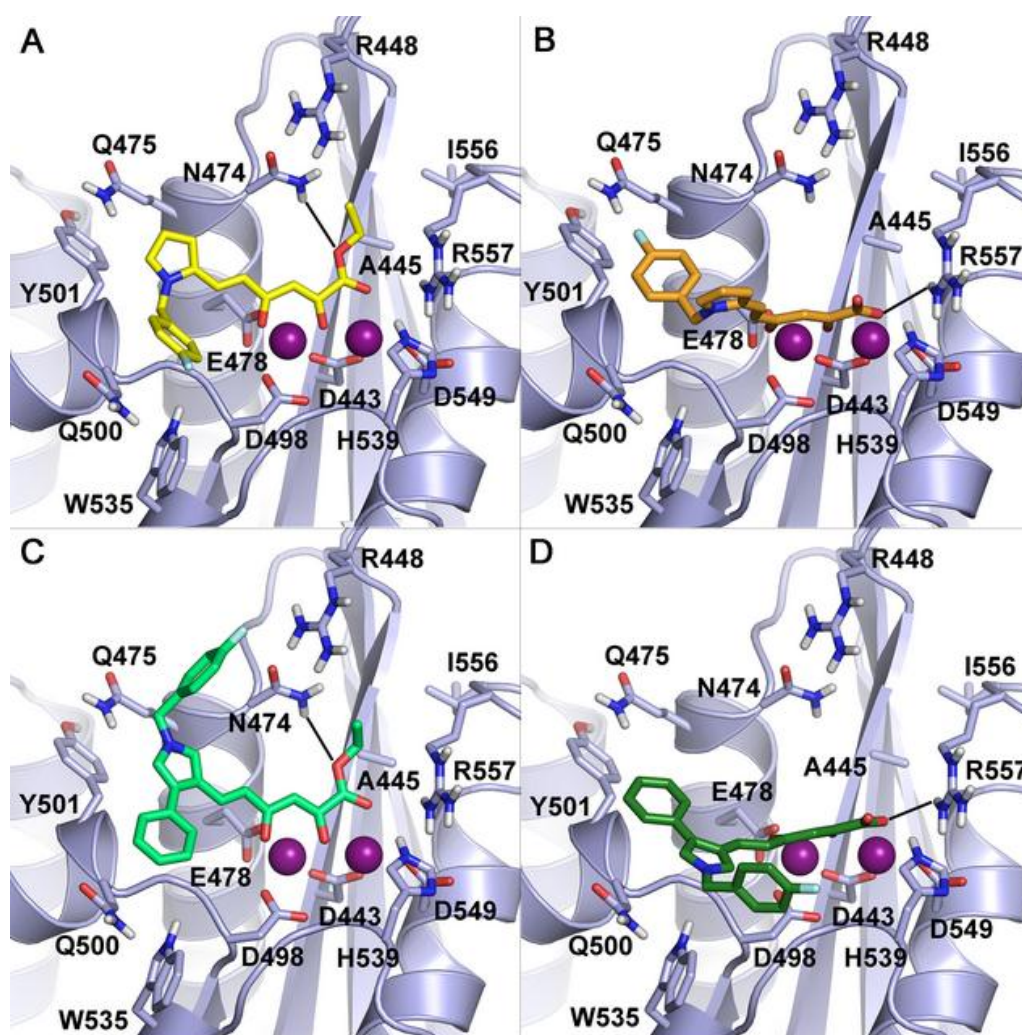


Figure 22. Molecular modeling of the binding modes of DKA derivatives into the HIV-1 RNase H active site. Panel A, RDS1643 (yellow); Panel B, RDS1644 (orange); Panel C, RDS1711 (light green); Panel D, RDS1712 (dark green). The receptor is shown as purple ribbons, amino acids involved in ligand binding are highlighted as sticks. The active site ions Mg²⁺ ions are represented as magenta spheres.

4.4 Catalytic efficiency of mutant HIV-1 RTs

Based on the interaction patterns predicted by docking calculations for the DKA derivatives, mutation into Ala of residues R448, N474, Q475, Y501, R557 within the p66 subunit of HIV-1 RT were selectively performed. However, it is important to note that N474, Q475 and Y501 residues are highly conserved, playing crucial structural and functional roles as part of the RNase H primer grip. In fact, mutations of the latter residues have been reported to drastically reduce the HIV-1 replication rate (Julias et al. 2002) and, more generally, mutations within the RNase H primer grip motif can strongly affect RNase H enzymatic activity (Rausch et al. 2002). Hence, to verify whether the selected mutant RTs were suitable for quantitative assays, a kinetic analysis on both their RNase H and RDDP catalytic efficiencies was performed (Table 3, Fig. 23). Consistent with previous observations (Rausch et al. 2002) all the RNase H primer grip mutants showed a drastically reduced, but still measurable, catalytic efficiency for their RNase H activity (Table 3). Interestingly, results showed that, with respect to wt RT, both k_{cat} and K_M values of all mutant RTs decreased, with the former being more affected than the latter, showing that mutations affect more the efficiency of the enzyme machinery in the maximum of velocity respect to substrate amount than the affinity of RT for the substrate itself. In particular, compared to wt RT, the catalytic efficiency of

Table 3. Comparison of HIV-1 wt and mutant RTs DNA polymerase independent RNase H and RDDP activities kinetics

	RNase H			RDDP		
	k_{cat} (min^{-1})	K_M (nM)	k_{cat}/K_M	k_{cat} (min^{-1})	K_M (nM)	k_{cat}/K_M
Wt	112.7 ± 1.4	126.7 ± 5.0	0.89	23.11 ± 0.88	0.94 ± 0.03	24.6
R557A	24.09 ± 2.9	40.9 ± 1.0	0.60	19.24 ± 1.48	0.94 ± 0.10	20.4
R448A	43.9 ± 9.3	85 ± 22	0.52	14.56 ± 1.35	0.90 ± 0.01	16.1
Q475A	10.7 ± 1.9	100 ± 11	0.11	8.44 ± 0.51	1.04 ± 0.18	8.1
N474A	2.62 ± 0.55	30.0 ± 0.04	0.08	23.47 ± 0.88	$1.19 \pm .03$	19.7
Y501A	0.25 ± 0.07	29.4 ± 9.0	0.008	20.21 ± 0.3	1.34 ± 0.03	15.0

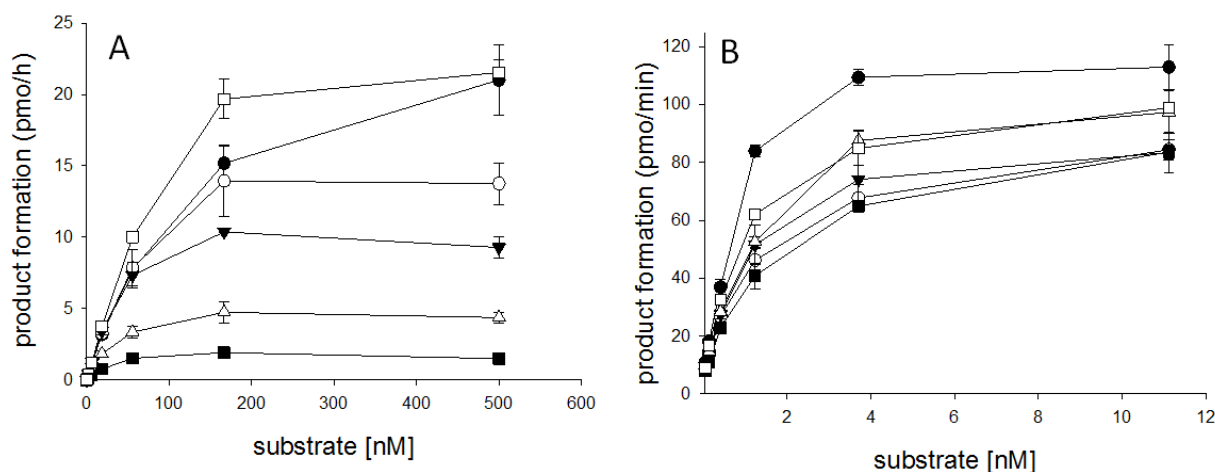


Figure 23. Comparison of the kinetics of polymerase-independent RNase H and RDDP activities of HIV-1 RT mutants. Panel A. Polymerase-independent RNase H cleavage for all HIV-1 RT mutants was measured in 100 μ L reactions containing increasing amount of RNA/DNA hybrid substrate and fix amount of enzymes. Panel B. RDDP activity was measured in 25 μ L volume containing 100 μ M poly(A)-oligo(dT), increasing concentrations of dTTP and fix amount of enzymes. The kinetic analysis (values reported in table 3) was performed according to Lineaweaver–Burke plot of the both RNase H and RDDP activities. (\square) wt RT , (\circ) R448A RT, (Δ) N474A RT, (\bullet) Q475A RT, (\blacksquare) Y501A RT and (\blacktriangledown) R557A RT.

N474A and Q475A RTs showed an almost 10-fold ratio decrease and the Y501A RT showed a 100-fold reduction. In contrast, the k_{cat}/K_M ratio of the R448A and R557A mutants RTs showed no reduction. Finally, none of the mutant RTs showed significant changes in the RT-associated RDDP function compared to wt RT, with sole exception of Q475A RT that demonstrated a 3-fold decrease in the RDDP catalytic efficiency.

4.5 Evaluation of the effects of DKA derivatives on mutant RTs

In order to verify experimentally the interactions individuated by computational studies between DKA derivatives and amino acid residues, all studied DKA derivatives were evaluated for their effects on the RNase H function of all mutant RTs, using the RHI BTP as positive control (Table 4). Results show that the inhibitory potency towards RNase H was drastically reduced for all the DKAs when tested on N474A RT, confirming that the N474 amino acid residue is crucial for DKA binding. In the case of ester derivatives, the loss of the H-bond with the N474 side chain might explain the lower inhibitory activity of these compounds against the N474A mutant RT. However, the increase in the IC_{50} observed for the acidic ligands suggests that the additional functional/structural role

for N474, as part of the RNase H primer grip motif, at the RNase H active site where its mutation to Ala impairs the geometry of the site.

When tested on R557A RT only a moderate effect on the inhibitory potency was observed. Interestingly, this effect was higher for acidic derivatives than for their ester counterparts. Indeed, as predicted by docking calculations, acidic derivatives are able to make a salt-bridge with the R557 side chain in the WT RT, which cannot be established in the R557A mutant RT.

A different behavior was observed when DKAs were assayed against Q475A RT. In fact, in this case, changes in the RNase H inhibition rate by ester compounds were generally higher to those measured for acidic derivatives. In particular, esters RDS1643, RDS1822, RDS2400, RDS1759 and

Table 4. Inhibition of the HIV-1 RT-associated RNase H activity of selectively mutated p66/p51 HIV-1 RT heterodimers by DKAs

	RNase H ^a IC ₅₀ (μM)					
	WT	R448A RT	R557A RT	N474A RT	Q475A RT	Y501A RT
RDS1643	8.6 ± 1.3	10.9 ± 2.1	17.0 ± 2.3	79.9 ± 5.7	91.6 ± 11.8	> 100 (86%) ^b
RDS1644	16.1 ± 2.3	19.3 ± 1.6	44.9 ± 0.7	> 100 (55%)	5.5 ± 1.5	11.6 ± 5.1
RDS1711	8.0 ± 0.2	100 ± 2	50.5 ± 4.7	>100 (100%)	>100 (83%)	>100 (100%)
RDS1712	7.7 ± 0.5	8.1 ± 0.3	19.6 ± 3.8	>100 (62%)	>100 (80%)	>100 (80%)
RDS1759	7.3 ± 0.03	8.6 ± 0.1	16.2 ± 3.0	89.4 ± 5.8	96.7 ± 1.4	>100 (100%)
RDS1760	19.4 ± 0.8	20.6 ± 2.3	63.6 ± 0.7	>100 (79%)	6.3 ± 2.3	>100 (80%)
RDS1822	6.3 ± 1.8	6.5 ± 3.5	17.4 ± 3.4	93.6 ± 9.6	71.2 ± 4.5	>100 (76%)
RDS1823	87 ± 5.1	88.5 ± 5.7	>100 (68%)	100 ± 2	7.4 ± 1.5	6.4 ± 1.6
RDS2291	8.2 ± 1.2	10.0 ± 2.0	20.7 ± 4.5	>100 (56%)	>100 (76%)	>100 (85%)
RDS2292	19.3 ± 2.6	27.2 ± 3.2	58.4 ± 3.3	>100 (84%)	3.4 ± 0,6	>100 (100%)
RDS2400	11.2 ± 1.1	15.1 ± 2.9	25.1 ± 5.4	62.8 ± 12.0	>100 (55%)	>100 (70%)
RDS2401	28.4 ± 5.4	24.7 ± 1.8	61.6 ± 5.7	>100 (65%)	28.2 ± 4.1	29.8 ± 6.7
BTP	0.20 ± 0.05	0.15 ± 0.02	0.22 ± 0.05	0.09 ± 0.01	0.19 ± 0.03	0.07 ± 0.005

^aCompound concentration (± standard deviation) required to inhibit HIV-1 RT-associated RNase H activity by 50%.

^bPercentage of enzyme activity measured in the presence of 100 μM compound concentration.

RDS2291 exhibited an at least 10-fold increase in the IC_{50} value with respect to wt RT, while their acidic counterparts exhibited a 3 to 5-folds increase in IC_{50} values, with the exception of derivative RDS1823 that showed an 11-fold increase in IC_{50} value. Indeed, according to docking results the Q475A mutation significantly reduces the interaction surface accessible to ester derivatives within the RNase H active site. Conversely, acidic derivatives are allowed to interact more tightly with the Y501 side chain through their benzyl group (or through the 4-phenyl substituent in the case of RDS1712).

The RNase H inhibitory potencies of all ester derivatives were significantly lower, when tested on the Y501A RT mutant. Also their acid counterparts generally showed increased IC_{50} values, except compounds RDS1644 and RDS2401. It can be thus postulated that the Y501A mutation modifies the interaction pattern with the adjacent Q475 by inducing a conformational rearrangement of the protein binding site which can not be modeled with rigid protein docking experiments.

The R448A mutation generally produced no effect on DKAs potency, with the exception of derivative RDS1711 that showed a 12-folds increase in the IC_{50} value. These results are in agreement with docking studies on RDS1711 and RDS1712 showing that the former, but not the latter, can establish a cation- π interaction with the R448 side chain in the WT enzyme through its benzyl group (Fig. 22C-22D), in agreement with the hypothesis of the different binding orientations of esters and acid derivatives.

4.6 Characterization of the mechanism of DKA inhibition in cell-based assays

Compound RDS1759 was found to be the only derivative able to selectively inhibit HIV-1 replication in cell-based assays and its RNase H function in biochemical assays (Table 2), without showing inhibition of RDDP function (data not shown). Therefore, we chose the ester/acid DKA couple RDS1759/RDS1760 to investigate in more detail their mechanism of action in cell-based assays. FACS and qPCR analyses were performed to detect which step of viral replication is targeted by these inhibitors. MT4 cells were infected with the NLENG1-ES-IRES wt HIV-1 containing a Green Fluorescent Protein (GFP) reporter system and treated with 10 μ M concentration of RDS1759 and RDS1760 DKAs at the time of infection or 10 hours post infection (p.i.), since this time point is considered to occur at the end of the reverse transcription window

(Arts & Hazuda 2012). High mean and low mean fluorescence indicates expression from integrated viral DNA and unintegrated viral DNA respectively, as described previously (Gelderblom et al. 2008). Samples were collected and analyzed by FACS at 48 and 72 hours p.i. quantifying i) the percentage of GFP positive cells (%eGFP), indicating the relative number of infected cells, that is overall reduced by reverse transcription inhibitors such as EFV; ii) the percentage of High Mean Fluorescence (%HMF), indicating the relative number of infected cells with integrated viral DNA, which is selectively affected by integration process inhibitors such as RAL (Fig. 24A-C). Data on viral replication showed that ester derivative RDS1759 reduced %eGFP cells by 68% and 43% at 48

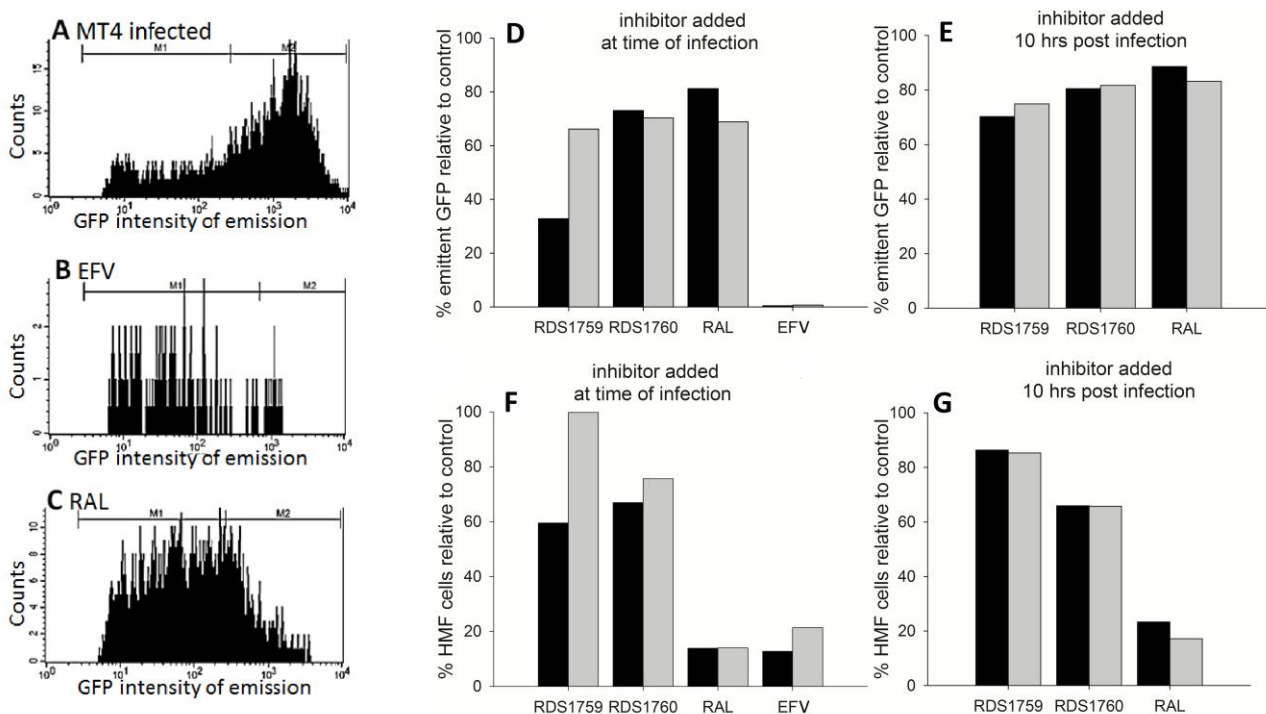


Figure 24. Inhibition of HIV-1 replication by DKAs. MT4 cells were infected with NLENG1-ES-IRES wt HIV-1 containing a GFP reporter system. Panel A-C. Samples were analyzed 48 hours post infection quantifying the number of emitting GFP cells (eGFP) versus the GFP intensity of emission, categorized in low intensity (M1), indicating expression from unintegrated viral DNA, and high intensity (M2), indicating integrated viral DNA expressing GFP. Panel A. MT4 infected (no inhibitor). Panel B. MT4 cells treated with 100 nM EFV. Panel C. MT4 cells treated with 200 nM RAL. Panel D-G. Samples were analyzed 48 (gray) and 72 (black) hours p.i., quantifying the percentage of total (M1 and M2) emitting GFP cells (panel D-E) and the percentage of High Mean Fluorescent cells (HMF) (M2) (Panel F-G) normalized to the percentage of the untreated control. Drugs (10 μ M RDS1759, 10 μ M RDS1760, 100 nM EFV, 200 nM RAL) were added at the time of infection (Panels D and F) and 10 hours p.i. (Panels E and G).

and 72 hours p.i., respectively (Fig. 24D-G). These results showed an inhibition pattern analogous to that observed for EFV, used as positive control, and suggested that RDS1759 inhibits the retrotranscription process as well. Surprisingly, inhibition of retrotranscription by RDS1759 was found to be time dependent since it was significantly reduced at 72 hours p.i.. In order to confirm this mechanism of action, drugs were added 10 hours p.i., and results showed a strong impairment of the effect of RDS1759 on %eGFP (only 30% on inhibition). Differently from RDS1759, the acidic derivative RDS1760 showed a HIV-1 inhibition pattern similar to that observed for RAL, used as positive control for IN inhibition, suggesting that RDS1760 mainly affects the integration step of the viral replication process. Subsequently, the viral DNA genomes formed during infection in the presence of the two DKAs were investigated by qPCR, total viral DNA and 2-LTRc DNA in the early phases of viral replication. First, 10 μ M of RDS1760 and RDS1759 were added at the time of infection and DNA samples were collected after 4, 6, 8, 10, 24 and 48 hours (Fig. 25A-B). Then, DKAs were added 10 hours p.i. and DNA samples were collected after 24 and 48 hours (Fig. 25C-D). Results showed that RDS1760 followed the RAL profile in 2-LTR accumulation after 24 and 48 hours either if added at the time of viral infection or 10 hours later. 2-LTR circles accumulation has been described when HIV-1 integration was impaired (Delelis et al. 2010). Moreover, RDS1760 caused a 30% decrease in total amount of viral DNA, which is higher than observed for RAL which was used as positive control and inhibited all integration events. Therefore, we could not exclude a partial inhibition of reverse transcription by RDS1760, even though its main target appears to be IN. Conversely, derivative RDS1759 induced a strong reduction in the formation of total viral DNA and followed the EFV profile until the time point at 10 hours. However, such a reduction was partially reversed at 24 hours, confirming a time dependent mode of action. Consistent with absence of IN inhibition, RDS1759 showed no accumulation of 2-LTRc DNA compared to untreated control. These results clearly indicate that RDS1760 primarily acts on IN, while RDS1759 selectively inhibits reverse transcription in a time-dependent manner. To further confirm this hypothesis, we determined the viral inhibition rate by RDS1759 at 24 and 48 hours, observing an important shift in the EC_{50} values from 0.17 μ M to 1.16 μ M, respectively (Fig. 26). No shift of the EC_{50} value was observed with EFV.

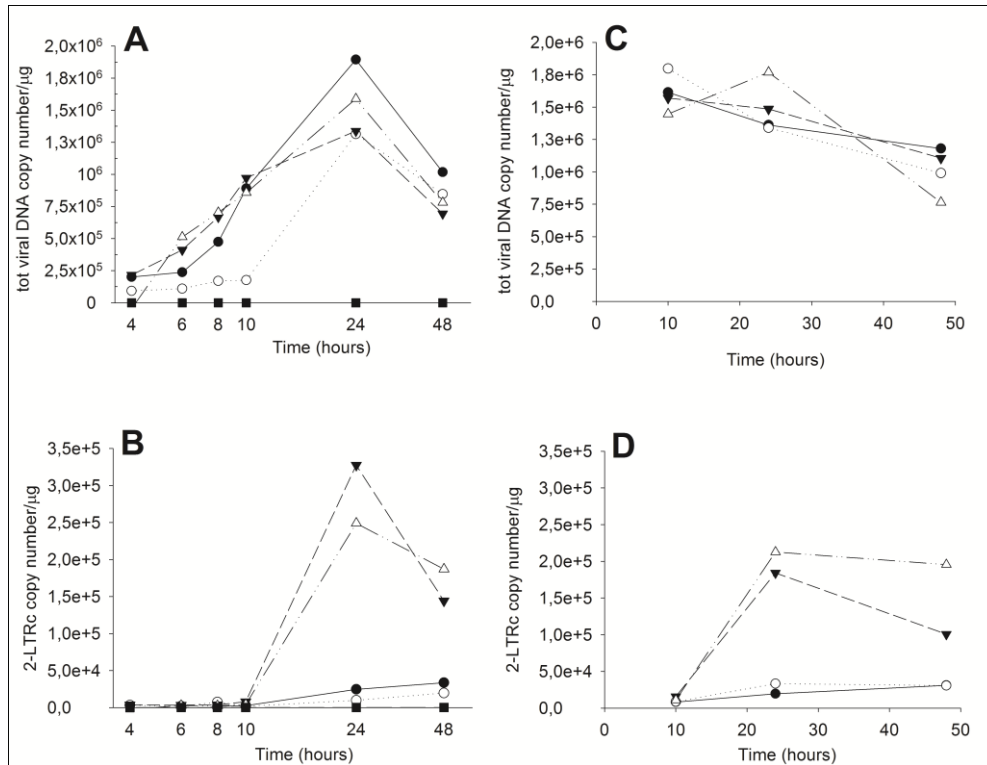


Figure 25. qPCR kinetics of total and 2-LTRc DNA forms during a single round of HIV replication in presence of inhibitors. MT4 cells were infected with HIV-1 in the absence (●) or in the presence of 10 μM RDS1759 (○), 10 μM RDS1760 (▼), 500 nM RAL (Δ) or 100 nM EFV (■), that were added at infection (Panel A-B) or 10 hours p.i. (Panel C-D). Samples were analyzed for total viral DNA and 2-LTRc at different time point p.i.

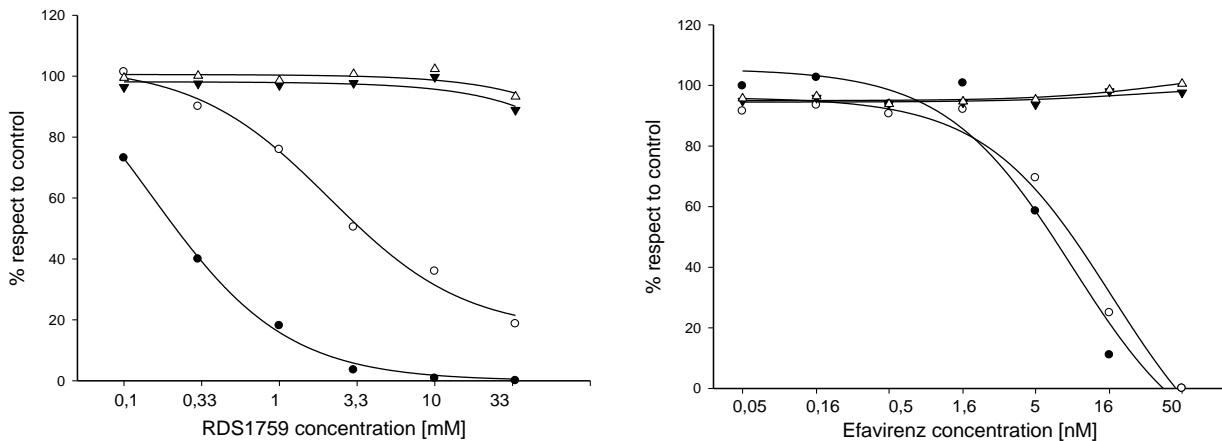


Figure 26. Time-dependent inhibition of HIV-1 replication by RDS1759. HIV-1 infected MT4 cells were treated at the time of onfection with increasing concentrations of RDS1759 (Panel A) and EFV (Panel B). Percentage of GFP emitting cells was measured at 24 hours p.i. (●) and 48 hours p.i. (○). MT4 cell viability was also evaluated at 24 hours p.i. (▼) and 48 hours (Δ).

The observed time dependent effect could be due either to cellular metabolism or to the fast dissociation of the ligand from the target. Therefore, to clearly distinguish between these two possibilities the amount of integrated viral DNA was determined at 24 and 48 hours p.i., adding RDS1759 12 hours before infection, at the time of infection, 12 hours p.i., and also adding each compound twice (at infection and 12 p.i.), using RAL as a control (Fig. 27). Addition of the compounds 12 hours before infection led to a consistent decrease of viral inhibition only for RDS1759, highlighting the possibility of cellular drug metabolism. As described previously, the efficiency of RDS1759 is maximal when the drug is added with the virus (time 0) or when the compound is added twice (time 0 and time 12 hours p.i.). When RDS1759 is added 12 hours p.i., inhibition of integration occurred but to a lesser extent compared to RAL. Taken together, these data demonstrate that RDS1759 displays a weaker stability compared to RAL. More importantly, RDS1759 efficiently targets the reverse transcription step, whereas the integration step is inhibited less efficiently.

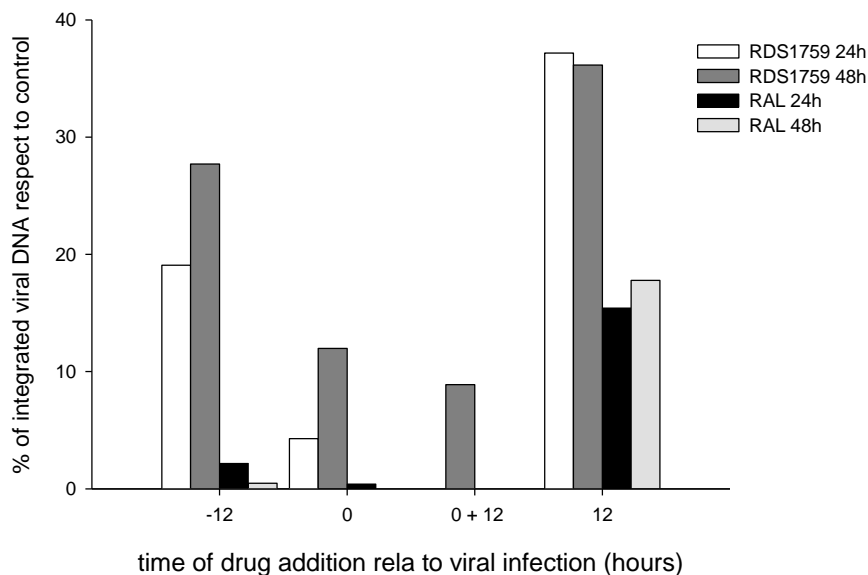


Figure 27. Effect of the time of RDS1759 addition on HIV-1 replication. HIV-1 infected MT4 cells were treated with 10 μ M RDS1759 or 200 nM RAL at different time points. Samples were collected at 24 (RDS1759 white box, RAL black box) and 48 hours (RDS1759 gray box, RAL pale gray box) and integrated viral DNA was measured.

4.7 Discussion

It has been previously reported that DKAs may act on both HIV-1 RNase H and IN functions and that some derivatives could inhibit one or both activities in the low micromolar range (Shaw-Reid et al. 2003) (Tramontano et al. 2005). More recently, a wider study on DKAs inhibition of both RNase H and IN functions categorized the compounds according to their ester or acidic function, with IN function preferentially inhibited by acidic DKAs and RNase H function equally inhibited by both ester and acid derivatives (Costi et al. 2013). In addition, even though a number of RNase H specific inhibitors have been identified, not one was specifically shown to actually inhibit reverse transcription in cell culture.

In the present study we defined the binding site of 12 DKAs on the HIV-1 RNase H domain and the investigated their mode of action in cell culture. We synthesized new couples of diketoester and DKA derivatives with various structural features that were shown to inhibit RNase H and/or IN in the low micromolar range. In particular, some esters proved to selectively inhibit RNase H activity with little or no effect to IN. A docking model for DKAs binding within the RNase H domain suggested interactions between this series of compounds and a number of highly conserved residues surrounding the RNase H active site: R448, N474, Q475, Y501, R557 (Alcaro et al. 2010). Interestingly, a different binding orientation was proposed for ester and acid derivatives into the RNase H domain because of the steric hindrance of the alkylic ester chain. Different interactions are thought to occur with residue Q475, and the lateral chain of R448 is thought to interact with the aromatic substituents on the pyrrole ring of diketoesters such as derivative RDS1711. These selected residues were changed to alanine by site directed mutagenesis. As these residues have critical functional roles, the catalytic efficiency was measured for both their RNase H and RDDP enzymatic activities, demonstrating a decrease of k_{cat}/K_M ratio for these RNase H primer grip mutants. In contrast, these mutations had no significant effects on RDDP function. Biochemical assays on these mutants RTs showed an inhibition pattern by DKAs consistent with the calculated model and corroborated the hypothesis of a different binding orientation for esters and acids. In particular, mutation Q475A was discriminating between the two groups since, with respect to wt RT, the ester DKAs decreased their inhibition potency while the acidic counterparts increased it. The difference in binding orientation between ester and acid derivatives was further confirmed by

the inactivity of ester RDS1711 on the R448A RT, while no change in IC_{50} value was observed for the acidic counterpart RDS1712; corroborating the hypothesis that an interaction occurs between R448 and the benzyl group of RDS1711 that is absent in the RDS1712/RT complex.

Importantly, in the present work we report a DKA derivative, RDS1759, that selectively inhibits the RNase H activity in the low micromolar range in biochemical assays, without effect on either IN or RDDP. RDS1759 also inhibits HIV-1 replication in cell-based assays with no evident toxic effects. IN contrast the acid counterpart, derivative RDS1760, instead was shown to preferentially target IN.

To confirm that RDS1759 selectively target RNase H function in cell based assays, we performed FACS analysis on MT-4 infected cells and qPCR evaluation of early viral DNA products. Results showed that RDS1759 selectively target the reverse transcription process in cell-based assays, with less impact on integration events. This was however time dependent, with a decay of the inhibition of viral replication with time. Time of addition assays were performed to investigate this property and discriminate between cellular inactivation and fast dissociation from the target. Pre-incubation in cell culture before viral infection compromised the effect of RDS1759 against HIV-1, while chronic exposure to the ligand completely restored the inhibition, supporting the hypothesis of some intracellular ligand inactivation. The speculation that some esterase metabolism could occur, generating the acidic counterpart is not supported by comparison of late effects related to inhibition of integration such as 2-LTRc DNA accumulation, that still occur for RDS1760 at 48 hours p.i. The more lipophilic nature of the ester DKA with compared to its acid counterpart may suggest, instead, a better diffusion into cellular compartments different from cytoplasm, where compound can be accumulated and/or metabolized, with a result loss of activity.

In conclusion we demonstrated a different binding orientation for ester and acid DKAs into RNase H domain, and proved that DKAs interact with highly conserved residues not involved in the catalytic motif (R448, N474, Q475, Y501, R557). Moreover we identified a selective RNase H active site inhibitor, RDS1759, which selectively inhibited reverse transcription in cell-based assays.

Chapter 5.

Site directed mutagenesis studies on HIV-1 RT shed light on the mechanism of action of a new RT-associated RNase H and RDDP dual inhibitor

5.1 Introduction

As described in the introduction, the DNA polymerase domain of the HIV-1 RT is located at the N-terminus of the p66 subunit and exhibits the classical “right hand” conformation, while the RNase H domain is located on the other side of the p66 subunit, at the C-terminus, 60 Å from the polymerase active site. These two domains, separated by the connection domain, proved to be strongly interconnected and a functional interdependence has been suggested (Shaw-Reid et al. 2005), since mutations at the N-terminus of the HIV-1 RT P226A, F227A, G231A, Y232A, E233A, and H235A can affect RNase H activity (Palaniappan et al. 1997), whereas deletions at the C-terminus can strongly decrease DNA polymerization (Hlzl et al. 1988). Such structural and functional interdependence is confirmed by the fact that i) mutations in RNase H domain were reported to influence nucleotide RT inhibitors (NRTIs) resistance (Gopalakrishnan et al. 1992) (Palaniappan & Wisniewski 1997) (Brehm et al. 2007), ii) the non-nucleoside RTIs (NNRTIs), i.e. nevirapine and EFV, binding to RT has been shown to increase RNase H activity (Herman & Sluis-Cremer 2013) and iii) RNase H inhibition has been linked to an increase in the AZT excision rate (Brehm et al. 2007).

A number of compounds have been reported to inhibit both RT functions *in vitro* (Distinto et al. 2013). In particular, hydrazones have been reported to inhibit RNase H function binding to an allosteric pocket close by the NNRTIs binding site (Himmel et al. 2006). More recently, a second hydrazone binding site, located in the RNase H domain, has been proposed (Felts et al. 2011) and further investigated (Gong et al. 2011) (Christen et al. 2012).

With the aim of finding new HIV-1 RNase H inhibitors, we recently performed a successful ligand based virtual screen identifying new derivatives based on the scaffold of hydrazonoindolin-2-one

(Fig.26) that are active on both RNase H and RDDP functions in the low micromolar range (Distinto et al. 2012). This scaffold, further derivatized (Meleddu et al. submitted), consistently inhibited both enzymatic activities, in presence of different substituents. In order to dissect their binding sites a new derivative (Z)-4-(2-(2-(2-oxoindolin-3-ylidene)hydrazinyl)thiazol-4-yl)benzotrile (RMNC6) was synthesized (Fig. 26) that is able to inhibit both RNase H and RDDP RT activities with IC_{50} values of 1.4 and 9.8 μ M, respectively (Table 5). A combination of biochemical and molecular modeling studies were performed to generate information that can be used in further rational drug design. Blind docking analysis suggested that RMNC6 could bind to two different sites: the first, close to the polymerase active site, the second one close to the RNase H active site. Conserved residues located close to both RDDP and RNase H primer grip regions were established as potentially critical for RMNC6 binding. Analysis of the susceptibility of the different point mutants to inhibition by RMNC6 showed a general agreement with the docking model, supporting the hypothesis that isatine derivatives may bind to two different RT binding pockets.

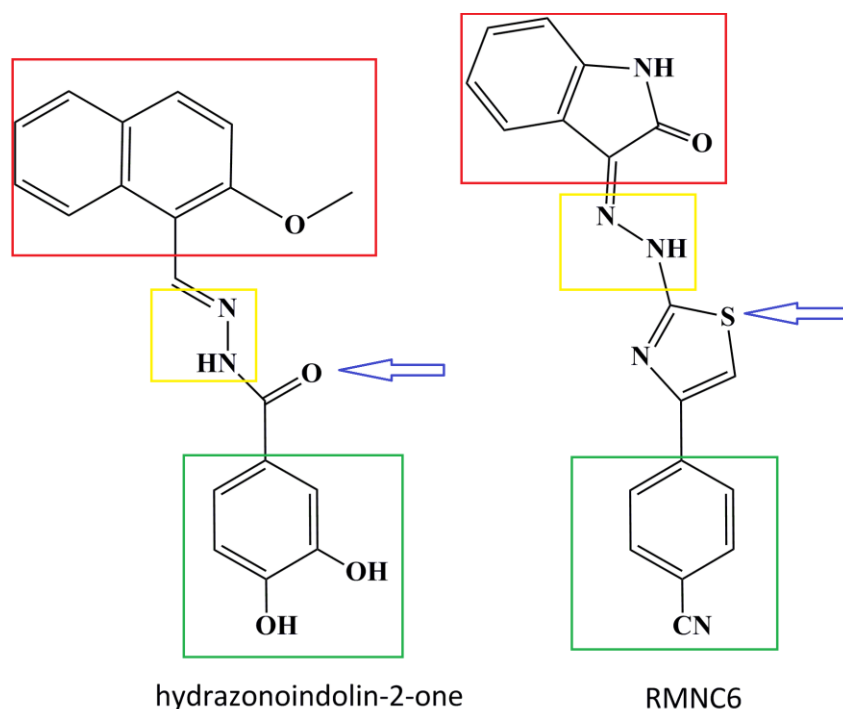


Figure 28. Chemical structure of hydrazoneindolin-2-one derivative and RMNC6. The main structural features are highlighted in color: an aromatic portion (red square); a hydrazone spacer (yellow square); a source of hydrogen bonds (blue arrow); a second aromatic ring (green square).

5.2 Comparison with known RNase H inhibitors.

Firstly, since many RNase H inhibitors such as DKA derivatives (Tramontano et al. 2005) act by chelating the cation cofactors in the catalytic site, we verified the possible RMNC6 chelating properties. We recorded its UV spectra in the absence and presence of Mg^{2+} ions, showing no significant changes in RMNC6 maximum of absorbance in the presence of 6 mM $MgCl_2$, excluding the involvement of chelation in the mechanism of action (not shown). Secondly, since it is known that some RNase H inhibitors such as VU destabilize the RT heterodimer by binding to an allosteric pocket in the RNase H domain at the interface between p66 and p51 subunits (Masaoka et al. 2013) the alterations of the HIV-1 RT thermal stability was determined by performing differential scanning fluorimetry analysis (Cummings et al. 2006) in the presence of increasing concentrations of RMNC6 as well as known inhibitors such as the NNRTI EFV, the RNase H active site inhibitor BTP and the allosteric RNase H inhibitor 2-(3,4-dihydroxyphenyl)-5,6-dimethylthieno[2,3-d]pyrimidin-4(3H)-one (VU) (Chung et al. 2012) as controls. In accordance with previous studies (Masaoka et al. 2013), we observed a T_m increase of < 2.0 °C in the presence of Mg^{2+} and BTP and a T_m decrease of 0.5–5.5 °C in the presence of VU. In contrast, both EFV and RMNC6 did not significantly affect

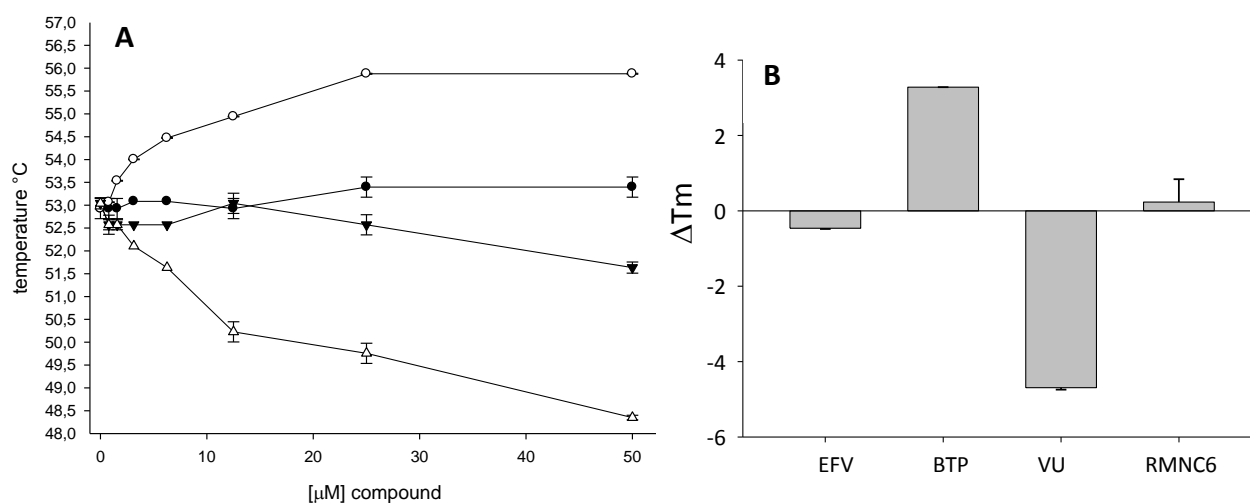


Figure 29. Effect of RT inhibitors on the thermal stability of p66/p51 HIV-1 RT. Panel A. The melting temperature of HIV-1 RT was measured in presence of increasing concentrations of different inhibitors: (▼) EFV, (○) BTP, (△) VU and (●) RMNC6. Panel B. Maximum HIV-1 RT thermal shift (ΔT_m) observed in the presence of 50 μ M concentration of compounds. ΔT_m values are the average of triplicate analysis, standard deviations are indicated as bars.

RT thermal stability, suggesting that RMNC6 may have an allosteric binding mode different from VU and possibly similar to EFV (Fig. 29).

5.3 Comparison with EFV: Yonetani-Theorell analysis and NNRTI resistant mutants.

To investigate the RMNC6 mode of action with respect to EFV, we performed a Yonetani-Theorell analysis on the interaction between RMNC6 and EFV with RDDP function. Such analysis allows to discriminate if two compounds are kinetically mutually exclusive or non-exclusive measuring reaction velocity at several fixed concentrations of the inhibitor while titrating the second inhibitor. The reciprocal of velocity ($1/v$) is then plotted as a function of concentration for the titrated inhibitor. If the two compounds are binding in a mutually exclusive fashion, this type of plot results in a series of parallel lines. If the two compounds binds independently, the lines in the Yonetani-Theorell plot will converge at the x-axis (Copeland 2013). Results showed that the RMNC6 and EFV are not kinetically mutually exclusive (Fig. 30). Interestingly, however, the calculated interaction constant α had a value of 1.2, suggesting a negative interference between the two compounds: EFV binding negatively influenced RMNC6 binding and vice versa. Because it is known that HIV-1 RT mutations K103N and Y181C and Y188L confer resistance to the NNRTIs EFV, the effect of RMNC6 on these mutant RTs was also tested (Table 6). Results showed no significant variation in IC_{50} values for RMNC6 inhibition of mutant RTs relative to wt RT on both RT-associated functions, demonstrating no implication for these residues in the RMNC6 binding and, hence, suggesting that RMNC6 mode of action differs from NNRTI, such as EFV.

Table 6. Effects of RMC6 on RNase H and RDDP activities of wt and NNRTI resistant HIV-1 RTs.

RT	<i>RMNC6</i>				<i>BTP</i>		<i>EFV</i>	
	RNase H		RDDP		RNase H		RDDP	
	IC_{50} (μ M) ^a	fold ^c	IC_{50} (μ M) ^b	fold ^c	IC_{50} (μ M) ^a	fold ^c	IC_{50} (nM) ^b	fold ^c
Wt	1.3 ± 0.3	1	9.8 ± 1.4	1	0.19 ± 0.03	1	23 ± 4.1	1
K103N	2.3 ± 0.1	1.8	13.6 ± 1.0	1.3	0.22 ± 0.08	1.2	176 ± 25	7.6
Y181C	2.1 ± 0.6	1.6	5.4 ± 0.3	0.5	0.23 ± 0.05	1.2	49.7 ± 9.1	2.2

^aCompound concentration (\pm standard deviation) required to inhibit HIV-1 RT-associated RNase H activity by 50%.

^bCompound concentration (\pm standard deviation) required to inhibit HIV-1 RT-associated RDDP activity by 50%.

^cFolds of difference with respect to wt RT.

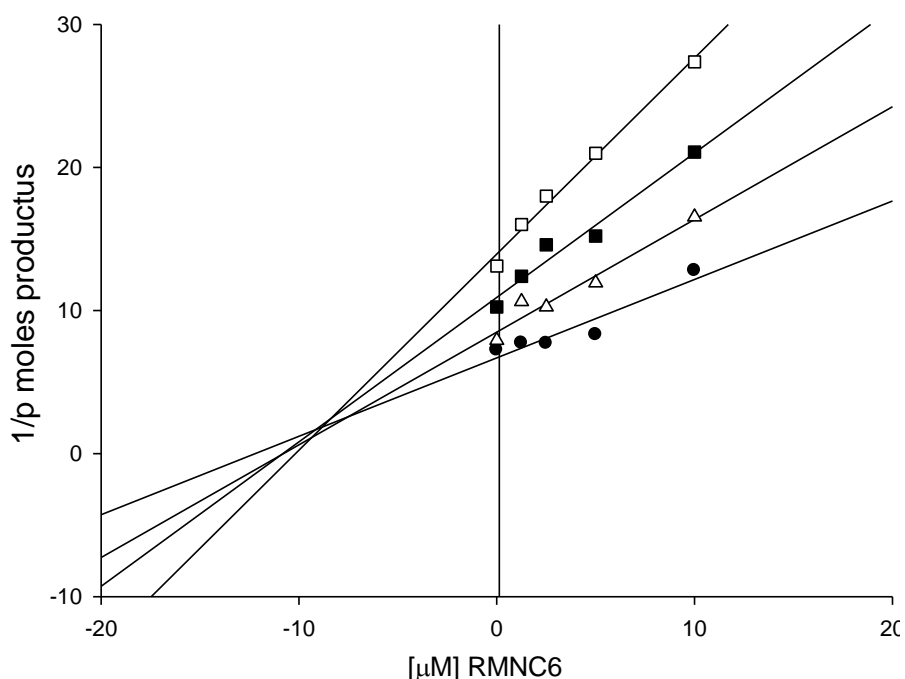


Figure 30. Yonetani–Theorell plot of the combination of RMNC6 and EFV on the HIV-1 RT RDDP activity. HIV-1 RT was incubated in the presence of RMNC6 alone (●) or in presence different concentrations of EFV: 4 nM (▲), 8 nM (■), 16 nM (□).

5.4 Blind docking analysis.

To create further insight into the RMNC6 binding mode blind docking studies on the whole structure of wt HIV-1 RT and RMNC6 was performed employing the QM-polarized ligand docking protocol utilizing Glide version 4.5, qsite version 4.5, jaguar 7.0 and maestro 8.5 (Schrodinger Inc, Portland, USA). Due to the flexibility of the target and the different shapes of known inhibitors (Fig. 31), it was decided to carry out ensemble docking experiments. The major conformational changes in the NNRTI binding pocket were taken into account to perform a clusterization of the available RT complexes. In particular, the orientation of Y181, Y188, Y183 and primer grip β 12- β 13 hairpin were considered (Fig. 31) (Paris et al. 2009). A representative of each different cluster was picked (Fig. 31) and the three dimensional structure of HIV RT was retrieved from the Protein Data Bank.

The obtained [RMNC6•RT] complexes were subjected to a post-docking procedure based on energy minimization and successive binding free energies calculation. The binding free energies ($\Delta G(\text{Bind})$) were obtained applying molecular mechanics and continuum solvation models using the molecular mechanics generalized Born/surface area (MM-GBSA) method ((Kollman et al. 2000). By comparing the ΔG -MMGBSA values (table 7), we found that blind docking calculations indicated the presence of two sites that are energetically favored for isatine derivatives binding (Fig. 32). The first binding site (pocket 1), the most energetically favored, is located close to the DNA polymerase catalytic site and is contiguous to the NNRTI binding pocket, having an “L shape”. In this large space, RMNC6 can dock in two different orientations. In the first orientation I (orientation A), the compound is accommodated in a pocket located between polymerase catalytic domain and NNRTI binding pocket. This pocket was recently described as allosteric pocket of HIV-1 RNase H function (Himmel et al 2006, Himmel et al 2009). It is characterized by Y181 and Y188 residues in closed conformation, different from the open conformation that characterize most NNRTIs (Fig. 33A). The docking results suggest that RMNC6 possibly makes critical interactions

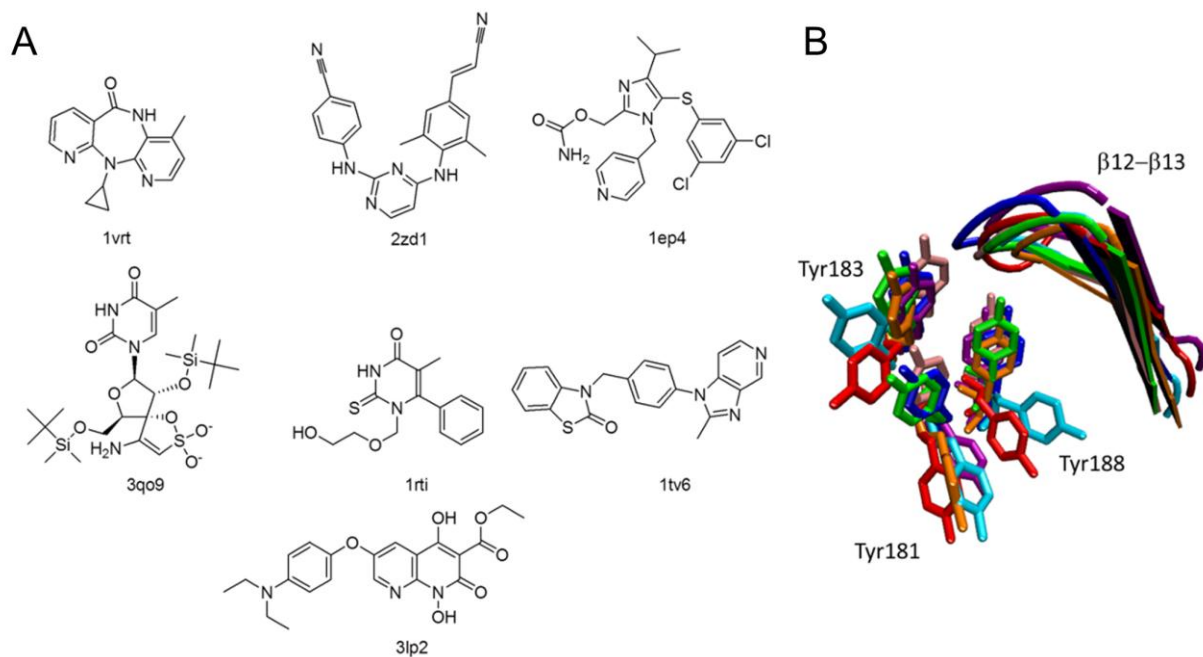


Figure 31. Details of co-crystals selected for docking analysis A. Chemical and crystal structures pdb codes of co-crystallized NNRTIs selected for the ensemble docking procedure. Panel B. Stereoview of the primer grip region and residues 181, 183 and 188 are shown in color, relative to the different crystal structures examined . with amino acid residues V108, Y188, P227, W229 and L234. According to the second orientation

with amino acid residues V108, Y188, P227, W229 and L234. According to the second orientation (orientation B), RMNC6 binding could involve amino acid residues P95, L100, V106, Y188, P225, L234, W229, P236, and Y318 (Fig. 33C). In particular, the hairpin formed by the β 12 and β 13 sheets (Jacobo-Molina et al. 1993) was involved with different residues in both putative orientations. The second putative binding pocket (pocket 2) is located in the RNase H domain, between the RNase H active site and the substrate-handle region, close to the interface of the two subunits p66 and p51. Docking modeling suggested that in this site RMNC6 could be partially sandwiched between different secondary structural units, the sheet β 21 and the helix α H in the p51, and the helix α B in the p66 subunit (residues 500-508) (Fig. 34). Since the large number of possibilities suggested by the docking modeling, we wanted to better investigate the binding mode via site directed mutagenesis.

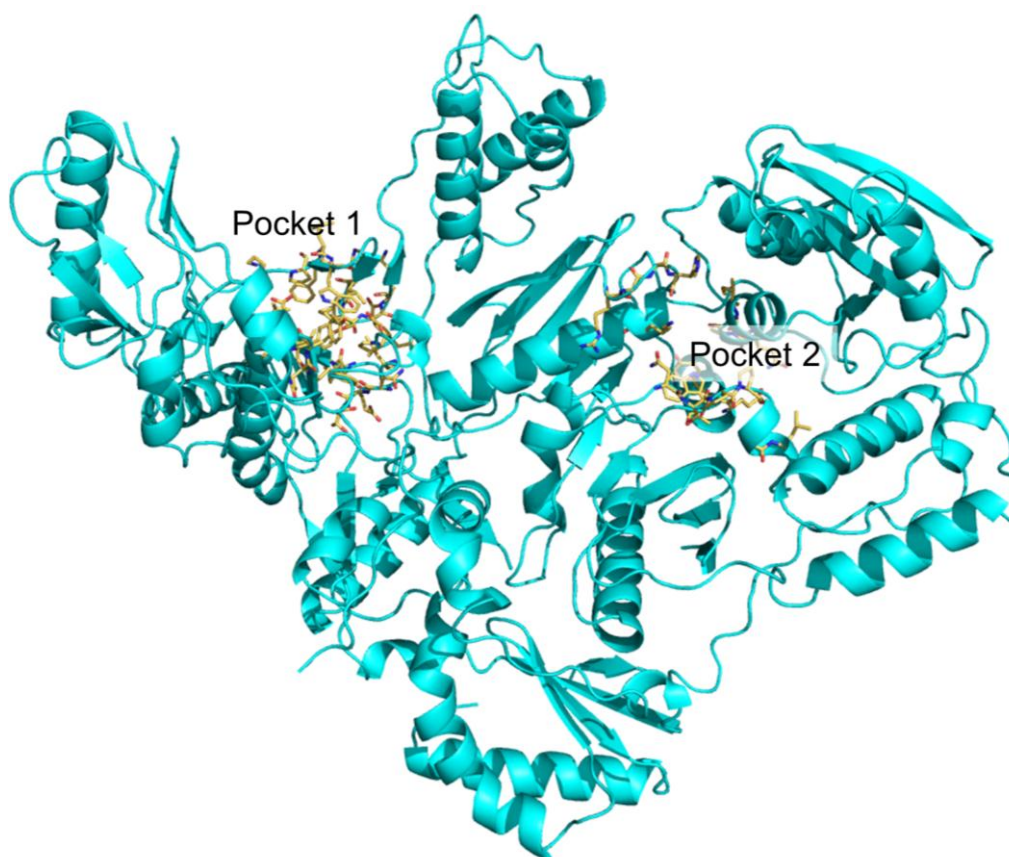


Figure 32. Binding sites of RMNC6 identified with blind docking experiments on the whole wt HIV-1 RT structure. HIV-RT shown in cyan ribbon. Residues of the two binding pockets are shown in yellow sticks.

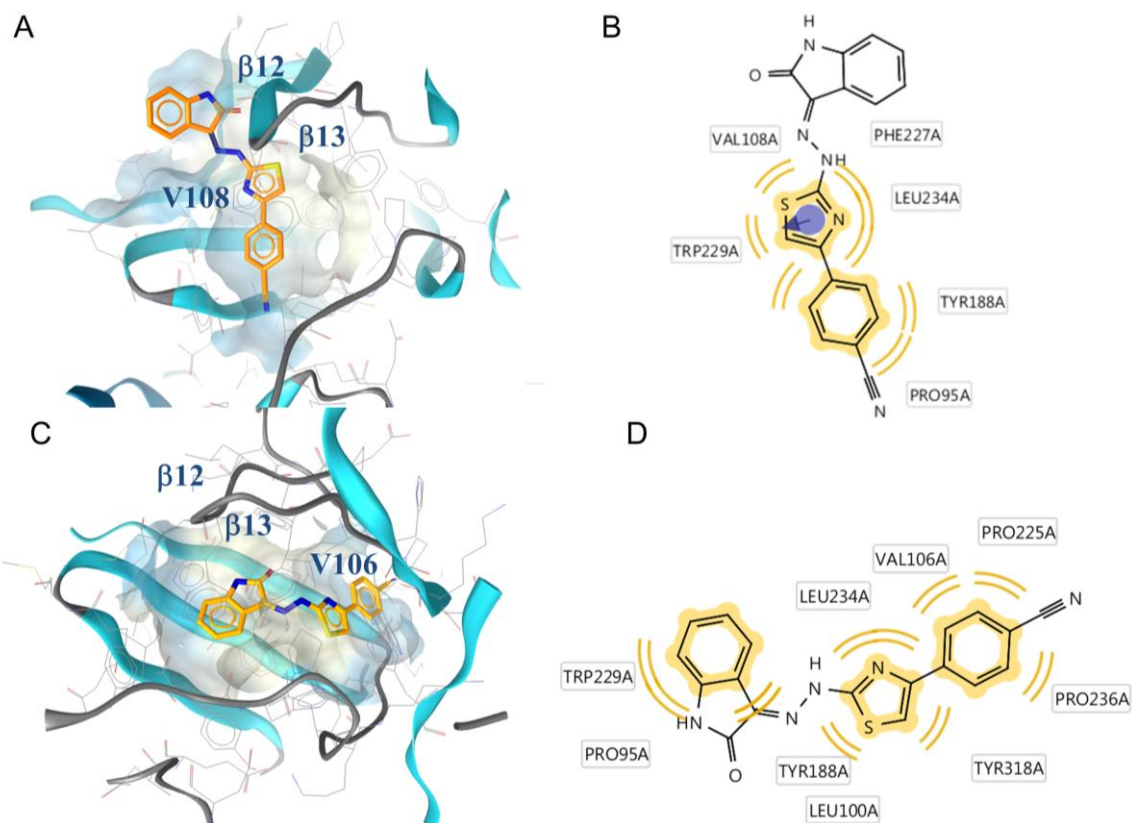


Figure 33. Putative binding mode of RMC6 and critical residues identified for RMNC6 binding in pocket 1. Panel A. orientation A. Panel C:orientation B. Panel B-D) 2D depiction of RMNC6 and its respective interactions with RT residues: pale yellow sphere indicate hydrophobic interactions with lipophilic residues. while the violet sphere represents the aromatic π - π stacking interaction.

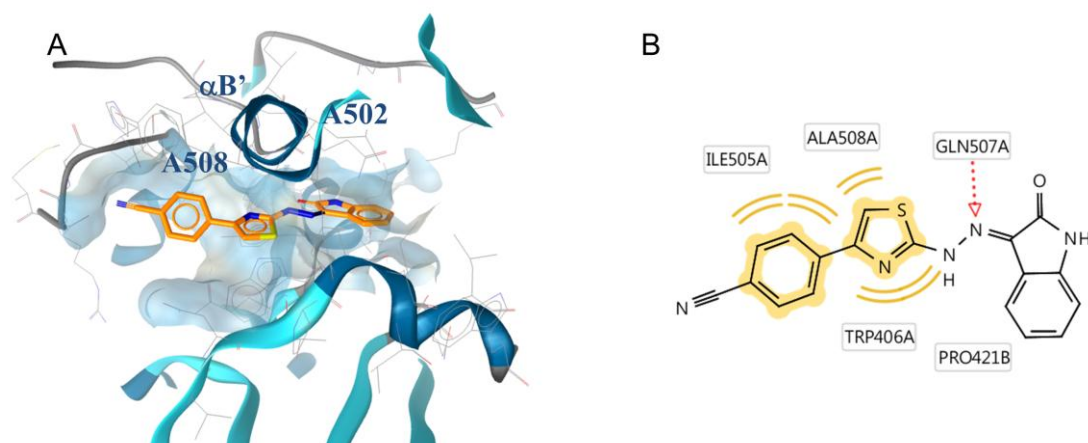


Figure34. Putative binding mode of RMC6 and critical residues identified for RMNC6 binding in the pocket 2. Panel A. Putative binding mode of RMC6 and critical residues identified for RMNC6 binding in the pocket 2. Panel B. 2D depiction of RMNC6 and its respective interactions with RT residues. pale yellow sphere indicate hydrophobic interactions with lipophilic residues. The red arrow indicates an hydrogen bond acceptor interaction.

Table 7. Ensemble docking results: binding free energies of [RMNC•RT] complexes. In bold are indicated the most favored binding orientations for pocket 1 (red) and pocket 2 (blue).

RTconformation (pdb codes)	Pocket	ΔG_{MMGBSA} (Kcal*mol)	Orientation
1ep4	1	-41.23	
1ep4	2	-36.22	
3lp2	1	-44.85	A
3lp2	2	-42.58	
1rti	1	-33.26	
1rti	2	-40.49	
1tv6	1	-51	B
1tv6	2	-48.74	
1vrt	1	-35.9	
1vrt	2	-32.44	
2zd1	1	-41.96	
2zd1	2	-32.06	
3q09	1	-39.25	
3q09	2	-38.48	

5.5 Influence of the amino acid residues in pocket 1 on HIV-1 RT inhibition by RMNC6.

Given the calculated docking model, we selectively mutated a large number of residues in both pockets. Considering the extent of pocket 1, its surface was deeply explored by single site mutagenesis. The hairpin constituted by the sheets $\beta 12$ and $\beta 13$ was identified as potentially involved in RMNC6 binding for both orientations and therefore alanine scanning mutagenesis was performed on amino acid residues 224-231. Residues V108 and V106 were identified to be important for inhibitor binding to RT in orientation A and B, respectively, and therefore they were also mutated into Alanine. We then tested the effects of RMNC6 on both RNase H and RDDP functions of these mutant RTs using BTP and EFV as controls (Table 8). Interestingly, when the mutant RTs RNase H function was assayed showed a 6-fold reduction in IC_{50} value against E224A RT compared to wt RT RMNC6, and a 4- and 10-fold reduction against V108A and V106A RTs, respectively. In contrast, no major difference in IC_{50} value was observed against the other mutant RTs (Table 8). When the mutant RTs RDDP function was assayed, a similar pattern was found even

though the extent of reduction in the IC₅₀ values was lower (1.4, 3.3 and 2.5 for E224A, V106A and V108A, respectively).

Table 8. Effects of RMNC6 on RNase H and RDDP activities of HIV-1 RTs mutated in amino acid residues in pocket 1.

RT	<i>RMNC6</i>				<i>BTP</i>		<i>EFV</i>	
	RNase H		RDDP		RNase H		RDDP	
	IC ₅₀ (μM) ^a	fold ^c	IC ₅₀ (μM) ^b	fold ^c	IC ₅₀ (μM) ^a	fold ^c	IC ₅₀ (nM) ^b	fold ^c
V106A	5.3 ± 0.6	4.1	25.1 ± 2.3	2.5	0.16 ± 0.03	0.8	35.4 ± 2.2	1.5
V108A	13.1 ± 2.5	10.1	33.0 ± 5.2	3.3	0.18 ± 0.04	0.9	21.3 ± 3.6	0.9
Y188A	3.3 ± 1.5	2.5	20.9 ± 4.0	2.1	0.19 ± 0.08	1.0	28.3 ± 7.4	1.2
E224A	7.9 ± 1.1	6.1	13.8 ± 4.2	1.4	0.15 ± 0.03	0.8	24.9 ± 0.7	1.0
P225A	1.7 ± 0.2	1.3	3.1 ± 0.3	0.3	0.13 ± 0.06	0.7	19.5 ± 2.9	0.9
P226A	1.9 ± 0.1	1.5	18.9 ± 0.7	1.9	0.29 ± 0.08	1.5	18.9 ± 2.4	0.8
F227A	0.7 ± 0.1	0.5	15.2 ± 0.9	1.5	0.22 ± 0.04	1.2	61.5 ± 1.4	2.7
L228A	1.5 ± 0.1	1.2	13.1 ± 1.9	1.3	0.10 ± 0.06	0.5	21.8 ± 3.8	0.9
W229A	1.9 ± 0.5	1.4	15.4 ± 2.8	1.6	0.15 ± 0.08	0.8	22.9 ± 5.2	1.0
M230A	0.5 ± 0.1	0.4	15.0 ± 3.5	1.5	0.14 ± 0.04	0.7	29.1 ± 2.2	1.3
G231A	1.7 ± 0.4	1.2	10.8 ± 2.4	1.1	0.25 ± 0.03	1.3	67.7 ± 3.5	2.9

^aCompound concentration (± standard deviation) required to inhibit HIV-1 RT-associated RNase H activity by 50%.

^bCompound concentration (± standard deviation) required to inhibit HIV-1 RT-associated RDDP activity by 50%.

^cFolds of difference with respect to wt RT.

5.6 Influence of the amino acid residues in pocket 2 on HIV-1 RT inhibition by RMNC6

Among the hypothesized RMNC6 interactions with the amino acid residues in pocket 2 we chose to mutate residues A502 to Phenylalanine and A508 to Valine with the aim to reduce the space available for RMNC6 accommodation. In addition, we also mutated residues Y501 and N474 into Alanine, since they were previously shown to be involved in interaction of DKAs with the RNase H domain (see chapter 4) and are known to play an important structural role in the functional geometry of the area, as part of the RNase H substrate primer grip motif, and are highly conserved, as indicated by the drastic reduction in viral infectivity of mutant viruses (Julias et al. 2002). Hence, we again tested the RMNC6 effects on both RNase H and RDDP functions of mutant RTs, using BTP and EFV as negative controls (Table 9). According to the model, when the mutant

RTs RNase H function was assayed, RMNC6 showed a 6- and 5-fold reduction in IC₅₀ value against A502F and A508V RTs compared to wt RT. In addition, RMNC6 showed a total loss of RT inhibition on the RNase H activity of N474A and Y501A RTs. Importantly, the active site inhibitor BTP showed a 2-fold reduction in RNase H inhibition only against N474A RT, confirming a difference in binding mode with respect to RMNC6. In contrast, when the RDDP function was assayed, RMNC6 did not show any significant change in potency of inhibition of mutant RTs compared to wt RT as expected.

Table 9. Effects of RMC6 on the RNase H and RDDP activities of HIV-1 RTs mutated in amino acid residues individuated in pocket 2.

RT	<i>RMNC6</i>				<i>BTP</i>		<i>EFV</i>	
	RNase H		RDDP		RNase H		RDDP	
	IC ₅₀ (μM) ^a	fold ^c	IC ₅₀ (μM) ^b	fold ^c	IC ₅₀ (μM) ^a	fold ^c	IC ₅₀ (nM) ^b	fold ^c
N474A	> 100	> 70	12.7 ± 1.7	1.3	0.92 ± 0.01	2.1	20.1 ± 5.1	0.9
Y501A	> 100	> 70	6.6 ± 0.1	0.7	0.07 ± 0.002	0.5	24.1 ± 3.5	1.1
A502F	13.0 ± 0.7	10.0	17.1 ± 2.1	1.7	0.17 ± 0.03	1.1	22.3 ± 1.5	0.9
A508V	6.5 ± 0.7	5.0	19.3 ± 2.8	1.9	0.16 ± 0.05	0.8	24.7 ± 2.4	1.1

^aCompound concentration (± standard deviation) required to inhibit HIV-1 RT-associated RNase H activity by 50%.

^bCompound concentration (± standard deviation) required to inhibit HIV-1 RT-associated RDDP activity by 50%.

^cFolds of difference with respect to wt RT.

5.7 Kinetic studies on mutants

These data on the partial loss in RMNC6 potency of RNase H inhibition observed for E224A, V108A and V106A RTs supported two different hypotheses. According to the first one, the reduced potency could be due to an impairment of a long-range effect of RMNC6 bound in pocket 1. According to the second one, the single mutations can lead to a long-range modification of pocket 2 that alters the compounds binding in pocket 2.

To examine this second hypothesis, the possibility of a long-range modification of the RNase H domain, we asked if these mutations could influence the RNase H function and evaluated the RNase H catalytic efficiency of all DNA polymerase domain mutants that exhibited a reduced RNase H inhibition by RMNC6. It is worth to note in this context, that residue E224 is highly conserved as it is involved in the DNA polymerase primer grip motive (Palaniappan & Wisniewski 82

1997). In addition, among the residues mutated in the RNase H domain, N474 and Y501 are also highly conserved since they are part of the RNase H primer grip motive and have been reported to possess a consistent reduction in RNase H activity (Rausch et al. 2002), see chapter 4, therefore we asked if A502F and A508V mutants also had altered in their kinetic parameters. Results showed a consistent reduction in k_{cat} value compared to wt RT for all the mutant RTs considered, and a slight reduction in K_M value for A508V, V106A, V108A and E224A, resulting in a loss of efficiency (k_{cat}/K_M) for V108A and E224A (2- and 3-fold, respectively), (Table 10). Overall, these results support the hypothesis of long-range effects on the RNase H domain of mutations in the polymerase domain, consistently with previously reported data (Palaniappan & Wisniewski 1997), that can affect RMNC6 binding to pocket 2.

Table 10. Comparison of DNA polymerase independent RNase H activity kinetics of wt and mutant HIV-1 RTs

RT	RNase H			
	k_{cat} (min^{-1})	K_M (nM)	k_{cat}/K_M	% of wt
wt	113 ± 1.4	127 ± 5.0	0.89	100
V106A	52.6 ± 5.6	69 ± 11	0.76	85.4
V108A	19.4 ± 3.3	48.8 ± 3.9	0.4	44.9
E224A	21.2 ± 4.3	78.6 ± 14	0.27	30.3
A502F	20.8 ± 1.0	273 ± 18	0.76	85.4
A508V	51.7 ± 4.9	74.9 ± 6.8	0.68	76.4

5.8 Discussion

Since both RDDP and RNase H activities of the HIV-1 RT are validated targets for drug development (Esposito et al. 2012; Distinto et al. 2013), but none of the approved drugs are able to inhibit both activities at the same time, the challenge of identifying a single molecule able to inhibit both functions at the same time is becoming more appealing in the attempt to minimize the occurrence of selection of drug resistant strains and reducing the administered drugs burden. In the past ten years, a number of compounds (Himmel et al. 2006; Esposito et al. 2011; Distinto et al. 2012) have

been reported to inhibit both RT-associated RNase H and RDDP functions. The third part of this work was focused on the characterization of the binding mode of a new scaffold identified in a virtual screening (Distinto et al. 2012). The RMNC6 derivative was able to inhibit both HIV-1 RT RNase H and RDDP functions in the low micromolar range and showed, via differential scanning fluorimetry, to behave differently from known RNase H active site inhibitors, that have been shown to stabilize RT against thermal denaturation (Su et al. 2010), and interface inhibitors, that have been shown to destabilize RT (Masaoka et al. 2013). Interestingly, RMNC6 behaved more similarly to the allosteric NNRTI EFV. Even though RMNC6 was not active against viral replication (data not shown), the dissection of its mode of action was particularly valuable.

Blind docking analysis suggested as favorite two putative binding pockets (Table 7 and Fig.32-34). In the pocket 1 RMNC6 exhibits two different binding orientations. In the orientation A in pocket 1 (Fig. 33A) the compound occupies an allosteric site located between the polymerase catalytic region and the NNRTI pocket 50 Å from the RNase H catalytic site, previously reported to be the binding site of hydrazones derivatives (Himmel et al. 2006), in the orientation B RMNC6 occupies the NNRTI pocket, where most known polymerase inhibitors bind. Pocket 2 is a site located between the RNase H active site and the substrate-handle region (Christen et al. 2012). Such *in silico* analysis support two possible modes of RMNC6 action: i) RMNC6 could preferentially bind to one of the two pockets and have both short- and long-range effects; ii) RMNC6 could bind to both sites and act by short-range effects on the two functions. According to the first mode of action, RMNC6 would exert its RDDP and RNase H inhibition by binding either into pocket 1 or into pocket 2. The binding into pocket 1 would have a short-range inhibition effect on RDDP activity and a long-range inhibition effect on the RNase H activity. So it would act opposite to NNRTIs such as nevirapine and EFV that were shown to destabilize the 3'-end of the DNA primer in the DNA polymerase active site and to promote RT-mediated polymerase-independent RNase H cleavages (Herman & Sluis-Cremer 2013). The binding into pocket 2, would have a short-range inhibition effect on RNase H activity and a long-range inhibition effect on the RDDP activity. Differently, according to the second mode of action, RMNC6 would bind to both individual RT pockets and its activity would be due to short-range inhibition effects, so that its binding to each site would be responsible for the inhibition of one function.

To investigate each of these possibilities we performed enzyme kinetics and site directed mutagenesis studies. The RMNC6 binding into pocket 1 (in orientation B), located in the polymerase domain, was the most energetically favored by modeling calculations (Table 7), however results of the assays with the mutant RTs led neither to incontrovertible evidence of RMNC6 binding, nor to a clear discrimination between the two proposed binding poses. The results, however, could not exclude the RMNC6 binding to pocket 1. In fact, given the magnitude of the pocket and the high RT flexibility, the very limited reduction in potency of inhibition of RDDP function by RMNC6 could be due to the fact RMNC6 could accommodate in pocket 1 switching between the two binding orientations, to compensate the loss of affinity introduced with the changes in amino acid residues. Also kinetic analysis of the interaction between RMNC6 and EFV showed no interference between the two compounds (Fig.30), even if they are not kinetically mutually exclusive, supporting the possibility that RMNC6 may bind in the large pocket 1 even in the presence of EFV.

Binding into pocket 2, located in the RNase H domain, had previously been reported for Hydrazones derivatives that exhibit inhibitory activity against RNase H function (Felts et al. 2011; Gong et al. 2011; Christen et al. 2012). When bound to this site RMNC6 might nudge the RNase H domain into a position in which the active site is no longer able to catalyze cleavage of RNA from the DNA:RNA duplex. RNase H inhibition of the mutant RTs in pocket 2 by RMNC6 strongly support the hypothesis that RMNC6 interacts with a pocket comprising amino acid residues N474, Y501 and A502, and that this binding is responsible for short-range inhibition of the RNase H function. The observed fully retained RDDP inhibition of these mutant RTs by RMNC6 also supports the hypothesis that RMNC6 could bind to both pocket 1 and 2, and that its RT inhibition is due to two different short-range effects. Analyses of the kinetic parameters, support this hypothesis since the partial loss of RMNC6 potency of RNase H inhibition against E224A, V108A and V106A RTs could be most probably due to a long-range effects of the mutation itself, that could alter the substrate binding in the RNase H domain (Palaniappan et al. 1997) as well as the RMNC6 binding in to the second site. This is also confirmed by alteration of the RNase H function kinetic parameters observed for these mutant RTs.

In conclusion we characterized a two-sites mechanism of action for the isatine-derivatived RNase H/RDDP dual inhibitor RMNC6, as a possibility for further development of RNase H/ RDDP dual inhibitors.

Chapter 6.

Conclusions

Since both HIV-1 RT-associated RNase H and RDDP functions are valid targets for drug development, the present work was focused on the identification and characterization of new promising RHIs. This goal was pursued by two different approaches: the characterization of the binding pocket of new RNase H active site chelating agents and the exploration of the mechanism of action of dual RNase H and RDDP inhibitors.

Given the similarities between the HIV-1 and PFV RNase H domains, determined by structural alignment and superimposition of the two RNase H domains, PFV RT was used as a tool to investigate its interactions with RHIs, with the purpose of identifying the corresponding residues involved in the interactions between HIV-1 RT RNase H and RHIs. We tested the effect of five HIV-1 RHIs, known to interact with different HIV-1 RT pockets, on the PFV RT: four selective RHIs (RDS1643, DHQ, BTP, VU6) and one HIV-1 RDDP and RNase H dual inhibitor (NSC657589). Moreover, for comparative purposes, we included the non-nucleoside RT inhibitor EFV in the study. All RHIs inhibited the PFV RNase H function at concentrations comparable to the ones reported for HIV-1 RNase H, suggesting similar binding to two proteins. Among the selective RHIs tested, RDS1643, DHQ and VU6 also inhibited the FV RT-associated RDDP activity, suggesting differences in the protein's structure and flexibility between PFV PR-RT and HIV-1 RT. NSC657589 confirmed its ability to inhibit both functions also in PFV RT. EFV was inactive on PFV PR-RT, indicating the lack of NNRTI binding pocket in that enzyme, as reported for other retroviruses with monomeric RTs. These results confirmed that NSC657589, as previously hypothesized, it does not bind to NNRTIs pocket. Since the structure of the PFV RNase H has been previously solved by NMR spectroscopy, NMR analysis was used to characterize the RDS1643 interactions with the protein. NMR titration and docking experiments identified a number of non-catalytic residues into the PFV RNase H active site region (T641, I647, Y672 and W703) that may be involved in RDS1643 binding of. Due to the high structural similarity of PFV and HIV-1 RNase H we were able to propose an inhibitor binding site in HIV-1 RNase H by using structural overlays. Sequence and structure alignments with HIV-1 RNase H suggested that the compound may interact with the corresponding

HIV-1 RT residues T473, L479, Y501 and V518, some of which are conserved as they are located in the RNase H primer grip area. We therefore demonstrate that PFV RNase H can be used as a model enzyme to analyze the binding of HIV-1 RHIs, and also to model the interactions between RT and RHIs using NMR. Furthermore, it can also be used to exclude the binding of inhibitors into the NNRTIs site.

The important insights that came from FV RT results makes the further investigation into the DKA binding mode into HIV-1 RNase H active site appealing. The prototype DKA RDS1643 was further developed into six ester/acid DKA couples used as chemical tool to explore their binding region on RT, and to demonstrate their mechanism of action in cell culture, with particular attention to discriminate between RNase H and IN, the other closely related viral-coded polynucleotidyl transferase. Among the compounds tested on both RNase H and IN functions, most of the ester derivatives showed selectivity for HIV-1 RNase H versus IN, while acids inhibited both functions and were generally more effective against IN. Molecular modeling and site-directed mutagenesis of the RNase H domain showed a different binding orientation for ester and acid DKAs, and proved that DKAs interact with highly conserved residues not involved in the catalytic motif (R448, N474, Q475, Y501, R557). In particular, an ester derivative, RDS1759, selectively inhibited RNase H activity and viral replication in the low micromolar range, making contacts with residues N474, Q475 and Y501 in the RNase H domain. Quantitative PCR studies and FACS analysis showed that RDS1759 selectively inhibits reverse transcription in cell-based assays. Overall, we provide the first demonstration that RNase H inhibition by DKAs can be related not only to their Mg^{2+} chelating properties, but also to specific interactions with highly conserved amino acid residues in the RNase H domain. Furthermore, RDS1759 is the first compound which, to the best of our knowledge, has been definitively proven to inhibit viral proliferation by inhibition of genomic RNA hydrolysis by RT, through interactions with conserved residues on RNase H domain of the enzyme, and hence offering important insights for rational optimization of RNase H active site inhibitors.

The second approach was focused on the identification and characterization of new RNase H/RDDP dual inhibitors. Starting from a previous virtual screening campaign (Distinto et al. 2012) wich identified a new isatine-based scaffold for dual functions RT inhibitors a new compound, RMNC6, was synthesized and shown to inhibit both RT-associated RNase H and RDDP activities

with IC_{50} values of 1.4 and 9.8 μ M concentration, respectively. RMNC6 showed a mode of RDDP inhibition different from the NNRTIs, retaining full potency of inhibition on NNRTI resistant mutant RTs: K103N, Y181C and Y188L. Hence, the possibilities of binding of this derivative into the whole HIV-1 RT through blind docking experiment and site-directed mutagenesis was explored. Two different RT pockets were identified: the first one close to the polymerase active site and contiguous to the NNRTI binding pocket, and the second one located in the RNase H domain. RMNC6 was assayed against enzymes selectively mutated on residues hypothesized to be critical for compound binding, which included conserved amino acid residues both in the polymerase and in the RNase H primer grip regions. The mutagenesis study supported the hypothesis of independent binding of RMNC6 in both pockets, since the mutation of amino acid residues in the pocket located in the RNase H domain (N474, Y501 and A502) strongly affected RNase H inhibition by RMNC6, while fully retaining its ability to inhibit the RDDP activity of these mutant RTs. Therefore, RT inhibition by RMNC6 seems to be due to its binding to two different RT pockets that lead to two different short-range effects. Moreover, we highlighted the role of mutations V106A, V108A and E224A that, affected the RNase H function in spite of their location far away from RNase H active site, confirming a strong interdependence between the two domains.

Overall we i) validated PFV RT as a useful tool for RNase H active site inhibitor development, ii) successfully identified an RNase H selective active site inhibitor (RDS1759) iii) characterized for the first time its broad interaction with conserved residues in the RNase H active site area, iv) confirmed its selective mechanism of action in cell based assays, v) characterized a two-sites mechanism of action for the isatine-derivatived RNase H/RDDP dual inhibitor RMNC6, opening the way for further characterization of its binding pocket needed to allow further rational optimization of the scaffold.

Acknowledgements

I would like to thank Prof. Tramontano, a mentor and example in the start of my work in research, and all my colleagues of the laboratory of Molecular Virology at the Department of Life and Environmental Sciences of the University of Cagliari: Francesca, Luca, Valeria, Marta, Nicole, Gianluca, Luana, with which I shared good and bad moments of the lab life, and all of the student that worked with us.

I would like to thank Prof. Elias Maccioni, Dr. Rita Meleddu and Dr. Simona Distinto for the long collaboration on RMNC project, for compound synthesis and helpful molecular modeling analysis in characterization of RMNC binding mode.

I would like to thank Dr. Stuart Le Grice and his lab team at HIV Drug Resistance Program, Center for Cancer Research, National Cancer Institute, National Institutes of Health Frederick, MD –USA, where I spent five months of my first year of PhD, learning advanced techniques of recombinant enzymes purification. There I made the first series of HIV-1 RT mutant enzymes and the experiments of differential scanning fluorimetry. They provided knowledge and technology, helpful discussions, and, not less important, a sincere friendship.

I would like to thank Prof. Roberto Di Santo and his collaborators for DKAs synthesis, Dr. Sandro Cosconati and his collaborators for helpful molecular modeling analysis in characterization of DKAs binding mode.

I would like to thank the team of Dr. Malcom Buckle and the team of Biophotonique des interactions moléculaires, Laboratoire de Biologie et Pharmacologie Appliquée (LBPA). Ecole Normale Supérieure Cachan cedex France, where I spent three months of my last year of PhD, learning viral replication cell based assays, qPCR, FACS analysis and BL3.

I would like to thank Prof. Birgitta M. Wöhrl and her collaborators for the fruitful collaboration on PFV-PR RT part of the project.

Last but not least, I would like to thank my family, Enrico, and one by one all the friends which always supported me and encouraged me to start and pursuing this fascinating job. Thank for contributing to make me grow and be as I am, loving me much more than I deserved.

References

- Abbondanzieri, E. a et al., 2008. Dynamic binding orientations direct activity of HIV reverse transcriptase. *Nature*, 453(7192), pp.184–9.
- Aguiar, R.S. & Peterlin, B.M., 2008. APOBEC3 proteins and reverse transcription. *Virus research*, 134(1-2), pp.74–85.
- Alcaro, S. et al., 2010. Computational analysis of Human Immunodeficiency Virus (HIV) Type-1 reverse transcriptase crystallographic models based on significant conserved residues found in Highly Active Antiretroviral Therapy (HAART)-treated patients. *Current medicinal chemistry*, 17(4), pp.290–308. Available at: <http://www.ingentaconnect.com/content/ben/cmc/2010/00000017/00000004/art00001> [Accessed March 2, 2014].
- Álvarez, M. & Menéndez-Arias, L., 2014. Temperature effects on the fidelity of a thermostable HIV-1 reverse transcriptase. *The FEBS journal*, 281(1), pp.342–51. Available at: <http://www.ncbi.nlm.nih.gov/pubmed/24279450> [Accessed February 25, 2014].
- Anon, Glide, version 5.8; Schrodinger, LLC, New York, NY, 2011.
- Anon, MacroModel, version 9.9; Schrodinger, LLC, New York, NY, 2012.
- Anon, Maestro, version 9.3; Schrodinger, LLC: New York, NY, 2012.
- Anon, 1981. Pneumocystis pneumonia--Los Angeles. *MMWR. Morbidity and mortality weekly report*, 30(21), pp.250–2. Available at: <http://www.ncbi.nlm.nih.gov/pubmed/6265753> [Accessed February 20, 2014].
- Arion, D. et al., 1998. Phenotypic mechanism of HIV-1 resistance to 3'-azido-3'-deoxythymidine (AZT): increased polymerization processivity and enhanced sensitivity to pyrophosphate of the mutant viral reverse transcriptase. *Biochemistry*, 37(45), pp.15908–17. Available at: <http://www.ncbi.nlm.nih.gov/pubmed/9843396>.
- Arts, E.J. & Hazuda, D.J., 2012. HIV-1 antiretroviral drug therapy. *Cold Spring Harbor perspectives in medicine*, 2(4), p.a007161. Available at: http://www.pubmedcentral.nih.gov/articlerender.fcgi?artid=3312400&tool=pmcentrez&render_type=abstract [Accessed January 13, 2014].
- Balzarini, J., 2004. Current status of the non-nucleoside reverse transcriptase inhibitors of human immunodeficiency virus type 1. *Current topics in medicinal chemistry*, 4(9), pp.921–44. Available at: <http://www.ncbi.nlm.nih.gov/pubmed/15134549> [Accessed February 25, 2014].

- Barré-Sinoussi, F. et al., 1983. Isolation of a T-lymphotropic retrovirus from a patient at risk for acquired immune deficiency syndrome (AIDS). *Science (New York, N.Y.)*, 220(4599), pp.868–71. Available at: <http://www.ncbi.nlm.nih.gov/pubmed/6189183> [Accessed January 15, 2013].
- Basu, V.P. et al., 2008. Strand transfer events during HIV-1 reverse transcription. *Virus research*, 134(1-2), pp.19–38. Available at: <http://www.ncbi.nlm.nih.gov/pubmed/18279992> [Accessed November 7, 2012].
- Beilhartz, G.L. & Götte, M., 2010. HIV-1 Ribonuclease H: Structure, Catalytic Mechanism and Inhibitors. *Viruses*, 2(4), pp.900–26. Available at: <http://www.pubmedcentral.nih.gov/articlerender.fcgi?artid=3185654&tool=pmcentrez&render type=abstract> [Accessed December 4, 2012].
- Berman, H.M. et al., 2000. The Protein Data Bank. *Nucleic acids research*, 28(1), pp.235–42. Available at: <http://www.pubmedcentral.nih.gov/articlerender.fcgi?artid=102472&tool=pmcentrez&rendert ype=abstract> [Accessed January 24, 2014].
- Boyer, P.L. et al., 2004. Characterization of the polymerase and RNase H activities of human foamy virus reverse transcriptase. *Journal of virology*, 78(12), pp.6112–21. Available at: <http://www.pubmedcentral.nih.gov/articlerender.fcgi?artid=416499&tool=pmcentrez&rendert ype=abstract> [Accessed March 1, 2014].
- Boyer, P.L. et al., 2007. In vitro fidelity of the prototype primate foamy virus (PFV) RT compared to HIV-1 RT. *Virology*, 367(2), pp.253–64. Available at: <http://www.pubmedcentral.nih.gov/articlerender.fcgi?artid=2720797&tool=pmcentrez&render type=abstract> [Accessed February 27, 2014].
- Brehm, J.H. et al., 2007. Selection of mutations in the connection and RNase H domains of human immunodeficiency virus type 1 reverse transcriptase that increase resistance to 3'-azido-3'-dideoxythymidine. *Journal of virology*, 81(15), pp.7852–9. Available at: <http://www.pubmedcentral.nih.gov/articlerender.fcgi?artid=1951314&tool=pmcentrez&render type=abstract> [Accessed January 2, 2013].
- Briggs, J.A.G. et al., 2004. The stoichiometry of Gag protein in HIV-1. *Nature structural & molecular biology*, 11(7), pp.672–5. Available at: <http://www.ncbi.nlm.nih.gov/pubmed/15208690> [Accessed February 24, 2014].
- Broder, S. & Gallo, R.C., 1984. A pathogenic retrovirus (HTLV-III) linked to AIDS. *The New England journal of medicine*, 311(20), pp.1292–7. Available at: <http://www.ncbi.nlm.nih.gov/pubmed/6208484> [Accessed January 15, 2013].
- Budihas, S.R. et al., 2005. Selective inhibition of HIV-1 reverse transcriptase-associated ribonuclease H activity by hydroxylated tropolones. *Nucleic acids research*, 33(4), pp.1249–56. Available at:

<http://www.pubmedcentral.nih.gov/articlerender.fcgi?artid=552956&tool=pmcentrez&rendertype=abstract> [Accessed March 20, 2013].

Champoux, J.J. & Schultz, S.J., 2009. Ribonuclease H: properties, substrate specificity and roles in retroviral reverse transcription. *The FEBS journal*, 276(6), pp.1506–16. Available at: <http://www.pubmedcentral.nih.gov/articlerender.fcgi?artid=2742777&tool=pmcentrez&rendertype=abstract> [Accessed January 2, 2013].

Chen, Y. et al., 2003. Mechanism of minus strand strong stop transfer in HIV-1 reverse transcription. *The Journal of biological chemistry*, 278(10), pp.8006–17. Available at: <http://www.ncbi.nlm.nih.gov/pubmed/12499370> [Accessed February 25, 2014].

Christen, M.T. et al., 2012. Structural basis of the allosteric inhibitor interaction on the HIV-1 reverse transcriptase RNase H domain. *Chemical biology & drug design*, 80(5), pp.706–16. Available at: <http://www.pubmedcentral.nih.gov/articlerender.fcgi?artid=3465473&tool=pmcentrez&rendertype=abstract> [Accessed January 2, 2013].

Chung, S. et al., 2012. Mutagenesis of human immunodeficiency virus reverse transcriptase p51 subunit defines residues contributing to vinylogous urea inhibition of ribonuclease H activity. *The Journal of biological chemistry*, 287(6), pp.4066–75. Available at: <http://www.ncbi.nlm.nih.gov/pubmed/22105069> [Accessed January 2, 2013].

Chung, S. et al., 2010. Structure-activity analysis of vinylogous urea inhibitors of human immunodeficiency virus-encoded ribonuclease H. *Antimicrobial agents and chemotherapy*, 54(9), pp.3913–21. Available at: <http://www.pubmedcentral.nih.gov/articlerender.fcgi?artid=2935023&tool=pmcentrez&rendertype=abstract> [Accessed November 7, 2012].

Chung, S. et al., 2011. Synthesis, activity, and structural analysis of novel α -hydroxytropolone inhibitors of human immunodeficiency virus reverse transcriptase-associated ribonuclease H. *Journal of medicinal chemistry*, 54(13), pp.4462–73. Available at: <http://www.pubmedcentral.nih.gov/articlerender.fcgi?artid=3133734&tool=pmcentrez&rendertype=abstract>.

Clavel, F. et al., 1986. Isolation of a new human retrovirus from West African patients with AIDS. *Science (New York, N.Y.)*, 233(4761), pp.343–6. Available at: <http://www.ncbi.nlm.nih.gov/pubmed/2425430> [Accessed February 24, 2014].

Coffin, J. et al., 1986. Human immunodeficiency viruses. *Science (New York, N.Y.)*, 232(4751), p.697. Available at: <http://www.ncbi.nlm.nih.gov/pubmed/3008335> [Accessed February 24, 2014].

Copeland, R.A., 2013. *Evaluation of Enzyme Inhibitors in Drug Discovery: A Guide for Medicinal Chemists and Pharmacologists* second., Wiley.

- Corona, A. et al., 2013. Active site and allosteric inhibitors of the ribonuclease H activity of HIV reverse transcriptase. *Future Med. Chem.*, 5(18), pp.2127–2139.
- Costi, R. et al., 2013. 6-(*N*-Benzyl-1*H*-pyrrol-2-yl)-2, 4-dioxo-5-hexenoic Acids as Dual Inhibitors of recombinant HIV-1 Integrase and Ribonuclease H, Synthesized by a Parallel Synthesis Approach. *Journal of medicinal ...*, (i). Available at: <http://medcontent.metapress.com/index/A65RM03P4874243N.pdf> [Accessed November 19, 2013].
- Cummings, M.D., Farnum, M. a & Nelen, M.I., 2006. Universal screening methods and applications of ThermoFluor. *Journal of biomolecular screening*, 11(7), pp.854–63. Available at: <http://www.ncbi.nlm.nih.gov/pubmed/16943390> [Accessed November 7, 2012].
- Damgaard, C.K. et al., 2004. RNA Interactions in the 5' Region of the HIV-1 Genome. *Journal of Molecular Biology*, 336(2), pp.369–379. Available at: <http://www.sciencedirect.com/science/article/pii/S0022283603014797> [Accessed February 17, 2014].
- Das, K. et al., 2011. Crystal structure of tert-butyldimethylsilyl-spiroaminooxathiole-dioxide-thymine (TSAO-T) in complex with HIV-1 reverse transcriptase (RT) redefines the elastic limits of the non-nucleoside inhibitor-binding pocket. *Journal of medicinal chemistry*, 54(8), pp.2727–37. Available at: http://www.pubmedcentral.nih.gov/articlerender.fcgi?artid=3361896&tool=pmcentrez&render_type=abstract [Accessed February 18, 2014].
- Das, K. et al., 1996. Crystal structures of 8-Cl and 9-Cl TIBO complexed with wild-type HIV-1 RT and 8-Cl TIBO complexed with the Tyr181Cys HIV-1 RT drug-resistant mutant. *Journal of molecular biology*, 264(5), pp.1085–100. Available at: <http://www.ncbi.nlm.nih.gov/pubmed/9000632> [Accessed February 25, 2014].
- Das, K. et al., 2005. Crystallography and the design of anti-AIDS drugs: conformational flexibility and positional adaptability are important in the design of non-nucleoside HIV-1 reverse transcriptase inhibitors. *Progress in biophysics and molecular biology*, 88(2), pp.209–31. Available at: <http://www.ncbi.nlm.nih.gov/pubmed/15572156> [Accessed November 7, 2012].
- Das, K. et al., 2008. High-resolution structures of HIV-1 reverse transcriptase/TMC278 complexes: strategic flexibility explains potency against resistance mutations. *Proceedings of the National Academy of Sciences of the United States of America*, 105(5), pp.1466–71. Available at: http://www.pubmedcentral.nih.gov/articlerender.fcgi?artid=2234167&tool=pmcentrez&render_type=abstract [Accessed February 18, 2014].
- Dash, C. et al., 2008. Examining the ribonuclease H primer grip of HIV-1 reverse transcriptase by charge neutralization of RNA/DNA hybrids. *Nucleic acids research*, 36(20), pp.6363–71. Available at: http://www.pubmedcentral.nih.gov/articlerender.fcgi?artid=2582618&tool=pmcentrez&render_type=abstract [Accessed January 2, 2013].

- Delelis, O. et al., 2007. Efficient and specific internal cleavage of a retroviral palindromic DNA sequence by tetrameric HIV-1 integrase. *PLoS one*, 2(7), p.e608. Available at: <http://www.pubmedcentral.nih.gov/articlerender.fcgi?artid=1905944&tool=pmcentrez&render type=abstract> [Accessed March 5, 2014].
- Delelis, O. et al., 2010. Impact of Y143 HIV-1 integrase mutations on resistance to raltegravir in vitro and in vivo. *Antimicrobial agents and chemotherapy*, 54(1), pp.491–501. Available at: <http://www.pubmedcentral.nih.gov/articlerender.fcgi?artid=2798554&tool=pmcentrez&render type=abstract> [Accessed February 28, 2014].
- Delviks-Frankenberry, K. a et al., 2008. HIV-1 reverse transcriptase connection subdomain mutations reduce template RNA degradation and enhance AZT excision. *Proceedings of the National Academy of Sciences of the United States of America*, 105(31), pp.10943–8. Available at: <http://www.pubmedcentral.nih.gov/articlerender.fcgi?artid=2491488&tool=pmcentrez&render type=abstract>.
- Dharmasena, S. et al., 2007. 3'-Azido-3'-deoxythymidine-(5')-tetraphospho-(5')-adenosine, the product of ATP-mediated excision of chain-terminating AZTMP, is a potent chain-terminating substrate for HIV-1 reverse transcriptase. *Biochemistry*, 46(3), pp.828–36. Available at: <http://www.ncbi.nlm.nih.gov/pubmed/17223704> [Accessed January 2, 2013].
- Ding, J. et al., 1995. Structure of HIV-1 RT/TIBO R 86183 complex reveals similarity in the binding of diverse nonnucleoside inhibitors. *Nature structural biology*, 2(5), pp.407–15. Available at: <http://www.ncbi.nlm.nih.gov/pubmed/7545077> [Accessed February 25, 2014].
- Distinto, S. et al., 2012. Identification of HIV-1 reverse transcriptase dual inhibitors by a combined shape-, 2D-fingerprint- and pharmacophore-based virtual screening approach. *European journal of medicinal chemistry*, 50, pp.216–29. Available at: <http://www.ncbi.nlm.nih.gov/pubmed/22361685> [Accessed November 2, 2012].
- Distinto, S. et al., 2013. Molecular Aspects of the RT/drug Interactions. Perspective of Dual Inhibitors. *Current pharmaceutical design*, 19(10), pp.1850–9. Available at: <http://www.ncbi.nlm.nih.gov/pubmed/23092286>.
- Divita, G. et al., 1995. Dimerization kinetics of HIV-1 and HIV-2 reverse transcriptase: a two step process. *Journal of molecular biology*, 245(5), pp.508–21. Available at: <http://www.ncbi.nlm.nih.gov/pubmed/7531247>.
- Doms, R.W., 2000. The plasma membrane as a combat zone in the HIV battlefield. *Genes & Development*, 14(21), pp.2677–2688. Available at: <http://www.genesdev.org/cgi/doi/10.1101/gad.833300> [Accessed February 24, 2014].
- Esposito, F. et al., 2011. Alizarine derivatives as new dual inhibitors of the HIV-1 reverse transcriptase-associated DNA polymerase and RNase H activities effective also on the RNase H activity of non-nucleoside resistant reverse transcriptases. *The FEBS journal*, 278(9),

pp.1444–57. Available at: <http://www.ncbi.nlm.nih.gov/pubmed/21348941> [Accessed January 2, 2013].

Esposito, F., Corona, A. & Tramontano, E., 2012. HIV-1 Reverse Transcriptase Still Remains a New Drug Target: Structure, Function, Classical Inhibitors, and New Inhibitors with Innovative Mechanisms of Actions. *Molecular biology international*, 2012, p.586401. Available at: <http://www.pubmedcentral.nih.gov/articlerender.fcgi?artid=3388302&tool=pmcentrez&render type=abstract>.

Feinstein, L. & Dimomfu, B., 2013. Global report: UNAIDS report on the global AIDS epidemic 2013. *Tropical Medicine and ...*. Available at: <http://www.popline.org/taxonomy/term/55091> [Accessed February 20, 2014].

Felts, A.K. et al., 2011. Identification of alternative binding sites for inhibitors of HIV-1 ribonuclease H through comparative analysis of virtual enrichment studies. *Journal of chemical information and modeling*, 51(8), pp.1986–98. Available at: <http://www.pubmedcentral.nih.gov/articlerender.fcgi?artid=3159817&tool=pmcentrez&render type=abstract>.

Figueiredo, A. et al., 2006. Potent nonnucleoside reverse transcriptase inhibitors target HIV-1 Gag-Pol. *PLoS pathogens*, 2(11), p.e119. Available at: <http://www.pubmedcentral.nih.gov/articlerender.fcgi?artid=1635531&tool=pmcentrez&render type=abstract> [Accessed April 13, 2014].

Freed, E.O., 2001. HIV-1 replication. *Somatic cell and molecular genetics*, 26(1-6), pp.13–33. Available at: <http://www.ncbi.nlm.nih.gov/pubmed/12465460> [Accessed February 24, 2014].

Freed, E.O. & Martin, A.M., 2007. HIVs and Their Replication. In D. M. Knipe & P. M. Howley, eds. *Fields Virology*. Philadelphia, PA 19106 USA: Lippincott Williams & Wilkins, pp. 2107–2185.

Fuji, H. et al., 2009. Derivatives of 5-nitro-furan-2-carboxylic acid carbamoylmethyl ester inhibit RNase H activity associated with HIV-1 reverse transcriptase. *Journal of medicinal chemistry*, 52(5), pp.1380–7. Available at: <http://www.ncbi.nlm.nih.gov/pubmed/19178289> [Accessed March 20, 2013].

Furfine, E.S. & Reardon, J.E., 1991. Reverse Transcriptase/RNase H from the Human Immunodeficiency Virus. , pp.406–412.

Ganser-Pornillos, B.K., Yeager, M. & Pornillos, O., 2012. Assembly and architecture of HIV. *Advances in experimental medicine and biology*, 726, pp.441–65. Available at: <http://www.ncbi.nlm.nih.gov/pubmed/22297526> [Accessed February 24, 2014].

- Gelderblom, H.C. et al., 2008. Viral complementation allows HIV-1 replication without integration. *Retrovirology*, 5(1), p.60. Available at: <http://www.retrovirology.com/content/5/1/60> [Accessed February 11, 2014].
- Goff, S.P., 2007. Host factors exploited by retroviruses. *Nature reviews. Microbiology*, 5(4), pp.253–63. Available at: <http://www.ncbi.nlm.nih.gov/pubmed/17325726> [Accessed November 12, 2012].
- Gong, Q. et al., 2011. Interaction of HIV-1 reverse transcriptase ribonuclease H with an acylhydrazone inhibitor. *Chemical biology & drug design*, 77(1), pp.39–47. Available at: <http://www.pubmedcentral.nih.gov/articlerender.fcgi?artid=3320797&tool=pmcentrez&render type=abstract> [Accessed January 2, 2013].
- Gopalakrishnan, V., Peliska, J. a & Benkovic, S.J., 1992. Human immunodeficiency virus type 1 reverse transcriptase: spatial and temporal relationship between the polymerase and RNase H activities. *Proceedings of the National Academy of Sciences of the United States of America*, 89(22), pp.10763–7. Available at: <http://www.pubmedcentral.nih.gov/articlerender.fcgi?artid=50422&tool=pmcentrez&rendertype=abstract>.
- Gottlieb, G.S. et al., 2002. Equal plasma viral loads predict a similar rate of CD4+ T cell decline in human immunodeficiency virus (HIV) type 1- and HIV-2-infected individuals from Senegal, West Africa. *The Journal of infectious diseases*, 185(7), pp.905–14. Available at: <http://www.ncbi.nlm.nih.gov/pubmed/11920314> [Accessed February 24, 2014].
- Di Grandi, M. et al., 2010. Small molecule inhibitors of HIV RT Ribonuclease H. *Bioorganic & medicinal chemistry letters*, 20(1), pp.398–402. Available at: <http://www.ncbi.nlm.nih.gov/pubmed/19939680> [Accessed March 20, 2013].
- Hachiya, A. et al., 2008. Amino acid mutation N348I in the connection subdomain of human immunodeficiency virus type 1 reverse transcriptase confers multiclass resistance to nucleoside and nonnucleoside reverse transcriptase inhibitors. *Journal of virology*, 82(7), pp.3261–70. Available at: <http://www.pubmedcentral.nih.gov/articlerender.fcgi?artid=2268505&tool=pmcentrez&render type=abstract> [Accessed January 2, 2013].
- Hartl, M.J. et al., 2010. Biophysical and enzymatic properties of the simian and prototype foamy virus reverse transcriptases. *Retrovirology*, 7, p.5. Available at: <http://www.pubmedcentral.nih.gov/articlerender.fcgi?artid=2835651&tool=pmcentrez&render type=abstract> [Accessed February 27, 2014].
- Hartl, M.J. et al., 2011. Regulation of foamy virus protease activity by viral RNA: a novel and unique mechanism among retroviruses. *Journal of virology*, 85(9), pp.4462–9. Available at: <http://www.pubmedcentral.nih.gov/articlerender.fcgi?artid=3126251&tool=pmcentrez&render type=abstract> [Accessed February 27, 2014].

- Hasel, W., Hendrickson, T.F. & Still, W.C., 1988. No Title. *Tetrahedron Computer Methodology*, 1(2), pp.103–116.
- Hazuda, D.J. et al., 2004. A naphthyridine carboxamide provides evidence for discordant resistance between mechanistically identical inhibitors of HIV-1 integrase. *Proceedings of the National Academy of Sciences of the United States of America*, 101(31), pp.11233–8. Available at: <http://www.pubmedcentral.nih.gov/articlerender.fcgi?artid=509174&tool=pmcentrez&rendertype=abstract> [Accessed February 3, 2014].
- Herman, B.D. & Sluis-Cremer, N., 2013. Transient kinetic analyses of the ribonuclease H cleavage activity of HIV-1 reverse transcriptase in complex with efavirenz and/or a β -thujaplicinol analogue. *The Biochemical journal*, 455(2), pp.179–84. Available at: <http://www.biochemj.org/bj/455/bj4550179.htm> [Accessed February 19, 2014].
- Herschhorn, A. & Hizi, A., 2010. Retroviral reverse transcriptases. *Cellular and molecular life sciences : CMLS*, 67(16), pp.2717–47. Available at: <http://www.ncbi.nlm.nih.gov/pubmed/20358252> [Accessed March 18, 2013].
- Himmel, D.M. et al., 2006. HIV-1 reverse transcriptase structure with RNase H inhibitor dihydroxy benzoyl naphthyl hydrazone bound at a novel site. *ACS chemical biology*, 1(11), pp.702–12. Available at: <http://www.pubmedcentral.nih.gov/articlerender.fcgi?artid=2963427&tool=pmcentrez&rendertype=abstract>.
- Himmel, D.M. et al., 2009. Structure of HIV-1 reverse transcriptase with the inhibitor beta-Thujaplicinol bound at the RNase H active site. *Structure (London, England : 1993)*, 17(12), pp.1625–35. Available at: <http://www.pubmedcentral.nih.gov/articlerender.fcgi?artid=3365588&tool=pmcentrez&rendertype=abstract> [Accessed December 31, 2012].
- HIZI, A., McGill, C. & Hughes, S., 1988. Expression of soluble, enzymatically active, human immunodeficiency virus reverse transcriptase in Escherichia coli and analysis of mutants. *Proceedings of the National ...*, 85(February), pp.1218–1222. Available at: <http://www.pnas.org/content/85/4/1218.short> [Accessed February 24, 2014].
- Huber, H.E. & Richardson, C.C., 1990. Processing of the primer for plus strand DNA synthesis by human immunodeficiency virus 1 reverse transcriptase. *The Journal of biological chemistry*, 265(18), pp.10565–73. Available at: <http://www.ncbi.nlm.nih.gov/pubmed/1693920> [Accessed February 25, 2014].
- Jacobo-Molina, A. et al., 1993. Crystal structure of human immunodeficiency virus type 1 reverse transcriptase complexed with double-stranded DNA at 3.0 Å resolution shows bent DNA. *Proceedings of the National Academy of Sciences of the United States of America*, 90(13), pp.6320–4. Available at: <http://www.pubmedcentral.nih.gov/articlerender.fcgi?artid=46920&tool=pmcentrez&rendertype=abstract> [Accessed June 30, 2013].

- Ji, X., Klarmann, G.J. & Preston, B.D., 1996. Effect of human immunodeficiency virus type 1 (HIV-1) nucleocapsid protein on HIV-1 reverse transcriptase activity in vitro. *Biochemistry*, 35(1), pp.132–43. Available at: <http://www.ncbi.nlm.nih.gov/pubmed/8555166>.
- Jorgensen, W.L., Maxwell, D.S. & Tirado-rives, J., 1996. Development and Testing of the OPLS All-Atom Force Field on Conformational Energetics and Properties of Organic Liquids. , 7863(15), pp.11225–11236.
- Julias, J.G. et al., 2002. Mutations in the RNase H domain of HIV-1 reverse transcriptase affect the initiation of DNA synthesis and the specificity of RNase H cleavage in vivo. *Proceedings of the National Academy of Sciences of the United States of America*, 99(14), pp.9515–20. Available at: <http://www.pubmedcentral.nih.gov/articlerender.fcgi?artid=123172&tool=pmcentrez&rendertype=abstract>.
- Kaminski, G.A. et al., 2001. Evaluation and Reparametrization of the OPLS-AA Force Field for Proteins via Comparison with Accurate Quantum Chemical Calculations on Peptides †. *The Journal of Physical Chemistry B*, 105(28), pp.6474–6487. Available at: <http://dx.doi.org/10.1021/jp003919d> [Accessed January 30, 2014].
- Kirschberg, T. a et al., 2009. RNase H active site inhibitors of human immunodeficiency virus type 1 reverse transcriptase: design, biochemical activity, and structural information. *Journal of medicinal chemistry*, 52(19), pp.5781–4. Available at: <http://www.ncbi.nlm.nih.gov/pubmed/19791799> [Accessed March 20, 2013].
- Klumpp, K., 2003. Two-metal ion mechanism of RNA cleavage by HIV RNase H and mechanism-based design of selective HIV RNase H inhibitors. *Nucleic Acids Research*, 31(23), pp.6852–6859. Available at: <http://www.nar.oupjournals.org/cgi/doi/10.1093/nar/gkg881> [Accessed November 27, 2012].
- Klumpp, K. & Mirzadegan, T., 2006. Recent progress in the design of small molecule inhibitors of HIV RNase H. *Current pharmaceutical design*, 12(15), pp.1909–22. Available at: <http://www.ncbi.nlm.nih.gov/pubmed/16724956>.
- Kohlstaedt, L.A. et al., 1992. Crystal structure at 3.5 Å resolution of HIV-1 reverse transcriptase complexed with an inhibitor. *Science (New York, N.Y.)*, 256(5065), pp.1783–90. Available at: <http://www.ncbi.nlm.nih.gov/pubmed/1377403> [Accessed February 25, 2014].
- Kollman, P.A. et al., 2000. Calculating structures and free energies of complex molecules: combining molecular mechanics and continuum models. *Accounts of chemical research*, 33(12), pp.889–97. Available at: <http://www.ncbi.nlm.nih.gov/pubmed/11123888> [Accessed February 10, 2014].
- Lansdon, E.B. et al., 2011. Structural and binding analysis of pyrimidinol carboxylic acid and N-hydroxy quinazolinedione HIV-1 RNase H inhibitors. *Antimicrobial agents and chemotherapy*, 55(6), pp.2905–15. Available at:

<http://www.pubmedcentral.nih.gov/articlerender.fcgi?artid=3101433&tool=pmcentrez&render type=abstract> [Accessed January 2, 2013].

Leo, B., Hartl, M.J., et al., 2012. Insights into the structure and activity of prototype foamy virus RNase H. *Retrovirology*, 9(1), p.14. Available at: <http://www.pubmedcentral.nih.gov/articlerender.fcgi?artid=3305377&tool=pmcentrez&render type=abstract> [Accessed February 26, 2014].

Leo, B., Schweimer, K., et al., 2012. The solution structure of the prototype foamy virus RNase H domain indicates an important role of the basic loop in substrate binding. *Retrovirology*, 9, p.73. Available at: <http://www.pubmedcentral.nih.gov/articlerender.fcgi?artid=3443672&tool=pmcentrez&render type=abstract> [Accessed February 27, 2014].

Linial, M., 2007. Foamy viruses. In D. M. Knipe & P. M. Howley, eds. *Fields Virology*. Lippincott Williams & Wilkins, pp. 2245–2262.

Liu, S. et al., 2008. Slide into action: dynamic shuttling of HIV reverse transcriptase on nucleic acid substrates. *Science (New York, N.Y.)*, 322(5904), pp.1092–7. Available at: <http://www.pubmedcentral.nih.gov/articlerender.fcgi?artid=2717043&tool=pmcentrez&render type=abstract> [Accessed January 2, 2013].

Masaoka, T. et al., 2013. Exploiting Drug-Resistant Enzymes as Tools To Identify Thienopyrimidinone Inhibitors of Human Immunodeficiency Virus Reverse Transcriptase-Associated Ribonuclease H. *Journal of medicinal chemistry*. Available at: <http://www.ncbi.nlm.nih.gov/pubmed/23631411>.

Maurin, C. et al., 2004. Spectroscopic studies of diketoacids-metal interactions. A probing tool for the pharmacophoric intermetallic distance in the HIV-1 integrase active site. *Journal of medicinal chemistry*, 47(22), pp.5583–6. Available at: <http://www.ncbi.nlm.nih.gov/pubmed/15481994> [Accessed February 28, 2014].

Mehellou, Y. & De Clercq, E., 2010. Twenty-six years of anti-HIV drug discovery: where do we stand and where do we go? *Journal of medicinal chemistry*, 53(2), pp.521–38. Available at: <http://www.ncbi.nlm.nih.gov/pubmed/19785437> [Accessed November 8, 2012].

Menéndez-Arias, L., 2008. Mechanisms of resistance to nucleoside analogue inhibitors of HIV-1 reverse transcriptase. *Virus research*, 134(1-2), pp.124–46. Available at: <http://www.ncbi.nlm.nih.gov/pubmed/18272247> [Accessed November 11, 2012].

Menéndez-Arias, L. et al., 2008. RNase H activity: structure, specificity, and function in reverse transcription. *Virus research*, 134(1-2), pp.86–103. Available at: <http://www.pubmedcentral.nih.gov/articlerender.fcgi?artid=2464458&tool=pmcentrez&render type=abstract> [Accessed December 9, 2012].

- Meyer, P.R. et al., 1999. A mechanism of AZT resistance: an increase in nucleotide-dependent primer unblocking by mutant HIV-1 reverse transcriptase. *Molecular cell*, 4(1), pp.35–43. Available at: <http://www.ncbi.nlm.nih.gov/pubmed/10445025> [Accessed April 12, 2014].
- Mizrahi, V. et al., 1990. Site-directed mutagenesis of the conserved Asp-443 and Asp-498 carboxy-terminal residues of HIV-1 reverse transcriptase. *Nucleic acids research*, 18(18), pp.5359–63. Available at: <http://www.pubmedcentral.nih.gov/articlerender.fcgi?artid=332210&tool=pmcentrez&rendertype=abstract>.
- Mizrahi, V., Brooksbank, R. & Nkabinde, N., 1994. acid 478, asparagine 494, and aspartic acid 498 residues in the ribonuclease H domain of p66/p51 human immunodeficiency virus type I reverse transcriptase. *Journal of Biological Chemistry*. Available at: <http://www.jbc.org/content/269/30/19245.short> [Accessed February 24, 2014].
- Mui, P.W. et al., 1992. Crystal structure of nevirapine, a non-nucleoside inhibitor of HIV-1 reverse transcriptase, and computational alignment with a structurally diverse inhibitor. *Journal of medicinal chemistry*, 35(1), pp.201–2. Available at: <http://www.ncbi.nlm.nih.gov/pubmed/1370694> [Accessed February 25, 2014].
- Munir, S. et al., 2013. Quantitative analysis of the time-course of viral DNA forms during the HIV-1 life cycle. *Retrovirology*, 10(1), p.87. Available at: <http://www.pubmedcentral.nih.gov/articlerender.fcgi?artid=3766001&tool=pmcentrez&renderertype=abstract> [Accessed November 4, 2013].
- Nettleship, J.E. et al., 2008. Methods for protein characterization by mass spectrometry, thermal shift (ThermoFluor) assay, and multiangle or static light scattering. *Methods in molecular biology (Clifton, N.J.)*, 426, pp.299–318. Available at: <http://www.ncbi.nlm.nih.gov/pubmed/18542872>.
- Nikolenko, G.N. et al., 2007. Mutations in the connection domain of HIV-1 reverse transcriptase increase 3'-azido-3'-deoxythymidine resistance. *Proceedings of the National Academy of Sciences of the United States of America*, 104(1), pp.317–22. Available at: <http://www.pubmedcentral.nih.gov/articlerender.fcgi?artid=1765458&tool=pmcentrez&renderertype=abstract>.
- Nowotny, M. et al., 2005. Crystal structures of RNase H bound to an RNA/DNA hybrid: substrate specificity and metal-dependent catalysis. *Cell*, 121(7), pp.1005–16. Available at: <http://www.ncbi.nlm.nih.gov/pubmed/15989951> [Accessed November 23, 2012].
- Palaniappan, C. et al., 1997. Mutations within the primer grip region of HIV-1 reverse transcriptase result in loss of RNase H function. *The Journal of biological chemistry*, 272(17), pp.11157–64. Available at: <http://www.jbc.org/content/272/17/11157.short> [Accessed February 13, 2014].

- Palaniappan, C. & Wisniewski, M., 1997. Mutations within the primer grip region of HIV-1 reverse transcriptase result in loss of RNase H function. *Journal of Biological Chemistry*, 272(17), pp.11157–11162. Available at: <http://www.jbc.org/content/272/17/11157.short> [Accessed February 13, 2014].
- Paris, K.A. et al., 2009. Conformational landscape of the human immunodeficiency virus type 1 reverse transcriptase non-nucleoside inhibitor binding pocket: lessons for inhibitor design from a cluster analysis of many crystal structures. *Journal of medicinal chemistry*, 52(20), pp.6413–20. Available at: http://www.pubmedcentral.nih.gov/articlerender.fcgi?artid=3182518&tool=pmcentrez&render_type=abstract [Accessed February 28, 2014].
- Pata, J.D. et al., 2004. Structure of HIV-1 reverse transcriptase bound to an inhibitor active against mutant reverse transcriptases resistant to other nonnucleoside inhibitors. *Proceedings of the National Academy of Sciences of the United States of America*, 101(29), pp.10548–53. Available at: http://www.pubmedcentral.nih.gov/articlerender.fcgi?artid=489975&tool=pmcentrez&render_type=abstract.
- Pfafferl, K.I. et al., 1998. Molecular characterization of proteolytic processing of the Pol proteins of human foamy virus reveals novel features of the viral protease. *Journal of virology*, 72(9), pp.7648–52. Available at: http://www.pubmedcentral.nih.gov/articlerender.fcgi?artid=110030&tool=pmcentrez&render_type=abstract [Accessed March 1, 2014].
- Ratner, L. et al., 1985. Complete nucleotide sequence of the AIDS virus, HTLV-III. *Nature*, 313(6000), pp.277–84. Available at: <http://www.ncbi.nlm.nih.gov/pubmed/2578615> [Accessed February 24, 2014].
- Rausch, J.W. et al., 2002. Altering the RNase H primer grip of human immunodeficiency virus reverse transcriptase modifies cleavage specificity. *Biochemistry*, 41(15), pp.4856–65. Available at: <http://www.ncbi.nlm.nih.gov/pubmed/11939780>.
- Rausch, J.W. & Le Grice, S.F.J., 2004. “Binding, bending and bonding”: polypurine tract-primed initiation of plus-strand DNA synthesis in human immunodeficiency virus. *The international journal of biochemistry & cell biology*, 36(9), pp.1752–66. Available at: <http://www.ncbi.nlm.nih.gov/pubmed/15183342> [Accessed January 2, 2013].
- Ren, J., 2000. Binding of the Second Generation Non-nucleoside Inhibitor S-1153 to HIV-1 Reverse Transcriptase Involves Extensive Main Chain Hydrogen Bonding. *Journal of Biological Chemistry*, 275(19), pp.14316–14320. Available at: <http://www.jbc.org/content/275/19/14316.long> [Accessed February 18, 2014].
- Ren, J. et al., 1995. High resolution structures of HIV-1 RT from four RT-inhibitor complexes. *Nature structural biology*, 2(4), pp.293–302. Available at: <http://www.ncbi.nlm.nih.gov/pubmed/7540934> [Accessed February 18, 2014].

- Ren, J. & Stammers, D.K., 2008. Structural basis for drug resistance mechanisms for non-nucleoside inhibitors of HIV reverse transcriptase. *Virus research*, 134(1-2), pp.157–70. Available at: <http://www.ncbi.nlm.nih.gov/pubmed/18313784> [Accessed December 5, 2012].
- Rinke, C.S. et al., 2002. Mutation of the catalytic domain of the foamy virus reverse transcriptase leads to loss of processivity and infectivity. *Journal of virology*, 76(15), pp.7560–70. Available at: <http://www.pubmedcentral.nih.gov/articlerender.fcgi?artid=136390&tool=pmcentrez&rendertype=abstract> [Accessed March 1, 2014].
- Roquebert, B. & Marcelin, A.-G., 2008. The involvement of HIV-1 RNase H in resistance to nucleoside analogues. *The Journal of antimicrobial chemotherapy*, 61(5), pp.973–5. Available at: <http://www.ncbi.nlm.nih.gov/pubmed/18325896> [Accessed January 2, 2013].
- Rosta, E. et al., 2011. Catalytic mechanism of RNA backbone cleavage by ribonuclease H from quantum mechanics/molecular mechanics simulations. *Journal of the American Chemical Society*, 133(23), pp.8934–41. Available at: <http://www.pubmedcentral.nih.gov/articlerender.fcgi?artid=3110985&tool=pmcentrez&rendertype=abstract> [Accessed November 5, 2012].
- Roy, J. & Linial, M.L., 2007. Role of the foamy virus Pol cleavage site in viral replication. *Journal of virology*, 81(10), pp.4956–62. Available at: <http://www.pubmedcentral.nih.gov/articlerender.fcgi?artid=1900213&tool=pmcentrez&rendertype=abstract> [Accessed February 27, 2014].
- Sarafianos, S.G. et al., 2001. Crystal structure of HIV-1 reverse transcriptase in complex with a polypurine tract RNA:DNA. *The EMBO journal*, 20(6), pp.1449–61. Available at: <http://www.pubmedcentral.nih.gov/articlerender.fcgi?artid=145536&tool=pmcentrez&rendertype=abstract>.
- Sarafianos, S.G. et al., 2009. Structure and function of HIV-1 reverse transcriptase: molecular mechanisms of polymerization and inhibition. *Journal of molecular biology*, 385(3), pp.693–713. Available at: <http://www.pubmedcentral.nih.gov/articlerender.fcgi?artid=2881421&tool=pmcentrez&rendertype=abstract> [Accessed November 11, 2012].
- Schäfer, W. et al., 1993. Non-nucleoside inhibitors of HIV-1 reverse transcriptase: molecular modeling and X-ray structure investigations. *Journal of medicinal chemistry*, 36(6), pp.726–32. Available at: <http://www.ncbi.nlm.nih.gov/pubmed/7681480> [Accessed February 25, 2014].
- Schatz, O. et al., 1990. Inactivation of the RNase H domain of HIV-1 reverse transcriptase blocks viral infectivity. *Gene regulation and AIDS*. Available at: <http://scholar.google.com/scholar?hl=en&btnG=Search&q=intitle:Inactivation+of+the+RNase+H+domain+of+HIV-1+reverse+transcriptase+blocks+viral+infectivity.#0> [Accessed January 17, 2014].

- Schatz, O. et al., 1989. *Point mutations in conserved amino acid residues within the C-terminal domain of HIV-1 reverse transcriptase specifically repress RNase H function*, Available at: <http://www.sciencedirect.com/science/article/pii/0014579389815595> [Accessed January 16, 2014].
- Shaw-Reid, C. a et al., 2005. Dissecting the effects of DNA polymerase and ribonuclease H inhibitor combinations on HIV-1 reverse-transcriptase activities. *Biochemistry*, 44(5), pp.1595–606. Available at: <http://www.ncbi.nlm.nih.gov/pubmed/15683243>.
- Shaw-Reid, C. a et al., 2003. Inhibition of HIV-1 ribonuclease H by a novel diketo acid, 4-[5-(benzoylamino)thien-2-yl]-2,4-dioxobutanoic acid. *The Journal of biological chemistry*, 278(5), pp.2777–80. Available at: <http://www.ncbi.nlm.nih.gov/pubmed/12480948> [Accessed January 2, 2013].
- Sluis-Cremer, N. et al., 2004. Proteolytic processing of an HIV-1 pol polyprotein precursor: insights into the mechanism of reverse transcriptase p66/p51 heterodimer formation. *The international journal of biochemistry & cell biology*, 36(9), pp.1836–47. Available at: <http://www.ncbi.nlm.nih.gov/pubmed/15183348> [Accessed November 6, 2012].
- Steitz, T. a, 1999. DNA polymerases: structural diversity and common mechanisms. *The Journal of biological chemistry*, 274(25), pp.17395–8. Available at: <http://www.ncbi.nlm.nih.gov/pubmed/10364165>.
- Su, H.-P., Yan, Y., Prasad, G.S., Smith, R.F., Daniels, C.L., Abeywickrema, P.D., Reid, J.C., Loughran, H.M., Kornienko, M., Sharma, S., Grobler, J. a, et al., 2010. Structural basis for the inhibition of RNase H activity of HIV-1 reverse transcriptase by RNase H active site-directed inhibitors. *Journal of virology*, 84(15), pp.7625–33. Available at: <http://www.pubmedcentral.nih.gov/articlerender.fcgi?artid=2897604&tool=pmcentrez&render type=abstract> [Accessed March 20, 2013].
- Su, H.-P., Yan, Y., Prasad, G.S., Smith, R.F., Daniels, C.L., Abeywickrema, P.D., Reid, J.C., Loughran, H.M., Kornienko, M., Sharma, S., Grobler, J.A., et al., 2010. Structural basis for the inhibition of RNase H activity of HIV-1 reverse transcriptase by RNase H active site-directed inhibitors. *Journal of virology*, 84(15), pp.7625–33. Available at: <http://www.pubmedcentral.nih.gov/articlerender.fcgi?artid=2897604&tool=pmcentrez&render type=abstract> [Accessed January 2, 2013].
- Suchaud, V. et al., 2012. Development of a series of 3-hydroxyquinolin-2(1H)-ones as selective inhibitors of HIV-1 reverse transcriptase associated RNase H activity. *Bioorganic & medicinal chemistry letters*, 22(12), pp.3988–92. Available at: <http://www.ncbi.nlm.nih.gov/pubmed/22607675> [Accessed January 2, 2013].
- Tomassini, J. et al., 1994. Inhibition of cap (m⁷GpppXm)-dependent endonuclease of influenza virus by 4-substituted 2,4-dioxobutanoic acid compounds. *Antimicrobial agents and chemotherapy*, 38(12), pp.2827–37. Available at:

<http://www.pubmedcentral.nih.gov/articlerender.fcgi?artid=188292&tool=pmcentrez&rendertype=abstract>.

Tramontano, E. et al., 2005. 6-[1-(4-Fluorophenyl)methyl-1H-pyrrol-2-yl]-2,4-dioxo-5-hexenoic acid ethyl ester a novel diketo acid derivative which selectively inhibits the HIV-1 viral replication in cell culture and the ribonuclease H activity in vitro. *Antiviral research*, 65(2), pp.117–24. Available at: <http://www.ncbi.nlm.nih.gov/pubmed/15708638> [Accessed January 2, 2013].

Tramontano, E., 2006. HIV-1 RNase H: recent progress in an exciting, yet little explored, drug target. *Mini reviews in medicinal chemistry*, 6(6), pp.727–37. Available at: <http://www.ncbi.nlm.nih.gov/pubmed/16787384> [Accessed January 14, 2014].

Tramontano, E. & Di Santo, R., 2010. HIV-1 RT-associated RNase H function inhibitors: Recent advances in drug development. *Current medicinal chemistry*, 17(26), pp.2837–53. Available at: <http://www.ncbi.nlm.nih.gov/pubmed/20858167>.

Trott, O. & Olson, A.J., 2010. AutoDock Vina: improving the speed and accuracy of docking with a new scoring function, efficient optimization, and multithreading. *Journal of computational chemistry*, 31(2), pp.455–61. Available at: <http://www.pubmedcentral.nih.gov/articlerender.fcgi?artid=3041641&tool=pmcentrez&rendertype=abstract> [Accessed February 20, 2014].

Tsibris, A.M.N. & Hirsch, M.S., 2010. Antiretroviral therapy in the clinic. *Journal of virology*, 84(11), pp.5458–64. Available at: <http://www.pubmedcentral.nih.gov/articlerender.fcgi?artid=2876604&tool=pmcentrez&rendertype=abstract> [Accessed January 2, 2013].

Wai, J.S. et al., 2000. 4-Aryl-2,4-dioxobutanoic acid inhibitors of HIV-1 integrase and viral replication in cells. *Journal of medicinal chemistry*, 43(26), pp.4923–6. Available at: <http://www.ncbi.nlm.nih.gov/pubmed/11150161> [Accessed February 3, 2014].

Yahi, N. et al., 2005. Structural analysis of reverse transcriptase mutations at codon 215 explains the predominance of T215Y over T215F in HIV-1 variants selected under antiretroviral therapy. *Journal of biomedical science*, 12(5), pp.701–10. Available at: <http://www.ncbi.nlm.nih.gov/pubmed/16200350> [Accessed December 13, 2012].

Yap, S. et al., 2007. N348I in the Connection Domain of HIV-1 Reverse Transcriptase Confers Zidovudine and Nevirapine Resistance. , 4(12).

Yonetani, T., 1982. The Yonetani-Theorell graphical method for examining overlapping subsites of enzyme active centers. *Methods in enzymology*, 87, pp.500–9. Available at: <http://www.ncbi.nlm.nih.gov/pubmed/6757651> [Accessed February 24, 2014].

Yu, S.F. et al., 1996. Human foamy virus replication: a pathway distinct from that of retroviruses and hepadnaviruses. *Science (New York, N.Y.)*, 271(5255), pp.1579–82. Available at: <http://www.ncbi.nlm.nih.gov/pubmed/8599113> [Accessed March 1, 2014].

Zamborlini, A. et al., 2011. Impairment of human immunodeficiency virus type-1 integrase SUMOylation correlates with an early replication defect. *The Journal of biological chemistry*, 286(23), pp.21013–22. Available at: <http://www.jbc.org/content/286/23/21013.full> [Accessed February 11, 2014].

i